Universitat Autònoma de Barcelona

FLEXOELECTRICITY IN BIOMATERIALS

Fabián Vásquez Sancho

Universitat Autònoma de Barcelona

POSTGRADUATE SCHOOL

PHYSICS DEPARTMENT

Ph. D. THESIS

FLEXOELECTRICITY IN BIOMATERIALS

Thesis submitted by

Fabián Vásquez Sancho

to apply for the Degree of Doctor at the Universitat Autonòma of Barcelona in the Doctoral Physics Program

Thesis Advisor: Gustau Catalan Bernabe

Thesis Tutor: Jordi Sort Viñas

prepared at Institut de Català de Nanocìencia i Nanotecnologia (ICN2)

defended on:

June 2018

The research work of this Ph. D. thesis has been founded from the ERC Starting Grant 308023.

Bellaterra, 2 Mayo de 2018

El Prof. Gustau Catalan, científico titular y lider del grupo **Oxide Nanophysics** del **Institut Català de Nanociència i Nanotecnologia (ICN2)**, en calidad de director de tesis y el Dr. Jordi Sort Viñas, profesor titular del Departamento de Física de la **Universitat Autònoma de Barcelona**, en calidad de tutor de tesis.

CERTIFICAN:

Que Fabián Vásquez Sancho, Bachiller en Física, ha realizado bajo su dirección y tutoría el trabajo que lleva por título ***"Flexoelectricity in Biomaterials"***. Dicho trabajo ha sido desarrollado dentro del programa de doctorado de Física y constituye su memoria de tesis doctoral, para optar por el grado de Doctor por la Univeristat Autònoma de Barcelona.

Dr. Gustau Catalan Bernabe
Oxide Nanophysics Group Leader
ICN2 - ICREA

Jordi Sort Viñas
Profesor Titular Dpto. Física
UAB

Jury :

Presidente :	Dra. Maria Pau Ginebra Molins	Biomaterial, Biomechanics and tissue engeeneering Universitat Politècnica de Catalunya Barcelona, España
Secretario :	Dr. Brian Joseph Rodriguez	School of Physics University College of Dublin Dublin, Ireland
Vocal :	Dr. Xavier Trepat Guixer	Integrative cell and tissue dynamics Institut for Bioengineering of Catalonia Barcelona, España
Suplente :	Maria de Carme Nogués Sanmiquel	Dep. Biologia Celular Universitat Autonoma de Barcelona Cerdanyola del Valles, España
Suplente :	Dr. Ignasi Fina Martinez	Institut de Ciència de Materiales de Barcelona UB Universidad de Barcelona Barcelona, España

To my family,

Acknowledgements

From the beginning I knew this project would be a major challenge for myself, not only because doing a PhD is already complicated, but also because I jumped into another field which I had never studied. In order to successfully finish this project I had the support of many people that i want to thank.

First, I want to thank the members of the tribunal for taking their time to read my thesis and come to evaluate it, I hope it is of your interest and may inspire you in your work.

To Gustau, my mentor (I can proudly say it), I am really happy that coincidences and life allowed me to do the doctorate under your guidance. From the academic point of view, I learned many things from you and I admire you. But also, I want to say, it is your humanity, principles and vision of life that amazed me the most. I will always be thankful for us, your students and coworkers, you were more than a boss. I know you will never change that.

Ku, my confidant, secretary, even my boss sometimes, but especially my friend. There are not enough words to honour you. I am here because of you and I have finished thanks to you. I am proud of being your friend, usted sabe como es...

To the past and present members of the group: Umesh, Amir, Jacke, James, Roque, Kumy, Lau, Amador, Neus, Ela, Pablo, Christina, Irene, Irena, Nathalie and Raquel. All of you were important in one way or the other during the time I was here. You were a escape and support during the stressful moments of the project, your friendship was, and always will be, very important for me. Raquel, your participation in this thesis was fundamental, without you this project wouldn't be half of what it is now; thanks because you did more than what was expected, especially while I was away.

To the technicians around the institute: Roque, Francisco, James, Javi, Juanlu, Rafa and Raul, many thanks for helping me with all my difficult requests and, most

of the time you did more than your job. You are essential to all the students here. Also, I want to thank Andrew, who helped me with writing in English of the thesis and made it all easier, your work was amazing.

To the rest of the people I met here at the ICN2, ICMAB and CNM: Nuria, Civan, Ceren, Rocio, Alba, Bahwna, Fede, Arindom, Ashley, Blai, the lady's maid (Mary and Gloria), thank you for making these years more entertaining.

Finally, I would like to dedicate this thesis is to my big and beautiful family because they mean a lot to me. I will change to Spanish for them.

A ambas familias Vasquez y Sancho, porque siempre he sentido el cariño y apoyo de todos: tíos y primos. Muchos siempre han estado pendientes de nosotros, nombrarlos es imposible pero ustedes saben que los queremos mucho.

Santos y Sara, muchas gracias por todo el apoyo. Ustedes son parte de la familia. El contar con ustedes para lo que fuera nos dio mucha tranquilidad a nostros dos y a los que están en Costa Rica. Nos ayudaron a encontrar una casa al presentarnos a Cesar, al que también le agradecemos por permitirnos hacer del piso nuestro primer hogar.

A todos los amigos que nos visitaron en Barcelona (La lista llegó a +40) que nos permitieron pasear y conocer. Pero especialmente a Bart que fue el más habitual y con el que compartí muchas caminata: Thanks man, you are always welcome where ever we are.

A los ticos en Barcelona: Carmen, Marina, Glory, Adri, Dani, Ku, Guillem, Roberto y Fede. Ustedes son nuestra familia en Barcelona. Muchas gracias por todo, fueron lo mejor de nuestra estancia aquí. El apoyo que nos dieron desde que llegamos y luego durante el embarazo significa mucho para nosotros. Los vamos a extrañar y saben que nuestra casa es su casa.

Jime, Sami, Don Johnny, doña Sonia, Jenny y Michael. Muchas gracias por ser tan comprensivos conmigo. Por apoyarnos en todo, mucho de lo que logramos es

gracias a ustedes. Los amo.

Mami y papi, Allan y Diego, esta tesis es también de ustedes. Les debo quien soy, muchas gracias por el apoyo que siempre he recibido de ustedes, por creer en mi. Los amo.

Por último y más importante a Kim y Eva que son la motivación, diaria las amo. Amor te debo este doctorado, es tan mío como tuyo, sabes que sin ti nunca lo hubiera logrado. De no ser por ti, no estaría en Barcelona, cambiaste mis planes y mi vida y ha sido lo mejor que me ha pasado.

Abstract

Natural materials are the result of millions of years of evolution and trial and error over time has equipped modern species with the most optimal materials in terms of availability of resources, minimal use of energy for all processes and of course, performance. Under these circumstances, flexoelectricity, a universal property of insulators, appears to play an important biological role.

Flexoelectricity is a mechanoelectric property that converts mechanical pressure into electricity by generating electrical polarization from strain gradients. Strain gradients (inhomogeneous deformations) occur in all kinds of solid materials, thanks to inhomogeneous pressures, porosity gradients, elastic constant gradients or structural defects. Furthermore, at lower size scales (the micro and nanoscales where cells and molecules operate), strain gradients can be orders of magnitude much higher than at the macroscopic scales, so one should expect flexoelectricity to have an important effect at the cell scale. The universality of the property and its importance at the microscale have motivated this Thesis, which examines flexoelectricity in biomaterials.

The usual way to observe and quantify flexoelectricity it is to bend a material and note that one of the surfaces is under tension and the other is under compression. This results in a strain gradient and therefore in flexoelectric a polarization across the material. But strain gradients can also be generated at the nanoscale by introducing structural defects or nano-mechanical inhomogeneities such as pores or micro-fractures. In this thesis, we have quantified the flexoelectricity of several bioceramics with the aim of determining the physiological role of flexoelectricity in important processes, such as bone remodelling and self repair. The thesis is structured as follows:

Chapter 1 introduces the topic of the mechanoelectric properties of piezoelectricity and flexoelectricity and gives an overview of the biomaterials studied in this

thesis.

In Chapter 2, a theoretical analysis of the mechanoelectric properties of inhomogeneous systems is developed. For biomaterials, flexoelectricity and piezoelectricity cannot be as easily separated as in the case of crystal or ceramic samples that are regular and with well defined properties. In this thesis, the use of biomaterials (which are often composites with ceramic parts and organic parts) has forced us to consider situations in which flexoelectricity and piezoelectricity may act together. Situations in which piezoelectricity is able to disguise itself as flexoelectricity or vice versa are presented, with the aim to lay the conceptual framework for the electromechanical measurements and results of the following chapters.

Chapter 3 describes the characterization and analysis of macroscopic measurements of flexoelectricity in hydroxyapatite and bones. Bending-induced polarization of both kinds of samples yielded very similar results, which demonstrates that hydroxyapatite can account for most of the bending-induced polarization of bones without needing to invoke collagen piezoelectricity.

Considering that flexoelectricity is more relevant at the microscale, where strain gradients are bigger, in Chapter 4, we developed a model to study strain gradients and flexoelectric fields around microcracks in bones. We determined that the magnitude of the electric fields generated by a loaded crack is large enough to induce apoptosis in osteocytes. Osteocyte apoptosys is known to be the first step in the bone remodeling process. Flexoelectricity therefore appears to act as the signal used by bones to determine the exact position of damage in the tissue and trigger its healing.

In Chapter 5, we performed in vitro experiments with osteocytes and osteoblast to probe whether flexoelectric fields are indeed able to affect cells. We observed not only that crack-generated flexoelectric fields experiments are able to induce apoptosys of cells in the short term, but in the long term culture experiments,

flexoelectricity is also able to stimulate mineralization and secretion of collagen 1a1 protein, an indicator of the state of differentiation of cells.

In Chapter 6, we explored the mechanoelectric properties of other ceramic-based biomaterials, such as teeth, coral skeleton and the club of a stomapod (thoughest known biomaterial). In the case of teeth, they are composed by the same constituents as bones, and they were therefore a good material to compare with bone. Meanwhile, coral skeleton is a material commonly used as a bone graft due to the similarities with bone in terms of mechanical properties and pore structure. By comparing flexoelectric properties of both materials, we were able to determine that they are also very similar, leading us to hypothesise that flexoelectricity comtatibility may be a helping factor in the good performance of coral-based bone grafts, a possibility we propose to explore in other candidates for bone grafts. Finally, the club of a kind of stomapod has an outstanding capacity to stand stress without fracture and this phenomenon motivated us to study the mechanoelectric properties of the club, as flexoelectricity is known to affect the mechanical properties of matter.

Finally, Chapter 7 gives a personal overview of the perspectives and future lines that could derive from this research, and the appendices provide useful information for anyone wishing to follow-up. The complete description of experimental procedures for electromechanical and biological experiments is in Appendix A, and Appendix B is the Mathematica algorithm that I programmed for calculating flexoelectric fields around cracks.

This thesis brings back the topic of mechanoelectric properties of biomaterials and gives the evidence of their importance in biological process such as bone remodeling.

Resumen

Los materiales producidos en la naturaleza, son el resultado de millones de años de evolución, este proceso de prueba y error ha dotado a las especies modernas con los materiales óptimos para sobrevivir. La evolución ha permitido la optimización de los biomateriales en función de la disponibilidad de recursos y minimización del uso de la energía. Considerando estos criterios la flexoelectricidad, una propiedad de todos los aislantes, parece jugar un rol importante moldeando la vida.

La flexoelectricidad es una propiedad mecanoeléctrica que convierte una presión mecánica en electricidad mediante la generación de polarización por gradientes de deformación. Los gradientes de deformación (deformaciones inhomogéneas) aparecen en todo tipo de materiales sólidos, debido a presiones inhomogéneas, defectos strucutrales y gradientes de porosidad y de constantes elásticas. Además, a escalas pequeñas (micro y nano escala en las que la células operan), los gradientes de deformación puede llegar a ser órdenes de magnitud mucho mayores que a la macro escala. Por lo tanto, se puede esperar que la flexoelectricidad pueda tener un efecto importante a la escala de las células. La universalidad de esta propiedad y su importancia en la micro escala motivó esta Tesis doctoral, que examina la flexoelectricidad en biomateriales.

La manera más simple de observar y cuantificar la flexoelectricidad es doblar un material y notar que una de las superficies se encuentra en tensión y la otra en compresión. Esto resulta en un gradiente de deformación y por tanto, en una polarización a través del material. Pero los gradientes de deformación pueden generarse también a la nano escala mediante la introducción de defectos o inhomogeneidades. En esta tesis, hemos cuantificado la flexoelectridad de varias biocerámicas con la intención de determinar el rol fisiológico de la flexoelectricidad en procesos importantes como la remodelación y autorepación de los huesos.

La tesis tiene la siguiente estructura:

El Capítulo 1 introduce la piezo y flexoelectricidad y describe los biomateriales estudiados en esta tesis.

En el Capítulo 2, se realiza una discusión más profunda sobre ambas propiedades mecano-eléctricas. En el caso de los biomateriales, la flexoelectricidad y la piezoelectricidad no pueden ser estudiados de la misma manera en la que se hace clasicamente en cerámicas y cristales que son regulares y tienen propiedades bien definidas. Al trabajar con biomateriales nos vimos forzados a considerar situaciones en las que la flexoelectricidad y piezoelectricidad pueden actuar a la vez o, incluso, situaciones en las que la piezoelectricidad is capaz de imitar los efectos de la flexoelectricidad y vice versa. Estos casos son presnetados para entender mejor las medidas y los resultados de los capítulos posteriores.

El Capítulo 3 describe las medidas macroscópicas de flexoelectridad en hidroxiapatita y huesos. La polarización inducida al doblar ambas muestras demostraron que la hidroxiapatita es capaz de generar tanta flexoelectricidad como el hueso,y por tanto la polarización del hueso puede ser explicada por la flexoelectricidad de la hidroxiapatita sin necesidad de considerar la piezoelectricidad del colágeno.

Considerando que la flexoelectricidad es más relevante en la micro escala, donde los gradientes de deformación son más grandes, en el Capítulo 4, se desarrolla un modelo para estudiar los gradientes de deformación alrededor de micro fracturas en huesos. Se determinó que la magnitud de los campos elélectricos generados alrededor de una fractura a la que se le aplica cierta fuerza, lo suficientemente grande como para inducir el proceso de la apoptosis en los osteocitos. Este proceso se sabe que es el primer paso para iniciar el remodelado de los huesos. Por lo tanto, la flexoelectricidad es la señal usada en el tejido para determinar la posición exacta de un daño en el hueso y facilicitar su autoregeneración.

En el Capítulo 5, realizamos experimentos in vitro con osteocitos y osteoblastos para determinar si los campos flexoeléctricos son capaces de afectar las células.

Observamos que los campos eléctricos en experimentos cortos son capacees de inducir la aopotosis de las células, but en cultivos celulares de más de una semana, la flexoelectricidad favorece el crecimiento celular y la secresión de la proteína Colageno 1a1, un indicador del estado de diferenciación de las células.

Finalmente, in el Capítulo 6, se exploran las propiedades mecanoeléctricas de otros biomateriales afines a la tesis como los dientes, corales, y el martillo de un tipo de camarón mantis. En el caso de los dientes, son de interes porque están compuestos de los mismos constituyentes que el hueso, y representaban un buen material comparativo con los huesos. Por otro lado, el mineral de coral es un material comunmente utilizado como injerto en el hueso debido a que tiene propiedades mecánicas y estructuras porosas muy parecidos al hueso. Al comparar las propiedades flexoelélectricas del coral y el hueso se puede determinar si la flexoelectricidad es un factor facilitador para la adaptación de los injertos, una posibilidad que proponemos explorar en otros materiales utilizados como injertos. Por último, estudiamos el martillo que utiliza un tipo de camarón mantis para romper otras biocerámicas, este martillo tiene una capacidad asombrosa para soportar golpes sin fracturarse, esta caracterísitica nos motivó para estudiar también sus propiedades mecanoeléctricas.

Contents

List of Figures

CHAPTER 1

Introduction

The combination of built-in structural flexibility and mechanical texture at the microscale - the scale in which cells operate and build - is inherent to biological tissues, and constitutes an optimal environment for flexoelectricity.

1.1 Flexoelectricity

Flexoelectricity is a universal property of insulators which enables them to polarize due to inhomogeneous deformations. The flexoelectric effect was first proposed by Mashkevich and Tolpygo and the theory of flexoelectricity was developed in 1964, by Kogan[1]. However, the concept remains unfamiliar to most people, mainly because it is a phenomenon that scales in inverse proportion to feature size[2, 3], making it imperceptible at the macroscale without the use of proper measurement technology. Nevertheless, this situation of relative anonymity is slowly changing for several reasons. Firstly, the ability to develop materials and characterize them in the small size-scales where flexoelectricity becomes important is now more accessible and technologically relevant. Secondly, as a universal property, flexoelectricity broadens the list of materials that can be used for applications. Finally, the possibility of creating electric fields within ferroelectrics by using strain gradients has enabled the development of new device applications such as ferroelectric memories that are operated mechanically and thus without electrode voltages[3], or photovoltaic cells where charge separation is provided by strain gradients[**?**].

1.1.1 Historical review

The concept of flexoelectricity was first identified theoretically in solids by Mashkevich and Tolpigo[4] from their studies of lattice dynamics in crystals. Later, Kogan developed the phenomenological theory describing the effect in crystals by analysing the effect of a phonon in centrosymmetric crystals and how this perturbation might produce an important polarization. According to his calculations, the deformation potential, which is known now as flexocoupling coefficient f_{ijkl}, should have a value between $1-10$ V. The effect in solid crystals was named only much later (in the 80's) by Indenbom, Loginov and Osipov[5], who based the name on a similar phenomenon discovered in liquid crystals by Meyer in 1969[6]. The term comes from the Latin word *flexus*, that means bend, related to the naturally occurring strain gradients in a bent plate.

Up to that point, the effect had been treated as a kind of piezoelectricity (Bursian called it "non-local piezoelectricity")[7]. In 1986, Tagantsev[8], developed a theory that demonstrated the independence of both phenomena and formulated a framework to calculate the flexoelectric constant from the dynamical perturbation of the crystal structure.

Initially, the small effect of flexoelectricity at macroscales delayed its experimental

investigation. However, the development of nanoscience and nanotechnology during the last thirty years, has increased the control stimulus on materials including strain and strain gradients. Importantly, because a strain gradient is a difference in strain divided by a relaxation length, at small length-scales strain gradients can be very big and, as consequence, flexoelectricity increases its magnitude at such scales, becomming relevant. In addition, the development of systematic experimental studies, led by the group of Prof. Eric Cross at Penn State, laid the foundation for the systematic study of flexoelectricity.

In the beginning of the 2000's, Ma and Cross, proposed different methods to measure flexoelectricity in solids[9] such as ceramics[10, 11] and nowadays, it is possible to find the flexoelectric coefficients of several perovskites[3]. But the results obtained are usually considerably larger than Kogan's prediction of the flexocoupling coefficient. This mismatch has been studied quite intensely and some candidates have been proposed to explain it, including parasitic piezoelectric contributions from polar nanoregions[12], defect concentrations gradients[13], residual ferroelectricity[14] and surface effects[8, 15]. The growing interest has also encouraged researchers to look at other types of materials, such as polymers[16–18], biomaterials[19] and even semiconductors[20].

1.1.2 Piezoelectricity versus flexoelectricity

Phenomenologically speaking, flexoelectricity is different from piezoelectricity, although both generate polarization as a response to a mechanical stimulus. Piezoelectric materials, which generate polarization from strain, must be non centrosymmetric (see Figure 1a). Strain, like stress, is not able to destroy centrosymmetry by itself (see Figure 1.1): it can change the polarization of the material only if the material is non centrosymmetric. In contrast, flexoelectricity generates polarization from strain gradients. Because the deformation gradient itself breaks spatial inversion symmetry, the change of polarization produced by flexoelectricity is not limited by the symmetry of the crystal, but depends instead on the inhomogeneous deformation that moves ions and the electronic clouds of atoms from their equilibrium position (see Figure 1c and 1d)[3].

The theory of flexoelectricity describes the generation of electric polarization by application of an elastic strain gradient and the phenomenon has to be treated in two different regimes: static and dynamic. The dynamic regime occurs in the case of a propagating sound wave[8]. In this thesis we are interested in the static regime, as in the bending of a plate, and unless stated otherwise, flexoelectricity refers to the

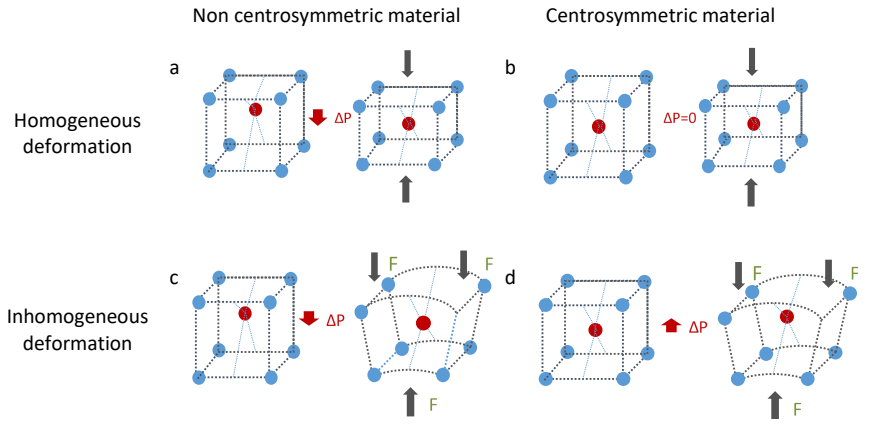

Figure 1.1: *Effects of mechanical stimulus on centrosymmetric and non-centrosymmetric crystals. Strains polarize only non-centrosymmetric materials (a and b). Centrosymmetry can be broken only with the presence of strain gradients (c and d).*

static regime. Following the theory of Kogan[1], the constitutive electromechanical equations are

$$P_i = \chi_{ij} E_j + d_{ijk} S_{jk} + \mu_{klij} \frac{\partial S_{kl}}{\partial x_j}, \tag{1.1}$$

where the first term on the right describes the dielectric polarization with χ_{ij} and E_j being the dielectric susceptibility and the macroscopic electric field respectively; the second term describes the piezoelectric response to stress σ_{jk} characterized by the piezoelectric tensor d_{ijk} in units of CN^{-1}. The last term describes the flexoelectric polarization, where the fourth rank tensor μ_{klij} is the flexoelectric coefficient and $\frac{\partial S_{ij}}{\partial x_k}$ is the gradient of the elastic strain along the x_j direction. In the absence of macroscopic electric fields, piezoelectricity and flexoelectricity are characterized by tensor relationship, as follows:

$$(P_i)_{E=0} = d_{ijk} \sigma_{jk} + \mu_{klij} \frac{\partial S_{kl}}{\partial x_j}. \tag{1.2}$$

The converse process for the case of flexoelectricity, generates a strain when an electric field gradient is applied to material, the converse flexoelectric effect is characterized by following relationship:

$$\sigma_{ij} = c_{ijkl} S_{kl} - \mu_{ijkl} \frac{\partial E_k}{\partial x_l}, \tag{1.3}$$

where c_{ijkl} is the elastic constant tensor and E_i is the electric field inside the material.

A more complete description of both electromechanical effects from the thermodynamic point of view, can be found in several reviews [3, 4, 7, 9, 21]. From Equation 1.2, it can be seen that piezoelectricity is governed by a third rank tensor, only available for non-centrosymmetric media, while flexoelectricity is governed by a fourth rank tensor, which is allowed in materials of any symmetry. As mentioned before, the main difference between piezoelectricity and flexoelectricity, is therefore that flexoelectricity is allowed in any material.

1.2 Determining the flexoelectric coefficient

Following the definition of flexoelectricity, two main methods are used to characterize the flexoelectric effect in the static regime, both represented in Figure 1.2. Both are able to measure only an effective flexoelectric coefficient, μ_{eff}; because materials present the Poisson effect, whereby deformations appear in a direction perpendicular to the strain. As a result, materials are simultaneously deformed in more than one direction, as are strain gradients, and the measured flexoelectric coefficient is thus a combination of different components of the flexoelectric tensor.

In this thesis, a 3-point bending system was the most used method. It is based on bending the material in cantilever-beam geometry at a certain frequency and measuring the displacement current or voltage.

The second method is based on a difference of pressure between two opposite faces of a material, which produces a strain gradient along the axis of the sample. This method was also proposed by Cross [9]. However, this geometry has the inconvenience that the strain gradient is strongly inhomogeneous since it concentrates at the sample edges, making it difficult to extract reliable values of μ_{eff} [22]. Still, for some samples whose lateral dimensions are too small to fit into the 3-point bending system, uniaxial stress gradients were the only available option. We used this method in the characterization of the mantis-prawn (stomapod) club and dentin-enamel junction in sections 6.1.2 and 6.2 respectively. The full description of the experimental setups is provided in Appendix A.

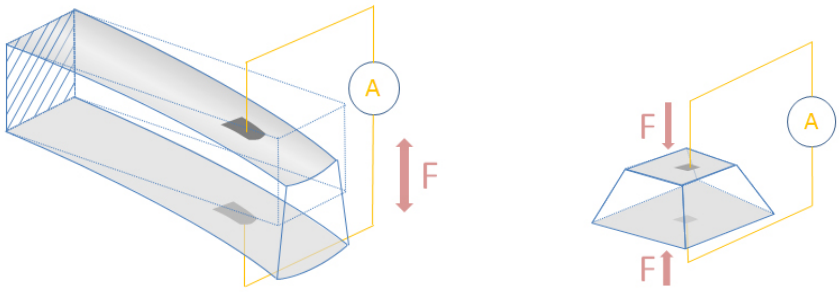

(a)

(b)

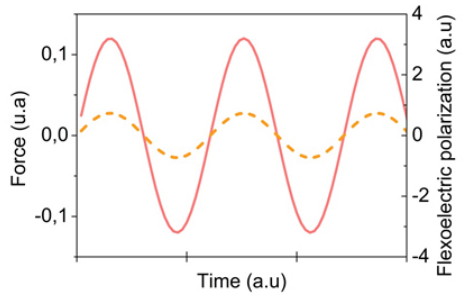

(c)

Figure 1.2: *Experimental methods to measure the effective flexoelectric coefficient. (a) Cantilever system. (b) Truncated pyramid method. (c) Flexoelectric polarization (in orange) in response to strain gradient produce by a force (in red).*

1.3 Biomaterials

As mentioned before, flexoelectricity is a universal property for all insulators, including crystals, ceramics and even polymers. Taking this into account, is the purpose of this thesis to determine if flexoelectricity is also present in biological-produced materials and, if so, to try to determine its physiological function. For the present thesis we will consider biomaterial made by nature.

Natural structural materials are built following certain principles: functionality, minimization of energy, and limited selection of components. Yet they have high performances in many physical properties. This high performance is often achieved by micro-structuration and materials combination. For example, micro-structured composite combination of minerals and protein in bones and nacre enhances their fracture toughness by two orders of magnitude above the coefficient of each individual component, as can be seen in Figure 1.3. These kinds of features are ubiquitous in nature, and have inspire d an entire research field, that of biommimetic materials, which searches for natural structures in order to understand their functionality and reproduce them with technology. In this thesis there is an order of increasing structural complexity in the materials we have studied. We start with a structurally homogeneous material such as hydroxyapatite ceramic, moving on to more complex compositestructures (bones, teeth, coral) and finishing with the most sophisticated mechanical composite, which is the stomatopod club. In terms of minaral composition, all of these structures are based around hydroxyapatite, with the exception of coral, which is made of calcite. Below I give an overview and justification for the study of each of these materials.

1.3.1 Bone

Bone is the dynamic tissue that forms the skeleton of vertebrates and acts as the main organ for support and protection of inner organs. In order to do so, bones must transfer forces along the body under controlled conditions of strain and stress. These functionalities, have led many scientists to study the mechanoelectric properties of bones.

1.3.1.1 Structure of bones

Bone is a complex structure. In general terms, bone can be considered as a family of materials with a common building block: collagen fibres mineralized with calcium

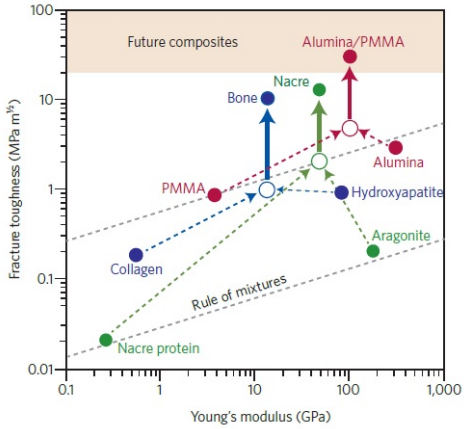

Figure 1.3: *Fracture toughness of biomaterials and its constituents. Mixture of materials enhance the mechanical properties of the final material, a common process used by nature. Taken from [23].*

phosphate[24]. For historical reasons, there are other materials with different names that, from a structural point of view, could be considered as bones e.g. dentine, enamel, mineralized tendons and even antler[25]. In this thesis, "typical" bone is considered as bone present in mammals, of which we have taken bovine femoral bone as a representative example.

Even though the discussion will be limited to typical bone, its structure has a hierarchical complexity that should be considered in order to understand the polarization of bone as a whole. The different levels of bone structure became evident as modern microscopes evolved. For example, higher levels of this hierarchy, such as osteons or lacunae, were identified with optical microscopes during the 17th century[26]. Different tissues within the bone, such as spongy and compact bone, were described by Monra in 1775[27]. More recently, the development of new microscopes, particularly polarizing and electron microscopes, has allowed other functional structures of bone to be identified at the molecular level, and in particular the intricate intertwining of collagen and hydroxyapatite.

The molecular level is the lowest level at which it is possible to find an organization in bone. At this level, bone can be considered as a composite of collagen, a fibrous protein, stiffened by a dense filling of hydroxyapatite crystal that surrounds the protein fibres[25, 28, 29]. Other components are also present at the molecular level, including water or non-collagen proteins. The mechanoelectric importance of water should not be underestimated since mechanic measurements of dry and wet

bone give different results[30]. Collagen is also of paramount importance, since it is known to be piezoelectric[31].

The inorganic constituents of bone were known to be calcium, phosphate and carbonate in 1799[32], and bone mineral was later identified as hydroxyapatite thanks to X-ray diffraction in 1926[33]. In bone, this mineral is known to contain high amounts of carbonate, thus, it is called carbonate hydroxyapatite (or dahllite)[24, 26]. Carbonate hydroxyapatite forms plate-shaped crystals (mineralized tendon) and needle-like crystals (femurs and calvaria) of 2-3 nm in thickness independently of the animal species[34]. The crystals usually have a preferred orientation along the collagen fibrils axis, but without a periodic correlation.

The space group and unit cell dimensions of hydroxyapatite were determined by Posner, et. al. as $P6_3/m$, and a = b = 9.432, c = 6.881[35] and since $P6_3/m$ space group is centrosymmetric, it should not be piezoelectric[35–37]. However, recent structural refinements and measurements of the mechanoelectric properties of hydroxyapatite are ambiguous, and will be discussed in Chapter 3.

The organic part of bone is mainly collagen Type I, from now on referred as just collagen. Collagen is formed by the aggregation of a protein called tropocollagen, which consists of three polypeptides of the same length, of which two have the same amino acid composition and one is different. The primary structure of the tropocollagen is [Gly (glycine)-X-Y]n, where X is commonly proline and Y hydroxyproline[38]. The three chains are held together by hydrogen bonds in a characteristic left handed triple helix.

Collagen molecules are organized into fibrils of 80-120 nm in diameter. Crystals of carbonated hydroxyapatite nucleate within the gaps inside the fibril which results in the compact composite of the organic and inorganic material, known as the second level in the hierarchical structure. Ordered and disordered arrays of fibrils are then formed, (third level), creating patterns of unidirectional arrays or fanning arrays (fourth level) which are the first micron structure inside bone. At the fifth level, bundles of arrays are formed and it is at this point on the scale where cellular networks are built[24, 26].

The sixth level consists of materials made by cells, for example, woven bone, parallel fibered bone and lamellar bone. Lamellar bone is the most common element in mammalian bone, while woven bone is found in tissues such as dentin and cementum from teeth. The next level includes elements formed inside tissue, such as trabecula, that is, lamellar packets and osteons that are cylindrical packets of lamellar bone[24, 26].

The eighth level is composed of different bone tissue: trabecular bone, also known as spongy or cancellous, and compact bone, the external shell of the bone. Compact bone, in contrast to spongy bone, is a solid mass that is found along the shafts of long bones (femur, tibia, radius, ulna) and is the principal component of flat bones (skull and ribs)[29].

1.3.1.2 Bone Cells

As mentioned before bone is a highly dynamic tissue, thanks to the presence of cells that continuously transform and remodel its structure in order to adapt it to the prevalent mechanical stress to which it is subject (Wolff's law).The transduction mechanism for Wolff's law appears to be electromechanical, as will be discussed later on[29, 39–41]. signals.

Bone has three specialized cells with different functions that, until now, are not fully understood, but basically work as follows:

Osteoblasts are mononucleated cells recruited from the mesechymal stem cells present in bone marrow[42]. They account for 4-6% of total cells in bone and are known for their bone building functions[42, 43]. Mature osteoblasts are located on the surface of the bones and are in charge of the bone matrix synthesis. This process implies the secretion of collagen and non collagen proteins to form the osteoids and consequently the initiation of mineralization by the synthesis of hydroxyapatite crystals. Finally, osteoblasts also contribute to the regulation of the osteoclastogenesis. As they mature, osteoblasts are able differentiate by taking two different pathways: (1) become osteocytes, as will be explained next, or (2) become bone-lining cells whose main role is to protect bone tissue against resorption.

Osteocytes, are differentiated osteoblasts embedded in the bone matrix. During the mineralization process, osteoblasts undergo morphological and ultrastructural changes, starting from being rounded-like cells and progressing to developing dendrites and becoming totally encased in the mineralized osteoids, and finally a reduction in the size of the cell. In addition, their amount of organelles decreases with protein synthesis and secretion[43, 44].

Osteocytes are the most abundant cells in bone, representing 90-95% of the total amount. They have a spider-like shape with up to 50 long branches that extend throughout the bone, forming a network of interconnecting canaliculi. This network facilitates the intracellular transport of ligands and interstitial fluid making it essential in coordinating the response of bone to mechanical, biological and electrical signals[44].

Osteocytes have the ability to regulate osteoblast behaviour by recruiting osteoclasts to locations where osteocytes have undergone apoptosis. An increment of the RANKL has been observed around regions with high amounts of dead osteocytes, making them an important protagonist in the process of bone remodelling[44, 45]. The issue of osteocyte apoptosis is important to this thesis because, as we will argue, flexoelectricity has the ability to cause localized osteocyte apoptosis near fractures or damaged regions in bones, thus linking flexoelectricity and bone repair.

Finally, the third type of bone-specific cells are the osteclast. Osteoclasts are multinucleated cells which originate from hematopoeitic stem cells lineage, under the influence of several factors. RANKL, secreted by osteoblasts and osteocytes is one of the factors that triggers osteoclasts recruitment to initiate the process of bone remodelling. During bone remodelling, an increase of acidity around its surface helps to dissolve hydroxyapatite crystals. Furthermore, it has been shown that osteoclasts produce factors that help to control osteoblasts and the activity of other cells.

To summarize at a very basic level, the role of the different cells in bone remodelling would be as follows: apoptosis of osteocites (caused e.g. by mechanical stress) releases RANKL that attracts osteoclasts to the damaged region and later osteoblasts. Osteoclasts "clean up" by dissolving the damaged region, while osteoblasts regenerate it by segregating bone mineral. Eventually, the osteoblasts become entombed in their own secreted bone composite, and then transform into osteocytes.

1.3.1.3 Mechanical properties of bone

Flexoelectric constitutive equations relate mechanical and electrical properties of materials. In the literature, it is possible to find a large range of values for each of the mechanical properties of bone (stiffness, strength, Young's modulus, among others), which implies differences not only in the variety of tissues but also in the measurement methodology used. These properties are usually obtained from bulk samples, and many attempts have been made to infer the properties of the intermediate levels of bone with varying degrees of success[24, 25].

The bulk elastic constants c_{ijkl} are related to the Young's modulus of the materials. Therefore, the elastic constants of bones directly determine the strain gradient distribution and thus the flexoelectric polarization. The elastic constants of compact bones, measured in the samples used in this thesis, plus the ones measured by other authors in different species are shown in table 1.1.

Table 1.1: *Elastic properties (in GPa) of different bones and species [25]*

	This work	Ashman et al.		Reilly and Burstein	
	Bovine	Canine	Human	Bovine	Human
E_1	6.0	12.8	12.0	10.4	12.8
E_2	12.0	15.6	13.4	10.4	12.8
E_3	19.0	20.1	20.0	23.1	17.7

Values of the elastic constants are average values in the three different directions specified by Voigt notation. As seen in table1.1, bone is an anisotropic material, in that it has different elastic constants depending on the orientation of the force applied. Therefore, the deformations are different in each direction. Bending within bones is believed to be an additional part of the design in order to meet the demands of axial strength vs dealing with stresses in different directions[46]. Therefore, curvatures and strain gradients are more common in bones than uniform deformation, which means that flexoelectricity is likely to be present potentially more so than piezoelectricity.

1.3.2 Teeth

From a material point of view, teeth may be considered as bone[25], since at the microscale they are formed by the common building block of hydroxyapatite and collagen. However, for historical reasons -and also because of their different physiological role- they were named differently[25]. Teeth in mammals are made of three main components: enamel, dentin and cementum.

Cementum is a thin layer of tissue covering the root of teeth. Cementum is attached to the outside of dentin and helps to fix teeth to the bone of the jaw, in which they lie. Also known as cement, cementum is essentially a modified bone, with cells called cementocytes, that are similar to osteocytes. Cementum, as bone, has collagen that is produced in part by cementocytes but mainly from the periodontal ligament. As it is a very thin interfacial layer, little is known about its mechanical and electrical properties.

Dentin is the major constituent of teeth and has a very similar composition to bone: 20% of organic material, 70% hydroxyapatite and 10% water. The main difference with respect to bone is that dentin does not have cells in it, all the cells in teeth moved into the pulp[25]. Furthermore, the orientation of collagen fibrils and, therefore hydroxyapatite crystallites are oriented normal to the dentinal tubules.

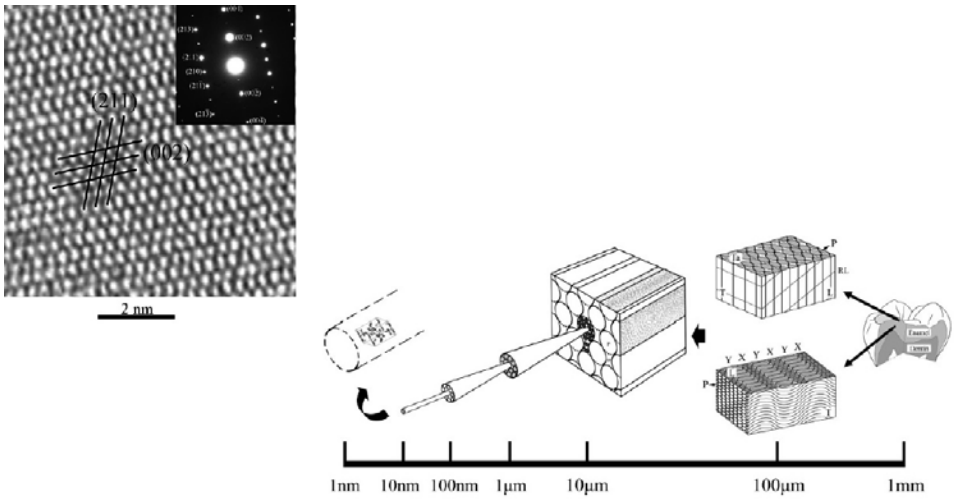

Figure 1.4: *Hierarchical organization enamel. At the lowest scale, hydroxyapatite organizes in highly ordered fibrils (inset). These fibrils tend to align into prisms that can take different directions at the highest levels. Taken from [47].*

Enamel is the exterior layer of teeth. It provides a hard surface for the trituration of food or as weapon in the case of some animals[25]. The most interesting part is that enamel is composed about 97% by weight of mineral with high crystalline order. As with bone, it has a hierarchical structure. Hydroxyapatite crystals, at the lowest level (nanometer range), are organized in a nanosized fibril-like structure. At the micrometer level, agglomerations of these fibrils can be observed. These structures are aligned parallel to each other and are called prisms. Eventually, at higher scales these prisms are arranged in different ways across the thickness of the enamel. Figure 1.4 shows the total organization of enamel[47].

1.3.3 Stomapod dactyl club

The stomapods are a group of tropical crustaceans with many interesting characteristics that have been explored recently by science, with an eye on biomimetic applications. For example, the eyes of these species are some of the most sophisticated found in nature. In comparison to human eyes, that have only three different types of color receptors, the mantis shrimp has 16 different types of color receptors and six polarization channels made by different nanostructures. A group of the University of Illinois has designed a biomimetic camera inspired by the stomapods eye which claim to be able to detect the disordered nature of cancerous cells[48].

In the case of *Odontodactylus scyllarus* (Figure 1.5(a)), a common stomapod from the tropical Indo-Pacific, their eyes also allow them to determine previous fractures or defects in the shells of mollusks that they hit with their club at a formidable acceleration of $10400g$[49]. This unique stomapod's club is of direct interest to this thesis, owing ti its outstanding mechanical properties. The most impressive feature is the club's ability to tolerate damage resulting from repetitive events. Furthermore, among the usual prey of this species are mollusks and crabs, whose outer shells are themselves regarded model systems for the study of toughness and damage tolerance. The extraordinary toughness of the stomapod's club motivates our interest in studying the flexoelectric properties of this material, as the highly localized stress generated by the impact could, in principle, lead to important flexoelectric effects.

The club is composed of two terminal segments named propodus and dactyl (Figure 1.5(b)). The dactyl is the most dense region of the whole exoeskeleton[49] and is divided in three different parts:the impact region, the periodic region and the striated region. Figure 1.5(c) shows the different regions of the club. The impact region is the most mineralized part, composed mainly of high crystalline hydroxyapatite with a preferable orientation of the (002) lattice planes parallel to the impact surface. By contrast, the periodic region shows no crystallinity, and is dominated by an amorphous mineral phase[49].

1.3.4 Coral skeleton

Corals are anthozoans, a word derived form the words 'flower' and 'animal' in Greek. It refers to the floral appearance of the polyp. Each coral colony consists of numerous small polyps, each with six (or multiples of six) tentacles, surrounding a mouth, leading to the main body cavity. These complex organisms are able to deposit calcium carbonate beneath them in a crystalline form called aragonite. The formation of a coral reef is the product of the action of several species that create the limestone substrate[50]. There is another group of corals, named soft corals that do not produce mineral protection. In this thesis we considered only stony corals that are made of aragonite.

Although all the stony species excrete aragonite, not all have the same mechanical properties. Mechanical properties change depending on the coral's morphology and are directly related to the pore concentration and size: for example, branched colonies are often stronger than massive colonies[51].

Aragonite, the mineral component of coral, is, like hydroxyapatite, a centrosym-

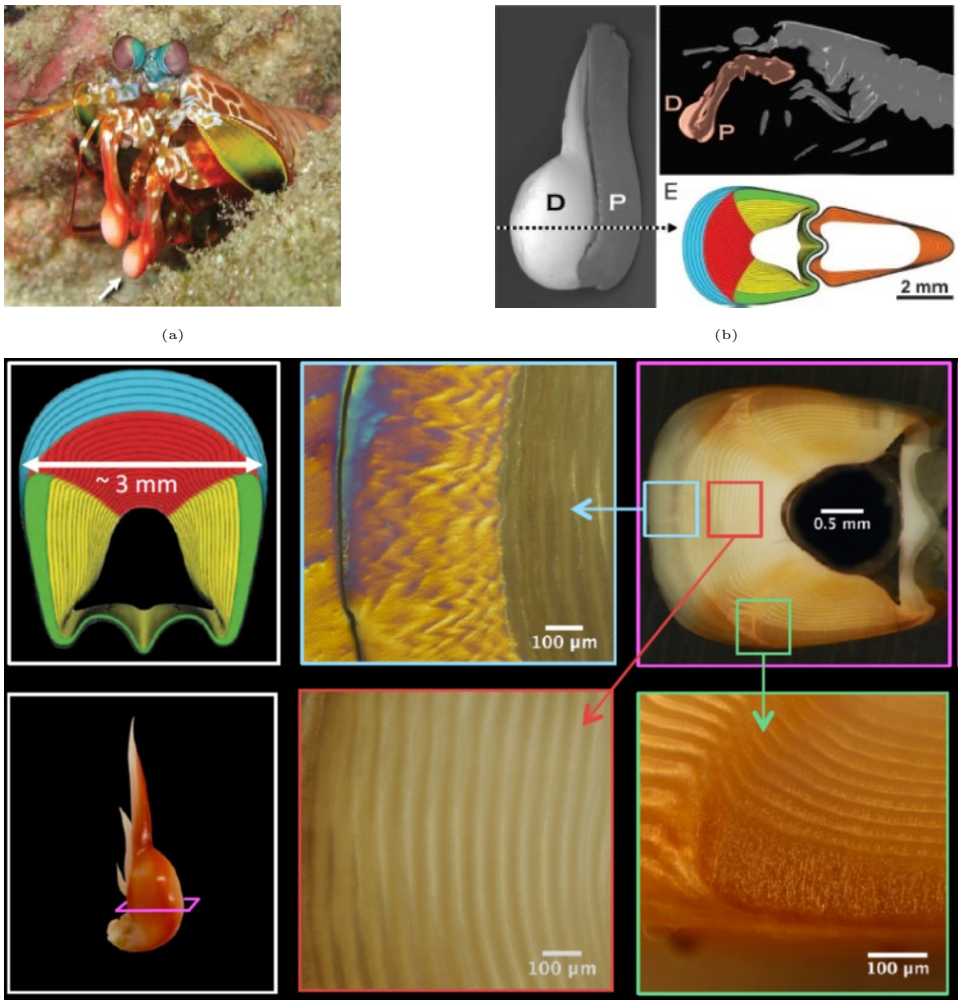

(a) (b)

(c)

Figure 1.5: *(a) Image of a Odontodactylus scyllarus, the white arrow indicates the dactyl club. (b) Division of the two main segments of the club: Dactyl and propodus. (c) Microscopic images of the parts of the dactyl. Taken from [49].*

metric crystal (space group Pmcn) lacking in piezo, pyro and ferroelectricity[52], so its electromechanical properties -if it has any at all- can only come from flexoelectricity. From the point of view of this thesis, the interest in coral mineral stems from the fact that a proven use of natural coral is as bone graft, due to its similar structure in terms of pore size and biocompatibility with pre-existing bone[53, 54]. The question we want to address is whether this biocompatibility includes having a similar flexoelectic coefficient.

CHAPTER 2

Theory of mechanoelectric properties in inhomogeneous materials

In Chapter 1, the theory of flexoelectricity and piezoelectricity was briefly accounted. The equations in that chapter are valid for crystals and ceramics were the mechanical properties can be considered homogeneous. However in biomaterials, usually, that is not the case owing to their hierarchical structures.

Hierarchical architectures are common to many species[23, 47, 55–57]. The main reason they developed was because such architectures help to increase flexural rigidity and also help deflect and stabilize cracks, thus increasing the fracture toughness of the whole tissue[23]. Being structurally inhomogeneous, they necessarily cause gradients and thus favour flexoelectricity.

In this chapter, we first analyze theoretically the electromechanical effects of strain gradients caused by gradients of elasticity or shape. From this analyzes we propose the equations to relate the experiments with effective constants of piezoelectricity or flexoelectricity.

In addition, and considering that bones have a piezoelectric ingredient (collagen), we analyze theoretically the electromechanical bending response of a heterogeneous piezoelectric beam and show that (i) it is a necessary and sufficient condition that the piezoelectric coefficient is not constant and not symmetrically distributed for a piezoelectric to be able to replicate the functional behavior of a flexoelectric and (ii) that such asymmetric piezoelectricity cannot be distinguished from true flexoelectricity in beam-bending experiments, even if the sample is turned upside down to change the sign of the piezoelectric vector; the disguise is, in this respect, perfect. Based on these results, we postulate an effective flexoelectric constant

given by the spatial distribution of piezoelectricity. Quantitative analysis of this pseudo-flexoelectric coefficient shows that even a relatively modest piezoelectric asymmetry can lead to an apparently giant effective flexoelectricity. More generally, the distinction between intrinsic flexoelectricity and gradient piezoelectricity is likely relevant for understanding the anomalously high (according to Kogan's theory) flexocoupling coefficients of some materials

2.1 Background

Polarization induced by other type of strain gradients have being studied in the past but not necessarily for biomaterials. In 2006 Cross proposed how to produce a "piezoelectric" device without the use of any piezoelectric material, but using flexoelectricity[9], by shaping a material in such a way that it generates a stress difference between two sides of a material. Biomaterials with different asymmetric shapes subjected to forces should also react in the same way (polarizing). This effect could be enhanced by gradients of elastic constants that were not considered by Cross and will be developed in the next section.

The converse effect will be the case where piezoelectricity is able to mimic flexoelectricity. This case is particularly pertinent for bones because, historically, Williams observed unexpected results on bent bones[58] which motivated doubts around his study. Williams himself did not observe a change in the phase polarization after flipping the samples as should be the case for a piezoelectric material.

Williams justified the bending-induced polarization of bones using what he called "gradient piezoelectricity". As was also mentioned by Fukada: " Since the structure of bone is very inhomogeneous, if there is any such orientation of [piezoelectric] collagen molecules, we might observe some residual polarization"[59]. Then the new analysis of Williams (motivated by Fukada) considered the piezoelectric coefficient as a function of the position $d_{yzz} = f(y) = d_0 + d'y$, where d_0 is a constant and d' is the linear change of the piezoelectric constant across the thickness of the sample. He defended this analysis instead of the incorporation of the strain gradient, first because he could not explain the reason for using strain gradient theory (the term flexoelectricty was not yet coined)[60]. And second because he was convinced that collagen was the only electromechanically-active constituent of bone, given centrosymmetry of hydroxyapatite. Since collagen distribution across bone is not regular, it was possible to consider that the bending induced polarization was a consequence of such irregularities.

Although Williams was able to obtain an expression to calculate the voltage across a bone cantilever, it appears that he lost interest in the phenomenon, mainly because he considered streaming potentials as a more relevant effect to explain polarization in real bones (with fluids)[60–63] and his analysis did not receive much attention. In the next sections, I will present a new model that reconciles the concept of variable piezoelectric constant (William's piezoelectric gradient) with flexoelectricity and shows that the two are,in fact, experimentally indistinguishable.

2.2 Electric polarization in hierarchical structures: flexolectricity mimics piezoelectricity

Let us assume a parallel-shaped sample with different elastic constants c_1 and c_2 at opposite faces with area A. For the sake of simplicity, let us assume that the variation of the elastic constant is linear with respect to the thickness of the sample. If a force F is applied there will be a strain gradient across the thickness of the sample h. Therefore, a polarization should appear in accordance with flexoelectric Equation 1.1. The average strain gradient across the sample will be the difference between the strains at each surface divided by the thickness

$$\frac{\partial S_z}{\partial x_z} = \frac{\frac{F}{Ac_1} - \frac{F}{Ac_2}}{h}. \tag{2.1}$$

and, therefore, the flexoelectric polarization is

$$P_z = \mu_{xz} \frac{F}{Ah} \left(\frac{c_2 - c_1}{c_1 c_2} \right) \tag{2.2}$$

A polarization induced by an elastic gradient, as far as we know, has not yet been measured, but the procedure to measure it should be similar to the one proposed by Cross for samples with shape gradients (truncated pyramids)[9]. In addition, many biomaterials, and certainly bone, are not completely inorganic and can have a piezoelectric response due to the organic matrix (collagen piezoelectricity), so the total polarization will be given by

$$P_z = e_{zz}\sigma_z + \mu_{zz} \frac{F}{Ah} \left(\frac{c_2 - c_1}{c_1 c_2} \right), \tag{2.3}$$

where e_{zz} is the piezoelectric constant. Equation 2.3 constitutes a general electromechanical model for biomaterials, incorporating both structural flexoelectricity and matrix piezoelectricity. It is experimentally impossible to separate both contributions with a single measurement of polarization as a function of stress, so we should therefore consider it as effective piezoelectricity, where each contribution could be competing or collaborating to the total polarization.

Defining the stress as

$$\sigma_z = \frac{F}{A}, \tag{2.4}$$

then the total polarization can be written as

$$P_z = \frac{F}{Ah}\left(\frac{c_2 - c_1}{c_2 c_1}\right)\mu_{eff}, \tag{2.5}$$

where μ_{eff} is defined as a combination of piezoelectricity and flexoelectricity:

$$\mu_{eff} = \frac{hc_1c_2}{c_2 - c_1}e_{zz} + \mu_{zz}. \tag{2.6}$$

As a complement, it is possible to rewrite Equation 2.3 in terms of a effective piezoelectric coefficient as

$$P_z = e_{eff}\sigma_z, \tag{2.7}$$

where e_{eff} is:

$$e_{eff} = e_{zz} + \frac{c_2 - c_1}{hc_1c_2}\mu_{zz}. \tag{2.8}$$

The previous model assumes a perfectly rectangular sample. However, biostructures have different shapes, usually not regular. When an object is subjected to a uniform force but its shape is not uniform, strain gradients can also appear as the irregular shape concentrates the strain in certain regions and deflects it from others. One well established method of measuring flexoelectricity is based on the possibility of inducing strain gradients by a difference of areas in a sample as illustrated in Figure 1.2(b). If we consider the form of a sample with different areas in opposite faces, Equation 2.1 should be rewritten as

$$\frac{\partial S_z}{\partial x_z} = \frac{\frac{F}{A_1c_1} - \frac{F}{A_2c_2}}{h}. \tag{2.9}$$

and the stress

$$\sigma_z = \frac{1}{2}\left(\frac{F}{A_1} + \frac{F}{A_2}\right), \tag{2.10}$$

therefore the total polarization is

$$P_z = \frac{F}{h}\left(\frac{A_2c_2 - A_1c_1}{A_2A_1c_2c_1}\right)\left[\left(\frac{hc_1c_2}{2}\frac{A_2 + A_1}{A_2c_2 - A_1c_1}\right)e_{zz} + \mu_{zz}\right], \tag{2.11}$$

and in terms of an effective piezoelectric constant can be written as

$$P_z = F\frac{A_2 + A_1}{2A_1A_2}\left[e_{zz} + \frac{2\mu_{zz}}{h(A_2 + A_1)}\left(\frac{A_2c_2 - A_1c_1}{c_2c_1}\right)\right] \tag{2.12}$$

The reality is that in nature shapes are more complex and probably not possible to solve analytically. However, rectangular or truncated cone shapes are relatively easy to prepare and analyze for controlled experiments as will be done in Chapter 6.

2.3 Bending induced polarization: piezoelectricity mimics flexoelectricity

If flexoelectricity can disguise as piezoelectricity, as seen in Section 2.2, then one can asks for the converse question: is it possible that, in the right conditions, piezoelectric materials can replicate the bending-induce polarization properties of flexoelectrics? In other words: is piezoelectricity able to mimic flexoelectricity? And if so, can we distinguish true flexoelectricity from gradient piezoelectricity?

To illustrate these questions, let us remind that polarization can be generated by flexoelectricity when the sample geometry, or the applied deformation is inhomogeneous (e.g., when a sample is bent[9, 11, 64–67]). For piezoelectricity, however, this is not necessarily true: bending a homogeneously poled piezoelectric beam does not induce any piezoelectric polarization, because there is no net strain: the piezoelectric polarization caused by stretching on the convex side is canceled by the opposite polarization induced by compression on the concave side. It follows from this example that, in a bending experiment, the total contribution of piezoelectricity to the polarization should be null.

In addition, whenever macroscopic piezoelectricity is evidenced by measuring polarization as a function of stress, space-inversion experiments such as flipping the sample upside-down, as in Figure 2.1(a), can be used to verify that the sign of the stress-generated charge changes sign[13], as it should given that piezoelectricity is given by an odd-parity tensor. By analogy with such experiments, it has been assumed that such space-inversion tests could thus be used to distinguish between piezoelectricity and flexoelectricity[15]. because flexoelectricity is given by an even-parity tensor. And, indeed, the bending-induced polarization of a flexoelectric cantilever is independent of its orientation, as it is shown in Figure 2.1(b). However, as we will see, there are conditions in which this inversion invariance is also true for piezoelectric cantilevers. In other words: in this section we are going to show that bending a piezoelectric can yield polarization and that this polarization, despite its piezoelectric origin, does not change sign when the sample is turned upside-down.

We begin by analyzing the response of a flexoelectric cantilever beam under bending. In this configuration, two electrodes are attached to the beam at the top

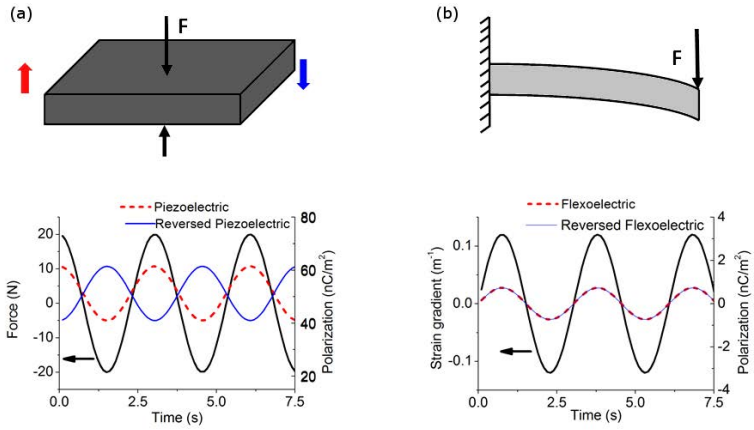

Figure 2.1: *(a) Piezoelectric polarization induced in a rectangular sample under tension or compression. The blue and red arrows represent the direction of the material polarization. (b) Flexoelectric polarization induced in a cantilever beam under bending. The polarization does not change sign by reversing the beam.*

and bottom faces (see Figure 2.2(a)). The top electrode is grounded, and the bottom electrode can undergo a change of electric potential as a result of deformation. The specific parameters are not important, but for this example the aspect ratio of the beam is fixed to $L/h = 10$, where L and h are the length and height of the beam with $h = 5$ μm. The magnitude of the flexoelectric coefficients are chosen as $\mu = \chi f$, where f is the transverse flexocoupling coefficient f_{13} and χ is the dielectric susceptibility at room temperature. For the sake of simplifying the discussion without loss of generality, we assume all other coefficients of the flexoelectric tensor to be zero. A representative value of $f = 10$ V for oxides[3] was chosen. The response of the beam is calculated using a self-consistent continuum model of flexoelectricity[68, 69][i]. Figure 2.2(a) shows the distribution of electric potential in the beam. The flexoelectric effect induces an electrical potential distribution, and an identical potential distribution is obtained by reversing the beam, as expected.

We also calculated the potential distribution corresponding to a beam of identical dimensions but where the electromechanical response is purely piezoelectric instead of flexoelectric. In Figure 2.2(b) it is clear that bending a homogeneous piezoelectric

[i]The model was developed by Prof. Abdollahi and he applied the model to the systems analyzed in this chapter

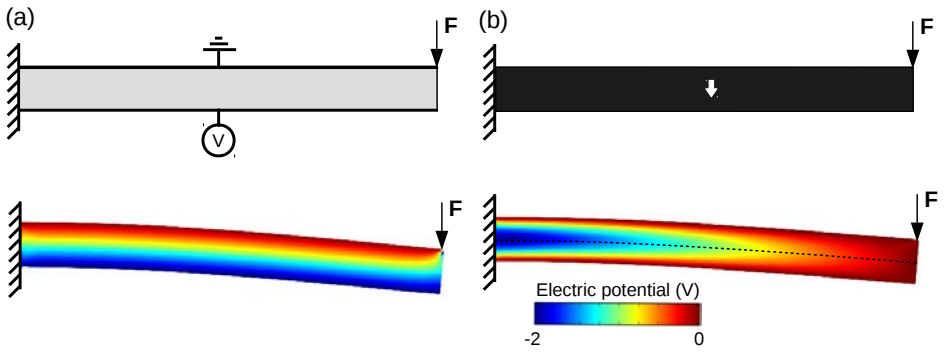

Figure 2.2: *(a)(top) Schematic of a flexoelectric cantilever beam under the point load F and (bottom) distribution of electric potential in the flexoelectric configuration. (b)(top) Schematic of a piezoelectric cantilever beam and (bottom) distribution of electric potential in the piezoelectric configuration. The white arrow represents the direction of the material polarization. In both setups, two electrodes are attached to the beam at the top and bottom faces.*

is unable to produce an electrical potential difference between the electrodes. The reason, as mentioned before, is that opposite stresses (compressive and tensile) are induced in the upper and lower halves of the beam respectively, thus leading to opposite piezoelectric effects and a zero net polarization. A piezoelectric coefficient of $e_{31} = -262\ pCN^{-1}$ corresponding to PZT [70] was used in the calculation, but the qualitative response is independent of the material parameters: bending a homogeneous piezoelectric beam simply cannot reproduce the flexoelectric response.

However, the balance of charges in a bent piezoelectric beam can be broken by replacing the top or bottom layers with a different piezoelectric or even a non-piezoelectric layer, as is in fact commonly done in piezoelectric bimorph sensors and actuators[71]. Such bimorph, in which the bottom layer is piezoelectric while the top layer is not, is illustrated in Figure 2.3(a).

The bimorph can be regarded as an extreme case of asymmetric piezoelectricity. The distribution of electric potential in this setup shows that the bottom electrode captures an electrical charge.

A bimorph piezoelectric cantilever thus generates a voltage just like a flexoelectric cantilever would. However, to exactly and indistinguishably mimic flexoelectricity, it is necessary that the sign (phase shift) of the piezoelectric charge does not change by reversing the beam. Figure 2.3(b) presents the reversed configuration together with its response. It can be seen that, indeed, the induced charge at the bottom electrode indeed does not change sign in comparison with Figure 2.3(a). A bent

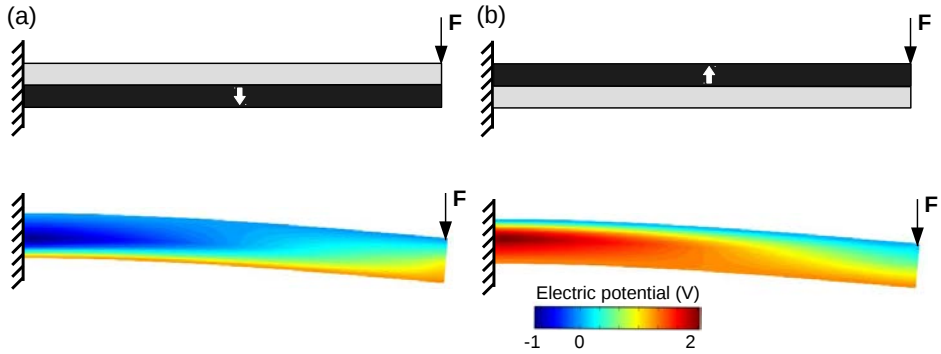

Figure 2.3: *(a)(top) Schematic of a cantilever beam under the point load F, where the dark layer is piezoelectric and (bottom) distribution of electric potential in this configuration. (b)(top) A reversed configuration (rotated by 180^o) of (a), and (bottom) distribution of electric potential in the reversed configuration. The white arrows represent the polarization direction of the layers. In both setups, two electrodes are attached to the beam at the top and bottom faces.*

piezoelectric bimorph is thus qualitatively indistinguishable from a bent flexoelectric beam.

2.3.1 Linear variation of piezoelectric coefficient

We can generalize the conclusions of the bilayer example by assuming a generic cantilever beam with an arbitrary distribution of piezoelectricity. A schematic of the beam is presented in Figure 2.4. By assuming that the beam consists of different piezoelectric layers sandwiched between two electrodes[72], the net polarization induced in the beam under the applied moment M is obtained as

$$P = C_M M c_{13} \frac{\sum_j \frac{d_{31j} t_j (z_M - z_j)}{K_j}}{\sum_j \frac{t_j}{K_j}}, \tag{2.13}$$

where C_M is the curvature per unit torque, c_{13} is the elastic constant in the transverse direction, d_{31} is the transverse piezoelectric coefficient, z_M is the neutral axis for torque inputs, z is the distance from reference to the center of each layer, t is the layer thickness, K is the dielectric permittivity, and j is the layer index. By considering infinite number of layers, i.e. $j \to \infty$ and $t \to 0$, and assuming that all the layers have the same dielectric permittivity, Equation (2.13) converts to an integral equation over the beam thickness h as

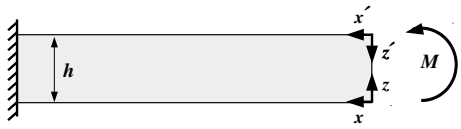

Figure 2.4: *Schematic of a cantilever beam under the moment M.*

$$P = \frac{\kappa c_{13}}{h} \int_0^h e_{31}(z)(\frac{h}{2} - z)dz, \tag{2.14}$$

where $e_{31}(z)$ is the distribution of piezoelectricity across the beam thickness and κ is the curvature obtained as $\kappa = M/YI$, Y is the Young's modulus and I being the moment of inertia. Equation 2.14 results in a zero net polarization if the piezoelectricity is symmetrically distributed about the centre of the beam, i.e. for any $d_{31}(z)$ such that $d_{31}(z) = d_{31}(h - z)$. Mathematically, the integrand is antisymmetric about the centre of the beam for any such symmetrical distribution of piezoelectricity. Conversely, as long as the piezoelectric coefficients are not symmetrically distributed across the sample, the bending-induced polarization will be non-zero.

In addition, the change of sign of the polarization in Equation (2.14) by flipping the beam can be demonstrated. In the flipped configuration, the coordinate system $x - z$ converts to the new system $x' - z'$, where $z' = h - z$, see Figure 2.4. Using this conversion and taking into account the negative sign of d_{31} in the flipped configuration, Equation (2.14) converts to an identical equation as a function of z', retaining its sign. Therefore, for a piezoelectric beam to be able to indistinguishably mimic flexoelectricity (i.e., for Equation (2.14) to yield a non-zero solution that is invariant with respect to space inversion), it is a necessary and a sufficient condition that the piezoelectric coefficient be asymmetrically distributed across the thickness of the beam. Two particular examples of this concept are the bimorph piezoelectric cantilever, for which $d_{31}(z)$ is a step-function, and surface piezoelectricity[3, 15, 73, 74], for which $d_{31}(z)$ can be viewed as two antisymmetric step functions.

Having shown that an asymmetric piezoelectric distribution can mimic a flexoelectric-like response, it is possible to define an effective flexoelectric constant as a function of the distribution of piezoelectricity. For a flexoelectric cantilever, the induced polarization as a function of beam bending is given by $P = \mu_{eff}\kappa$, where μ_{eff} is the effective flexoelectric constant and κ is the applied bending. By

equating this polarization to Equation (2.14), the effective flexoelectric constant can be defined as

$$\mu_{eff} = \frac{c_{13}}{h} \int_0^h d_{31}(z)(\frac{h}{2} - z)dz. \tag{2.15}$$

In order to get some quantitative estimates of how much "pseudo-flexoelectricity" can be generated by a gradient of piezoelectricity, we consider a simple linear distribution of piezoelectricity as $e_{31}(z) = mz + n$ as was done by Williams[60], where m is the slope of the linear gradient of piezoelectricity and $n = e_{31}(0)$. Plugging this function in equation (2.15) yields an effective flexoelectric coefficient of

$$\mu_{eff} = c_{13} m h^2/12. \tag{2.16}$$

Let us use this equation to analyze experimentally relevant cases. Experimental setups to quantify flexoelectricity commonly bend cantilever beams with a thickness in the order of $h = 1$ mm [9–11, 75, 76]. Therefore, to induce what is usually regarded as "giant" flexoelectric coefficient in the order of $\mu_{eff} = 1\ \mu C m^{-1}$, reported for important piezoelectric materials such as PZT and $BaTiO_3$ [9, 11, 76], the slope m should be in the order of 10 $pC(Nm)^{-1}$. For a 1 mm-thick beam, this represent a piezoelectric variation of $10^{-2}\ pCN^{-1}$ from the bottom to the top. When compared to the piezoelectricity of PZT and $BaTiO_3$, which is in the order of 100 pCm^{-2}[70, 77], such gradient represents only a 0.02 % fluctuation of the piezoelectric constant across the beam thickness. The conclusion is that, for materials with big piezoelectric coefficients, even a tiny gradient of piezoelectricity can yield an apparently giant flexoelectric coefficient, thus invalidating any quantification of flexoelectricity in the poled states of these materials.

The more relevant question, of course, is to what extent these results can also be extended to quantify the variation of effective piezoelectricity in the nominally *paraelectric* phase of ferroelectric materials. As has recently been reported, even in this nominally paraelectric phase, an asymmetric distribution of defects can result in a small but measurable piezoelectric coefficient[13]. The reported effective piezoelectric coefficients of nominally paraelectric perovskite electroceramics is in the order of 0.2 pCN^{-1}. Compared to this value, the same piezoelectric gradient of $10^{-2}\ pCm^{-2}$ across 1 mm, required to yield $\mu_{eff} = 1\ \mu C m^{-1}$ represents a 20% variation of the effective piezoelectric constant across the 1 mm thick beam in the paraelectric phase. Though this gradient is large, it does not seem unrealistic. And,

of course, a piezoelectric gradient 1000 times smaller can generate a flexoelectric coefficient of 1nC/m, which is in fact the expected flexoelectric coefficient for most materials based on the Kogan-Tagantsev theory of flexoelectricity. The conclusion is therefore that flexoelectricity and inhomogeneous parasitic piezoelectricity are, for all practical purposes, indistinguishable. Just as flexoelectricity can be utilized for imitating the functionality of piezoelectrics[9, 78–80], asymmetric piezoelectricity can be used to imitate the functionality of flexoelectrics.

This thesis is not concerned with the microscopic origin of polarization (true flexoelectricity vs gradient piezoelectricity), but with the existence, magnitude and physiological effects of gradient-induced polarization in biological systems. Whenever we quantify such gradient-induced polarization, it will be defined by an effective flexoelectric coefficient, irrespective of whether the origin is "true" flexoelectricity or parasitic piezoelectricity.

CHAPTER 3

Flexoelectricity in bones

This chapter describes our measurement of flexoelectricity in bones and hydroxyapatite, providing direct evidence that flexoelectricity contributes to the total polarization of bone, and examining its consequences at the micrometer range.

3.1 Hystorical background

In 1957, Japanese scientists Eiichi Fukada and Iwao Yasuda measured piezoelectricity in bones for the first time[81]. In the experiment, they applied a uniform strain to samples cut in different directions of the bone with respect to the long axis of human and ox bones. They found values of the piezoelectric constant ranging from 0.05 pCN^{-1} to 0.2 pCN^{-1} depending on the cutting direction. Additionally, they measured polarization even when all the inorganic material (the hydroxyapatite mineral) had been dissolved with acid, suggesting that the origin of piezoelectric signals comes from the collagen.

This discovery had profound implications for understanding the nature of signals that control the osteblastic and osteclastic stimuli[82] and gave a new perspective to understanding Wolff's Law [83, 84]: piezoelectricity would convert mechanical stresses into electrical signals to direct the bone-forming activity of the cells [41]. Although electricity has been used as a therapy for fracture treatment since the 1850's, it was not until the 1970's that the clinical usage of electricity for bone healing exponentially increased, in most cases without any well-established protocols [40]. Despite these limitations, electric stimulation of bones is still considered a potential cure for degenerative bone diseases such as osteoporosis[40].

Shortly after the discovery of polarization of bone by Yasuda and Fukada, new measurements were taken to prove the origin of the piezoelectric signal from collagen. Marino and Becker[85], who not only measured piezoelectricity of bones but also of collagen and hydroxyapatite separately confirmed the inability of hydroxyapatite to polarize under strains. They justified this due to the centrosymmetry of the crystal structure of hydroxyapatite, indicating that collagen was therefore solely responsible for the electromechanical polarization of bone[36, 41, 86–91].

At this point, Wendell Williams introduced the concept of "inhomogeneous piezoelectricity", as we discussed in Chapter 2, and produced several works that deserve special attention. His interest in the mechanoelectric properties of bone started by unsuccessfully exploring the p-n junction nature of bone and collagen[92], one of the hypothesis to explain the piezoelectric nature of bones. Later, he presented his results of piezoelectricity of bone and tendons in the Fifth Annual Biomaterials Symposium, in Clemson University. The measurements were done by using a bending system, from which he calculated the strain in a cantilever and used it to determine the piezoelectric coefficients, which he finally published in 1975[58]. This work is remarkable since his system is similar to those used nowadays

to measure flexoelectricity. Furthermore, he proposed using a fourth-rank tensor of strain gradient in order to explain the polarization of bone in a bending system.

He extended and analyzed this proposal in a publication one year later, inspired by Kogan's theory[59]. Interestingly, the article has an addendum of a discussion by E. Fukada, C. H. Lerchenth and W. Williams. Fukada, supported by Lerchenth, suggested that the classical theory of linear piezoelectricity was sufficient to explain Williams's results if he took into account the gradients of concentrations and inhomogenous strain. From his point of view, the polarization was caused by the inhomogeneous distribution of space charge and not by flexoelectricity (at that time the concept wasn't universally established).

In later publications relating to bones and fourth-rank tensor theory, Williams added: "This approach adequately described the observations, but its basic assumption could not be justified."[36, 60]. Another reason that flexolectricity was disregarded in the field was the proposition of polarization of bones by streaming potentials, an effect that is bigger in magnitude and takes into account the presence of fluids in bones. This new proposition was enthusiastically supported by Williams himself[61] and started to be more accepted as the main mechanoelectric effect in bones[41, 93]. A problem with streaming potentials, however, is that they cannot adequately account for electromechanical and physiological effects observed around cracks in bone ceramics.

3.2 Piezoelectricity of hydroxyapatite

As mentioned before, early experiments showed that hydroxyapatite samples under stressdid not polarize, suggesting that collagen must be the only contributor to the piezoelectricity of bones. However, more recent structural refinements[94] have suggested that hydroxyapatite might be piezoelectric after all, and functional measurements remain ambiguous. Thin films yield substantial piezoelectric coefficients[52], but thin films can easily become polarized by built-in fields, strain gradients, and/or defects[13]. Bulk ceramics, meanwhile, sometimes yield a small piezoelectricity[95] and sometimes no piezoelectricity at all[85]. These variations probably reflect differences in sample composition or morphology, making it all but impossible to make definitive statements about intrinsic properties.

In this study, different measurements were taken to determine whether our hydroxyapatite samples were piezoelectric. First, hydroxyapatite ceramics and commercially acquired ceramics from Berkeley Advanced Biomaterials, Inc., were

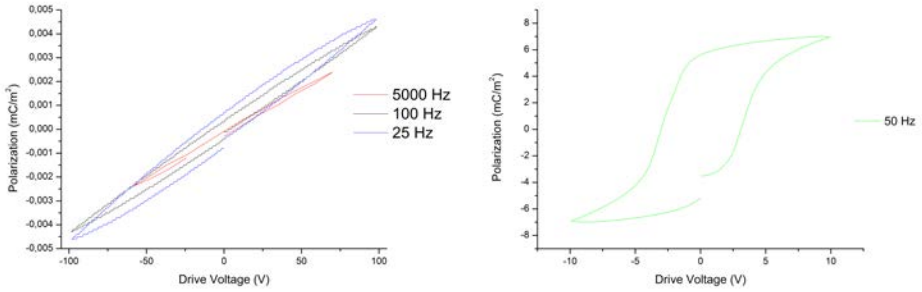

(a) (b)

Figure 3.1: *Polarization hysteresis loops of (a) hydroxyapatite at different frequencies and (b) PZT, a true ferroelectric material, for comparison.*

tested to discard ferroelectric like behaviour in Polarization-Voltage (P-V) curves. Figure 3.1 shows the measurements for hydroxyapatite samples at 25, 100 and 5000 Hz. In all the measurements, so called, "banana loops", typical of lossy dielectrics, were obtained providing no evidence of ferroelectric remanent polarization in hydroxypaptite at room temperature. As a reference, a P-V curve is shown for a reference ferroelectric, PZT ($Pb[Zr_xTi_{x-1}]O_3$), and in this case, there is a typical ferroelectric behaviour with a high remanent polarization.

In addition, the piezoelectricity of our hydroxyapatite was characterized by a direct load method[13], yielding piezoelectric coefficients smaller than 0.001 pCN^{-1}. This is at least two orders of magnitude smaller than the piezoelectricity of bone[96], and is comparable to the residual (defect-induced) piezoelectricity of $SrTiO_3$, a reference non-piezoelectric material used for comparison (see Figure3.2). Our bone ceramics are therefore not significantly piezoelectric, a result fully consistent with the reported lack of piezoelectricity in de-collagenized bones[85].

Macroscopic measurements, however, do not rule out the existence of piezoelectricity on a microscopic level[52]: piezoelectric grains with different orientation can in theory average out their aggregate contribution yielding no net macroscopic polarization even if there is polarization at the individual grain level. In order to examine this possibility, piezo response force microscopy (PFM) was performed to map out piezo response of the ceramic and see if there was a piezoelectric contrast between each grain. An EFM (electrostatic force microscopy) tip with a spring constant of 1.43 nN(mm)^{-1} and drive amplitude of 3 V was used for these measurements.

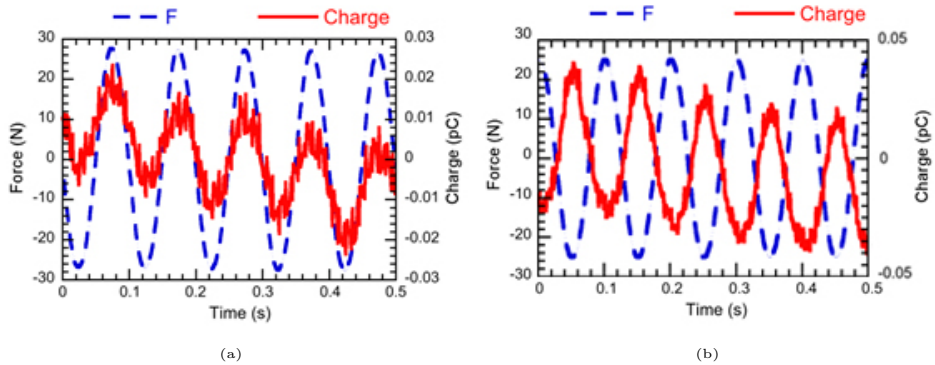

Figure 3.2: *Piezoelectric measurements of hydroxyapatite (left) and $SrTiO_3$(right). The piezoelectric coefficient is obtained by dividing the peak charge by the peak force applied.*

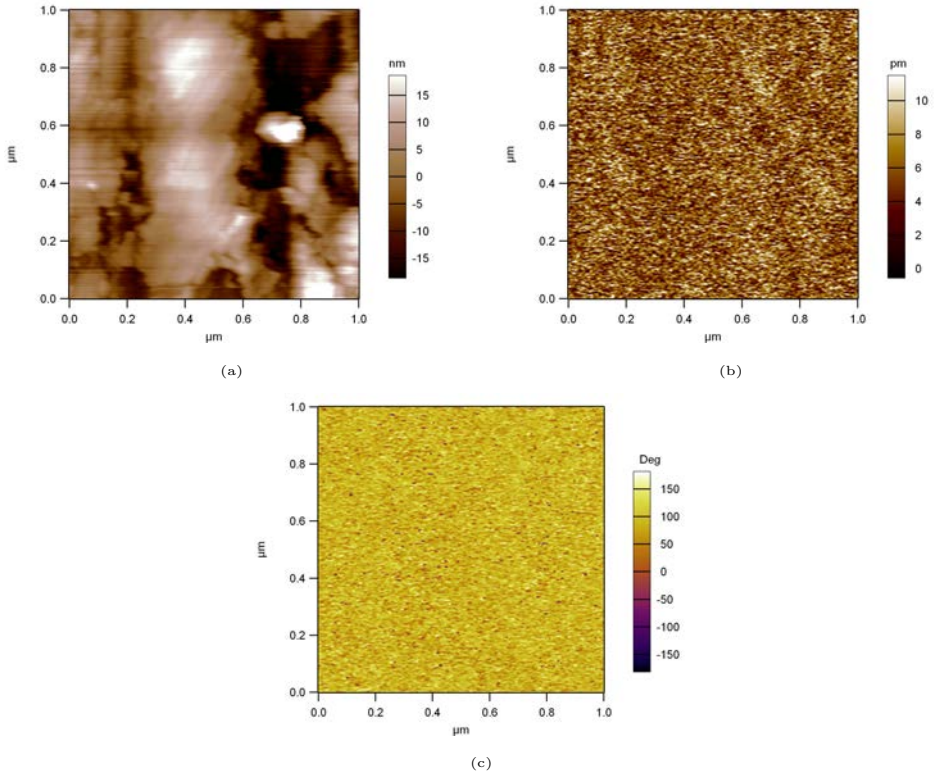

Figure 3.3: *Single frequency piezo response force microscopy images showing (a) topography, (b) amplitude and (c) phase image of a surface of hydroxyapatite, showing grains and pores as expected from a polycrystalline ceramic.*

Figure 3.3, shows the topography of the surface of the sample. The amplitude and phase of the piezoresponse did not show any contrast between the large central grain and the surrounding ones, implying that, at the microscopic level, grains do not present a contrasting piezoelectricity that could average out the macroscopically. Hydroxyapatite piezoelectricity is therefore discarded.

On the other hand, pure, hydroxyapatite has been shown to be able to direct the activity of osteoblasts towards damaged regions [97]. If hydroxyapatite is not piezoelectric, how does it manage to "communicate" to the cells where they have to work? This chapter examines the possibility that the mechanism whereby hydroxyapatite interacts electromechanically with cells is flexoelectricity.

3.3 Flexoelectricity of bones

The hypothesis that bone mineral generates electromechanical signals due to flexoelectricity is plausible. The combination of built-in structural flexibility and mechanical texture at the microscale - the scale in which cells operate and build - is inherent to biological tissues, and constitutes an optimal environment for flexoelectricity. For example, flexoelectricity has already been identified in stereocillia (inner ear micro-hairs), as an important ingredient of mammalian hearing[19].The highly textured and inhomogeneous structure of bones, with radial porosity gradients and curved walls, also lends itself to flexoelectric phenomena. Already in 1975, Williams[58] claimed that some electromechanical properties of bones, could perhaps be explained by "gradient polarization" or inhomogeneous piezoelectricity. Around the same time, Lakes [98] performed a theoretical analysis of the potential role of gradients in bones, an excellent theoretical analysis which unfortunately could not be substantiated due to lack of quantitative knowledge of their flexoelectric coefficients. Later, Fu reported the existence of bending-induced polarization in bones[99], attributing to collagen (wrongly, as is demonstrated in this chapter) the flexoelectric-like response of bones. Though these antecedents are few and scattered, together they provide tantalising evidence that there may be a role for flexoelectricity in bones. This role is experimentally quantified here.

Fresh bovine femurs were cut in beams oriented parallel to the bone axis and electroded for measuring flexoelectricity. The same femurs were also ground to powder, calcined and sintered into ceramic pellets (see the experimental section in Appendix A.1). A dynamic mechanical analyzer was used to deliver an oscillatory bending and a lock-in amplifier was used to detect the bending-induced

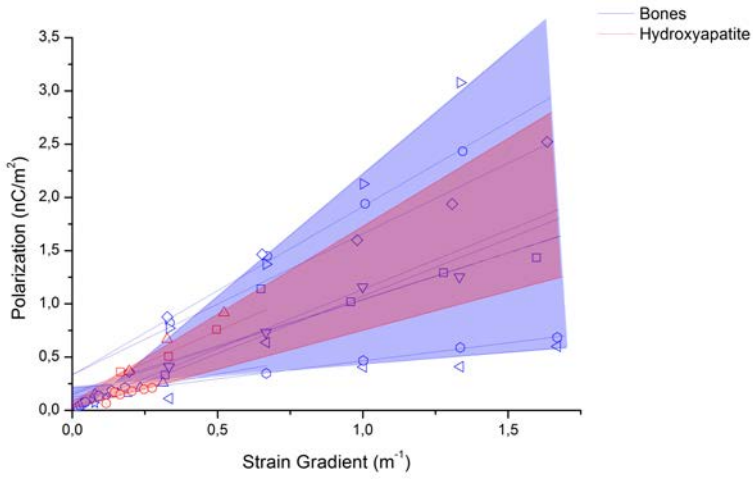

Figure 3.4: *Flexoelectric polarization of bone and hydroxyapatite samples as a function of the strain gradient. The flexoelectric coefficient is the constant of proportionality between a strain gradient (bending) and the bending-induced polarization. For greater accuracy, measurements were made for different applied forces (which induced different curvatures).The shadowed areas represent the dispersion of the data for bones (blue) and hydroxyapatite (red).*

polarization. The bending-induced polarization of bone, natural hydroxyapatite, and commercially-acquired synthetic hydroxyapatite is shown in Figure 3.4. The effective flexoelectric coefficients μ_{eff}, are extracted from the slopes of the linear fits of the polarization as a function of bending as is explained in the experimental section A.2.

Bones and hydroxyapatite presented some variation from sample to sample. The dispersion of the flexoelectric coefficient for each material is presented as the shadowed area: red for hydroxyapatite and blue for bones. The effective flexoelectric coefficients are between 0.4-2.6 nCm^{-1} for bone, and between 0.7-1.6 nCm^{-1} for hydroxyapatite. Collagen increases the mechanical toughness of bones, allowing them to withstand bigger bending than brittle ceramics of pure hydroxyapatite; nevertheless, for any given curvature, hydroxyapatite flexoelectricity is comparable to the flexoelectricity of bones. Hydroxyapatite flexoelectricity can by itself account for most of the bending-induced polarization of bones without needing to invoke collagen piezoelectricity.

As a comparison Table 3.1 shows the results of flexoelectricity of hydroxyapatite with other known flexoelectric coefficients of non-polar dielectric materials (values

taken from our measurements and in the case of STO from [65]).

Table 3.1: *Meachanoelectric properties of non-polar dielectric materials at room temperature*

	Flexoelectric coefficient (nCm^{-}1)	Dielectric constant (Fm^{-1})	Flexocoupling (V)
Hydroxyapatite	1.1 ± 0.5	9.74×10^{-11}	11 ± 4
STO[100]	6.1	2.65×10^{-9}	2.29
TiO_2	3 ± 1	7.52×10^{-10}	4 ± 1

Considering the anisotropy of the mechanical properties of bone, and the electromechanical anisotropy already reported in the seminal work of Fukada and Yasuda [81], the direction of the load is important for the polarization of a bone sample. Therefore, flexoelectricity was also measured at different cutting directions of the bone. The results in Figure 3.4 were made for bones cut parallel to the bone axis. In contrast, samples cut at two different transverse directions to the bone axis, measured with the same method, are shown in Figure 3.5. Both transversal directions presented flexoelectric coefficients higher than any sample cut longitudinal to the bone axis.

3.4 Evaluation of variable piezoelectric coefficient in bone

Taking into account the analysis of Section 2.3 we should consider the possibility that collagen's piezoelectricity is affecting the bending-induce polarization. Therefore, let us assume in the macroscopic samples of bones measured before that there was a linear variation of the collagen density and, therefore, there is a linear variation of the piezoelectric coefficient in the sample. According to Equation 2.16, for an effective flexoelectric coefficient of 1 nCm^{-1} the linear constant of variation should be $m = 4\ pC(Nm)^{-1}$. This is equivalent to a variation of 1 fCN^{-1} in 400 μm of thickness. Considering local measurements of bones, which showed variations of the piezoelectric constant in the order of 1 pCN^{-1} in the range of millimeters[100], it seems feasible that collagen piezoelectricity could be the real source of apparent flexoelectricity in our bone samples. However, hydroxyapatite ceramics do not have collagen or any piezoelectric organic molecules that could imitate flexoelectricity and the residual piezoelectric constant measured by direct methods is in the order

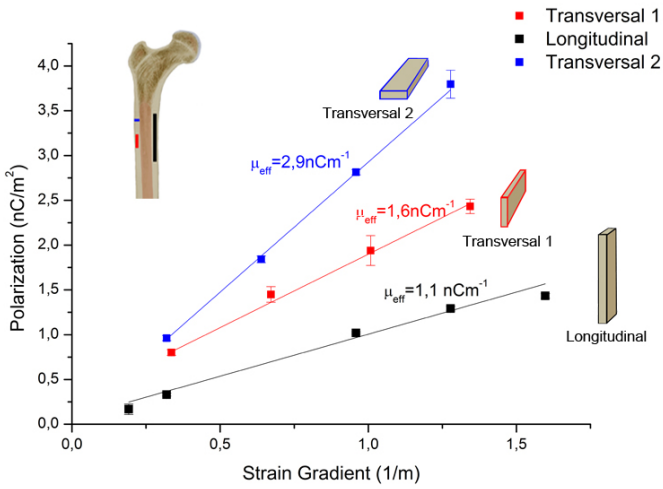

Figure 3.5: *Samples obtained along different directions of bone showed the flexoelectric anisotropy of bone. Transverse samples have a higher flexoelectric coefficient than the longitudinal sample in black.*

of 1 fCN^{-1}, and thus they would require a variation of 100% in the piezoelectric coefficient across the sample thickness, which seems highly improbable. And, yet, pure hydroxyapatite samples still present effective flexoelectric polarization of the same order of magnitude as bones, suggesting that the origin must be the same for both and, since in hydroxyapatite it cannot be piezoelectricity, flexoelectricity appears to be the most likely culprit.

Having measured the flexoelectrcity of bone mineral, the next important question is: considering that bones already can generate electromechanical voltages from streaming potentials and collagen piezoelectricity, what (if any) is the additional benefit of having a flexoelectric contribution from bone mineral? Strain gradients grow in inverse proportion to feature size[2, 3]. This means that although at macroscopic scales the average strain (and thus piezoelectricity and streaming potentials) can dictate the global response, at small scales the strain gradient, and thus flexoelectricity, can be much larger and dominate the local electromechanical response[99]. The next chapter examines the scaling hypothesis in detail, by focusing on the large strain gradients (and expected flexoelectric effects) associated with micro-fractures (cracks) in bones.

CHAPTER 4

Flexoelectricity around microcracks

Any material under a bending force can curve more as its thickness is reduced. That is, curvature (as strain gradients) increases by diminishing the scale. A dramatic manifestation of this principle takes place at the apex of cracks, which concentrate in a very small volume (crack junctions are atomically sharp) the maximum stress that a material can withstand before rupture. According to theoretical calculations, the flexoelectric polarization near a crack apex can exceed the piezoelectric polarization for even the best piezoelectric materials[101]. This chapter examines the possibility that crack-generated flexoelectricity could be capable of triggering the process of damage repair and remodelling.

4.1 Cracks in bones

The fracture of materials usually occurs when a force higher than a critical value of the material is surpassed. In an experiment it is easy to determine this critical value after preparing the sample with the right configuration and applying a force in a certain direction. With bones, the situation is a bit more complicated. First, a bone in normal conditions is usually under the action of several forces in different directions. Second, the anisotropy of bone also affects its fracture toughness[102]. Third, bones also behave differently if they are under tension or under compression. Finally, but perhaps most importantly, bone is a heterogeneous composite of two materials, hydroxyapatite and collagen, forming an intricate porous structure that makes it all but impossible to induce a straight crack propagating in a well defined direction. All these features of bones make it difficult to understand how bones break and fracture[25].

There are nevertheless some types of partial fracture (not implying complete breaking of a bone) which are quite common and can be studied. Micro-cracks are flaws formed due to cyclically applied stress. They are very common, but they usually represent no risk for the integrity of the bone thanks to the process of remodelling[25, 39, 103]. One of the most interesting features of bones is precisely their ability to stabilize (and eventually heal) cracks, preventing their spreading or coalescence. This happens thanks to bone's multiscale structural heterogeneity. In Figure 4.1 a comparison of the propagation of cracks in different materials can be seen. Bone is a combination of cases b, c and d. First, at higher levels of the hierarchy, layers of lamellae help to change directions of a crack or even divide it in two different cracks. This interface therefore makes the propagation of the crack difficult. Furthermore, voids and discontinuities at different levels of the bone can also stop the growth of cracks. Finally, at the lowest level, bone is a composite so that in order for a crack to spread, it needs to have enough energy to separate the mineral part and the collagen fibres. All these structural features help to stabilize cracks inside bones. But, do these craks have any physiological consequences? Also, after their growth has been arrested, how do microcracks get healed?

Cracks (especially) are a mechanical discontinuity inside bones, with great capacity for concentrating stress. In addition to cracks, other discontinuities are quite common inside bones, such as osteocytes lacunae, blood vessels and canaliculi and the stress concentration around them can also be impressive. For example, the effect of a blood vessel can be a concentration of three times the normal stress along

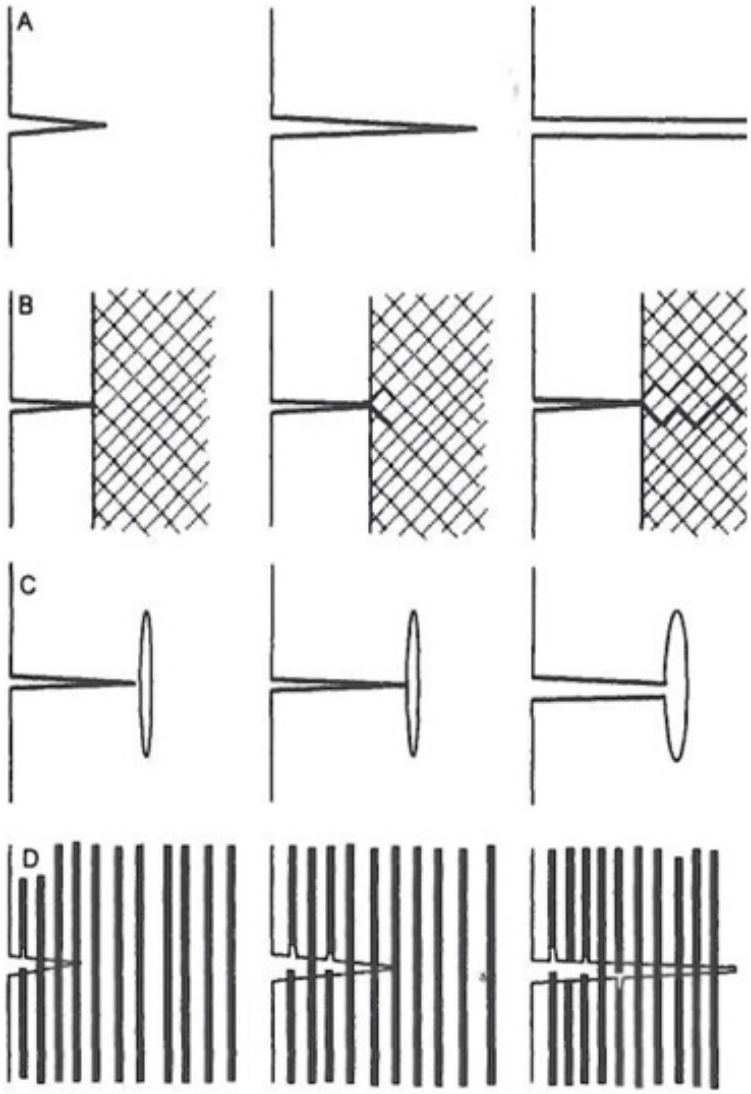

Figure 4.1: *(a) In brittle materials, once a crack started to travel it is unobstructed until the material is completely crack.(b) In materials with different layers cracks can take different pathways. (c) Voids in materials help to stop the crack propagation. (d) When cracks are formed in materials with to phases, one of them been a strong fiber, there most be enough energy to overcome the energy to separate the crystal, which is usually brittle, and the energy to overcome the strong fibers of collagen. Image taken from [25].*

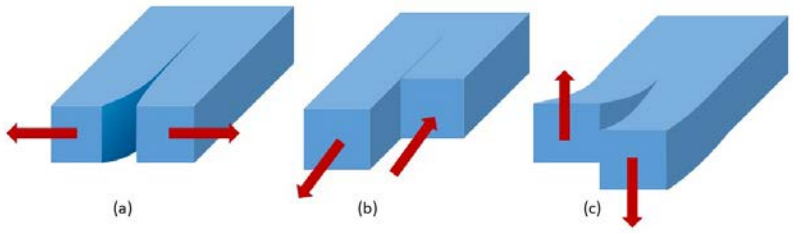

Figure 4.2: *Depending on the mode of load to a crack they are classified as: (a) Mode-I, opening mode, (b) Mode-II, sliding mode and (c) Mode-III, tearing mode.*

bones[104]. The stress around such discontinuities gives rise to deformations around them; therefore, since hydroxyapatite is flexoelectric, flexoelectric fields should be present. The next section deals with the strain gradients present around the tip of a crack that produces the flexoelectric fields.

4.1.1 Strain gradients around cracks

A crack can be created either because the material suffers an impact or due to fatigue that accumulates enough energy to separate the material, creating two surfaces. The crack can then be stabilized or else continue growing until the material breaks completely. Let us assume that a crack is stabilized but the material continues being subjected to loads. In fracture mechanics, three different types of cracks can be considered, depending on the mode of the load applied. In Figure 4.2, the three modes are represented. Crack Mode-I, also called opening mode, is the one that is loaded with a stress perpendicular to the propagation of the crack, but in the same plane as the crack. Mode-II, are between two surfaces that are loaded with forces parallel to the crack in plane in such a way that they slide on each other. Finally, in Mode-III, tearing mode, cracks are loaded with shear forces in a direction out of the crack plane.

Let us consider a Mode-I crack to determine the stress around the tip of the

crack. Mode-I cracks are the simplest to study. The goal of this exercise is to determine the order of magnitude of the forces acting around the tip of the crack, the deformations created around the tip and the gradients of such deformations.

From the analytical 'near field' solutions of the stress around a crack in a plane, developed by Irwin in 1958[105] in polar coordinates, we have

$$\begin{Bmatrix} \sigma_{xx} \\ \sigma_{yy} \\ \sigma_{xy} \end{Bmatrix} = \frac{K_I}{(2\pi r)^{1/2}} \begin{Bmatrix} \cos(\theta/2)[1 - \sin(\theta/2)\sin(3\theta/2)] \\ \cos(\theta/2)[1 + \sin(\theta/2)\sin(3\theta/2)] \\ \sin(\theta/2)\cos(\theta/2)\cos(3\theta/2) \end{Bmatrix}, \tag{4.1}$$

where K_I is the stress intensity factor of the material. A value of 3 $MPam^{-1/2}$ which was selected as the critical intensity factor for bone[25]. For higher values of K_I, a crack in a bone should continue growing.

By using the stress, it is possible to calculate the strain around the crack with:

$$S_{ij}^{el} = \frac{1+\nu}{Y}\sigma_{ij} - 3\frac{\nu}{Y}\sigma_m\delta_{ij}, \tag{4.2}$$

where ν is Poisson's ratio, Y is the Young's modulus, $\sigma_m = \frac{\sigma_{xx}+\sigma_{yy}+\sigma_{zz}}{3}$ is the average stress and δ_{ij} is Kronecker's delta. After substituting Equation 4.3 in Equation 4.2, the strain in each direction for polar coordinates are:

$$\begin{Bmatrix} S_{xx} \\ S_{yy} \\ S_{xy} \end{Bmatrix} = \begin{Bmatrix} \frac{K_I}{Y_{xx}(2\pi r)^{1/2}} \cos(\theta/2)[1 - \nu - \sin(\theta/2)\sin(3\theta/2)(1+\nu)] \\ \frac{K_I}{Y_{yy}(2\pi r)^{1/2}} \cos(\theta/2)[1 + \nu - \sin(\theta/2)\sin(3\theta/2)(1+\nu)] \\ \frac{K_I}{Y_{xy}(2\pi r)^{1/2}} \frac{1+\nu}{E_{xy}} \sin(\theta/2)\cos(\theta/2)\cos(3\theta/2) \end{Bmatrix}. \tag{4.3}$$

4.1.2 Flexoelectric fields around cracks

Once the strain of the material around the crack is obtained (Figure 4.3(a)), it is possible to obtain the strain gradient, which is what generates the flexoelectric field (see Figures 4.3(b) and 4.3(c)). All these calculations were made in Wolfram Mathematica and the code is shown in the appendix section B.1.

For the calculations $Y_{xx} = 6\ GPa$ and $Y_{yy} = 20\ GPa$, both values were obtained from our measurements in bones. Equations were transformed to Cartesians coordinates in order to compute the flexoelectric field:

$$\begin{Bmatrix} E_1 \\ E_2 \end{Bmatrix} = \begin{Bmatrix} f_{11}\frac{\partial S_{xx}}{\partial x} + f_{xy}\frac{\partial S_{yy}}{\partial x} \\ f_{22}\frac{\partial S_{yy}}{\partial y} + f_{yx}\frac{\partial S_{xx}}{\partial y} \end{Bmatrix}, \tag{4.4}$$

and the magnitude of the flexoelectric field is

$$E = \sqrt{E_1^2 + E_2^2}, \tag{4.5}$$

with f_{ij} as the flexocoupling tensor. The flexocoupling tensor was calculated with the effective flexoelectric coefficient μ_{eff} and the dielectric constant of bone ϵ

$$\mu_{eff} = f_{eff}\epsilon. \tag{4.6}$$

For the calculation in bones, $f_{xx} = f_{yy} = f_{xy} = f_{yx} = f_{eff} = 10\ V$ and the shear component was taken as null. We used $10\ V$ as a general case since we measured several samples and all the flexocoupling values ranged from $9.3\ V$ to $11.8\ V$. The same happened with the dielectric constant, in that all the samples showed different values ranging from 10 to 15.

As can be seen in Figure 4.4, the flexoelectric field is biggest at the crack tip and decays progressively away. As seen in both Figures 4.3 and 4.4, just in front of the tip of the crack, the magnitudes of the fields are enormous, in fact in the idealized mathematical model, the value goes to infinity at the crack tip in real life, of course, this cannot be the case, as the atomic junction is atomically sharp but not infinitely small, plus non-linear effects must also intervene to prevent non-physical divergences.

4.2 Effects of electric fields on cells

The presence of such big electic fields inside the body affects cells in tissues. This topic has been extensively studied in the last two centuries[40], since the discovery of intrinsic electric fields in tissues[106]. Electric fields inside the body have been demonstrated to affect cell growth, wound healing and even the menstrual cycle[40, 107]. And, of course, the nervous impulses that connect our brain to the rest of our organs are electrical signals. This evidence has also encouraged the scientific community to carry out studies on the regeneration process of tissues using extrinsic electric fields with bone as one of the most studied tissues[37, 40, 106, 108–110].

The consequences of electricity on cells may vary depending on the strength, duration and mode of the electric (or electromagnetic[108, 111]) stimulation[106]. The basic effects of an electric field on a cell can be described if we consider a cell as a conductive body (cytoplasm) with a dielectric layer (membrane) around it. One of the most consistent and studied effects of electrical stimulation in cells is the increase

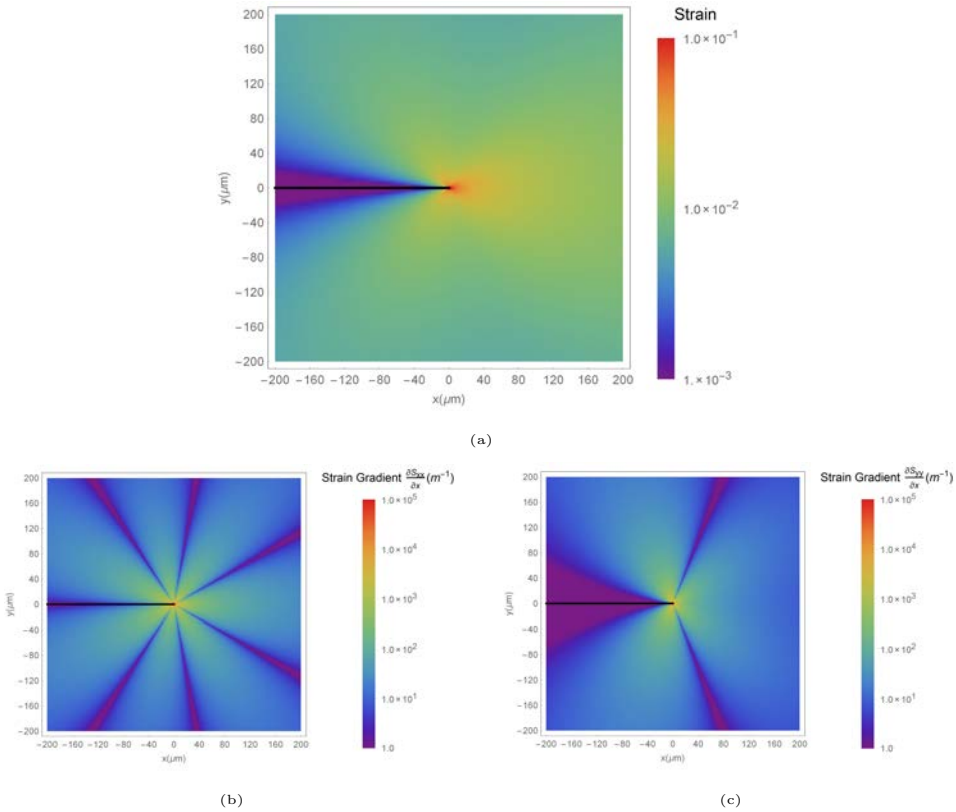

(a)

(b)

(c)

Figure 4.3: *(a) Due to the accumulation of stress around the tip of the crack, large deformations are induced in bone. Strain Gradients in the (b) longitudinal direction of the crack and (c) transverse direction of the crack.*

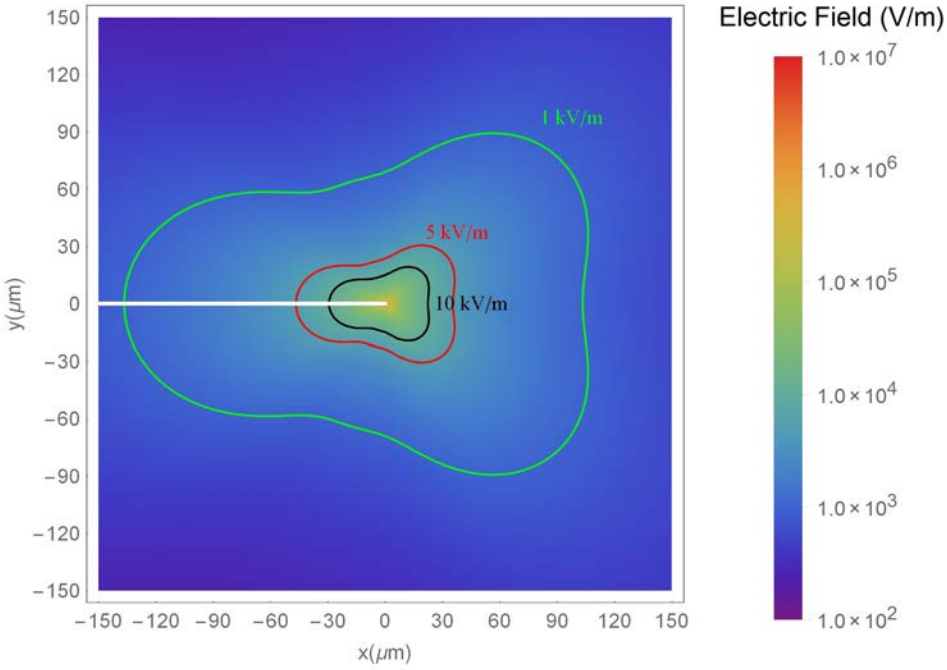

Figure 4.4: *Flexoelectric field around a microcrack in bone, and cytologically critical isoelectric lines. The green line defines the outermost region beyond which where the flexoelectric fields are weak enough not to damage the cells but intense enough to stimulate them, red line defines the intermediate regime where apoptosis is expected and the black line defines the region where cells are being directly killed by the intensity of the field.*

of intracellular calcium ion concentration[106] by different mechanisms[106, 112]. Such concentrations are important because calcium signaling affects the properties of cells during life[113] and controls apoptosis of cells, that is, the controlled death of cells [114].

Depending on the strength of a direct current (DC) electric field, different mechanisms can cause the influx of Ca^{+2} and increase its concentration inside the cell. In osteoblasts, Ca^{+2} concentration alters the process of the parathyroid hormone (PTH), which is responsible for bone resorption and when the PTH pathaway is affected, bone formation is promoted[40, 115]. Capacitive-pulse electrical stimulation is also able to promote bone generation in the same manner as in DC, although it has been demonstrated that it is dependent on the frequency of the applied pulses[40, 109].

New treatments are also being developed in order to produce apoptosis of osteosarcoma with high pulsed electric fields. Nanopulsed electric fields increase the membrane permeability without producing electroporation and this process starts the apoptosis of cells[112]. In addition, this technique minimizes Joule heating and shows no hyperthermic effects in other cells as happens with radiotherapy[116].

Finally, low frequency electric fields have also been shown to have the capacity to promote osteogenesis or apoptosis of osteoblasts when cells are exposed to electrical stimulus[117]. McCullen et al. found that the promotion of osteogenesis of human adipose-derived stem cells (hASCs) was improved without risk of damage by using electric fields in the range of 100-1000 Vm^{-1} with frequencies lower than 15 Hz. They observed detachment of cells and direct membrane breakdown with fields of 10-100 kVm^{-1}. Taking these values into account, they concluded that cells can be compromised with electric fields higher than 1 kVm^{-1} and the direct death of cells (necrosis) was observed above 10 kVm^{-1} at low frequencies. From these findings, we estimate an intermediate value: 5 kVm^{-1} for cell apoptosis. The study of McCullen et al. is relevant for the present research because low frequency (flexo)electric fields are expected to appear in bones under cyclic efforts such as walking, breading, chewing, etc. The critical electric field measured by McCullen have therefore been marked as isoelectric lines in the calculation of the flexoelectricity generated by a loaded crack (Figure 4.4).

The overlapping of the known cytologically-critical electric field onto the theoretical calculation of the crack-induced flexoelectric field show that the magnitudes and distances involved are cytologically relevant. The “electrically safe” limit of 1 kVm^{-1} is located at a distance of approximately 100 μm around the crack

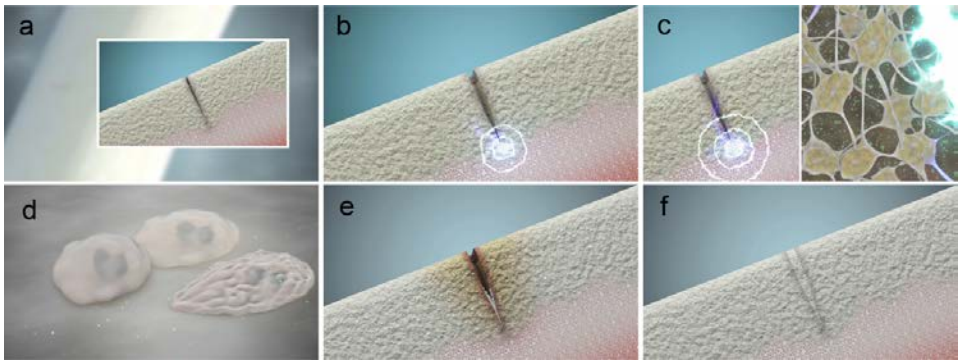

Figure 4.5: *(a)Microcracks can appear due to continues loading in our bones. (b) At the tips of the cracks flexoelectric fields are generated due to the strain gradients. (c) The electric fields induce apoptosis of osteocytes, liberating proteins. (d) Proteins recruit osteoclasts to do the resorption of the damage tissue. (e) and (f) Finally, osteoclasts recruit osteoblasts that are responsible for the formation of new bone.*

apex. Cells located within this radius are liable to suffer flexoelectric-induced apoptosis. Apoptosis of osteocytes is important because it is the first step of bone regeneration[45, 103]; when dead, osteocytes release chemical triggers that, as discussed in the introduction, signal the osteoclasts to initiate the repair of bone by cleaning the damaged region, followed by osteoblasts that segregate new bone mineral[25, 45, 103]. Electric fields also attract screening ions which create electrochemical gradients that assist osteogenesis[97, 118], further increasing the velocity of reparation of the damaged region[37]. The process we propose to start the regeneration of bone can be seen in Figure 4.5.

In previous chapters we demonstrated that piezoelectricity is able to mimic flexoelectricity. Therefore, we can consider a piezoelectric constant and calculate the electric field generated in bone for the extreme case of the crack due to stress around the crack(Figure 4.6). The maximum piezoelectric field is located in front of the crack where the maximum stress is accumulated. Nevertheless, the magnitude of such electric field is minimum in comparison with the flexoelectric field generated in the same range as it can be seen by comparing Figure 4.6 (piezoelectric field) and Figure 4.4 (flexoelectric field). Therefore, the importance of flexoelectricity is at small scales where the strain gradients are large and, the effect of piezoelectricity cannot imitate the enormous flexoelectric fields generated near the tip of a crack.

Osteoblasts are known to be attracted to the tip of cracks in pure bone mineral[97], suggesting that osteoblasts do indeed detect a crack tip as the centre

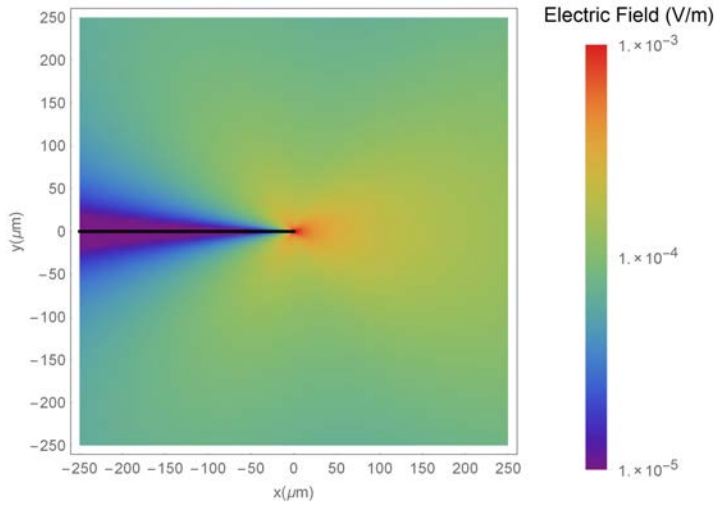

Figure 4.6: *Piezoelectric field around a crack tip due to the stress gradient.*

of damage. Furthermore, the apex is itself a movable entity: as the crack is healed, its apex will recede, continually pointing the osteoclasts and osteoblasts to the new position of the region to repair[45]. As the calculation shows, flexoelectricity is theoretically strong enough to act as the beacon in this process. The next obvious step is to see whether the theoretical prediction agrees with reality, i.e. to examine how cell cultures react to flexoelectric fields around cracks. To this end, experiments with cells are developed and analyzed in the following chapter.

CHAPTER 5

Cytological investigation of the flexoelectric effects of bone cracks

The main goal of this chapter of the thesis is to determine whether, according to the calculations made around the crack in the last section, flexoelectric fields do indeed have physiological roles in bones.

First, the survival of the osteocytes exposed to crack generation (see section 5.1.3) was evaluated. However, because the generation of a crack also includes a mechanical shock wave (associated with the release of stress upon cracking), it is important to separate the flexoelectric effect from the purely mechanical impact of the cracking event. In order to do so, a second series of experiments were performed on pre-cracked samples, i.e. where the cracks were made before cells were cultured on their surface samples. These samples were then mechanically stimulated (see section 5.1.2) by bending, so as to put a periodic mechanical load on the cracks in order to make them generate low-frequency flexoelectric fields.

The effects examined were (i) whether crack-generated strain gradients are able to induce apoptosis of cells in the inmediate vecinity of the crack and (ii) whether flexoelectric fields could also stimulate cells for the production of collagen and bone mineral.

5.1 Experiments description

5.1.1 Cell cultures

MC3T3-E1 mouse osteoblastic cells (ECACC General Cell Collection) were seeded in the different substrates..Experiments were performed on both osteoblasts and osteocytes, and the osteocytes were chosen mainly because the density of the cells was bigger than osteoblasts. Cell maturation to osteocytes was performed over 10-15 days[i] Details, of the cultivation process can be seen in appendix A.4.1.

Cell viability was analysed by Live/Dead staining before and after cracking in hydorxyapatite substrates by observing the samples in a fluorescence optical microscope (Zeiss Axio Observer). Live/death assays are able to show in green when the cytoplasm is healthy (live cells) and in red when the nucleous collapses (dead cells). A description of the commercial live dead assay can be found in the appendix A.4.2.

5.1.2 Single cantilever portable system

Once the cells were cultured on the samples with cracks, they were electromechanically stimulated. A clamped cantilever system with a piezoelectric actuator was designed in such a way that one end of the sample was clamped while the other end was pushed periodically by the piezoelectric actuator. In this way, a mechanical stress was applied to the cracked sample, thus causing accumulation of stress around the tip of the crack, thereby generating an alternating flexoelectric field. Such a design had to meet certain practical requirements. For example it should be small enough to fit inside the culture chamber, and it should be able to operate at small frequencies with a variety of displacements. Figure 5.1 shows the design and final custom-made device used for these experiments.

5.1.3 Crack generator

Samples with cells were cracked by using the system shown in Figure 5.2. The system is a three point bending system with a sharp knife driven by a micrometer screw. The load is applied parallel to the width of the sample. The system was designed for samples of different thicknesses, lengths and widths. Common dimensions of the samples were 12x6x1 mm.

[i]The culture, manipulation and evaluation of the experiments with cells ware made with the support of Dr. Raquel Nuñez, a postdoctoral biologist specialized in the culture of osteogenic cells.

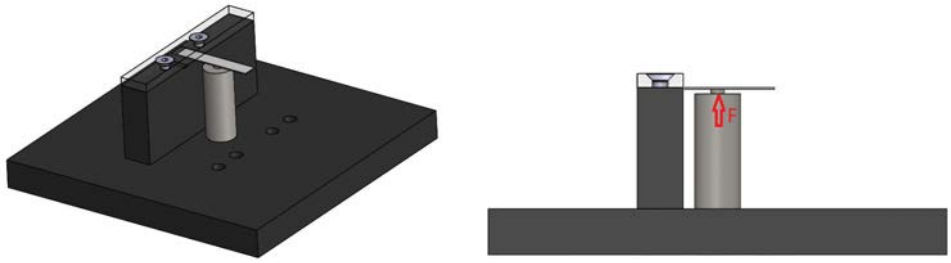

(a) (b)

Figure 5.1: *Schemes of the portable bending system used to stimulate the samples.*

(a) (b)

Figure 5.2: *Pictures of the crack generator. It is a three point bending system designed specifically to create cracks in samples with cells on them.*

5.2 Results

5.2.1 Effect of crack generation on cells

Figure 5.3(a) shows that cells (osteocytes) attached well to the surface, and no dead cells were detected before cracking. However, immediately after crack generation (Figure 5.3(b)), the around the crack died. Dead cells were detected up to 200 µm from the crack; further away, the rest of the osteocytes withstood the mechanical impact without apparent damage. In this case, cell apoptosis could occur due to a combination of both flexoelectric field generated around the crack and the mechanical shock of creating the fracture, as could happen when a bone fractures. For this reason, we also studied the effect of pure flexoelectricity on pre-cracked samples.

5.2.2 Flexoelectric effects on cells around microcracks

Once confirmed cellular apoptosis during crack formation, the effect of flexoelectricity in the cellular response was studied. To separate the flexoelectric effect from the mechanical effect, cells were cultured in hydroxiapatite pre-cracked substrates and analyzed before and after 2,5 minutes of bending at a frequency of 5 Hz. In this way, there is no mechanical shock to the system (the crack was formed before the cells were cultured). In addition, for this experiment we cultured osteoblasts and osteocytes in different samples in order to determine the effect of flexoelectricity the different types of cells. The first difference among these two cases is that osteocytes formed a much denser layer of cells than osteoblasts because, in order to differentiate osteoblasts until they become osteocytes, they were cultured during 10 days, allowing higher cell reproductions. Meanwhile osteoblasts were cultured in general for 3-4 days, therefore the cell density is lower for osteoblasts.

By Live/Dead staining, it was observed that in both cell types there was cellular death around the crack. However, the mortality was higher in samples with osteocytes (Figure 5.4). In addition, in the samples with osteoblasts, there were only dead cells adjacent to the tip of the crack, as can be seen in Figure 5.4(a). Meanwhile in the samples with osteocytes the density of death cells was highest near the tip of the crack, but extended further afield as is shown in Figure 5.4(b).

The cell viability in osteocytes after crack bending was quantified and compared to cell viability in samples without any cracks. Results show that 80% of the cells were viable after bending in the absence of a crack, whereas there was a significant

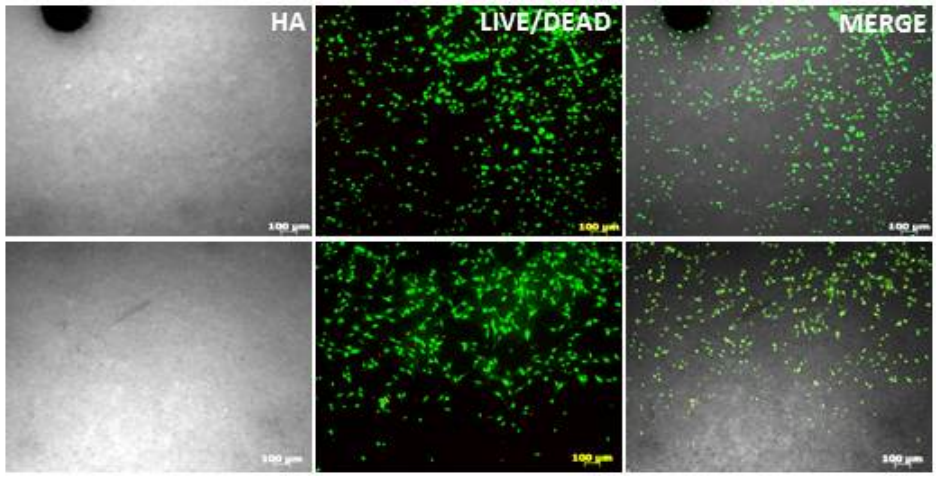

(a)

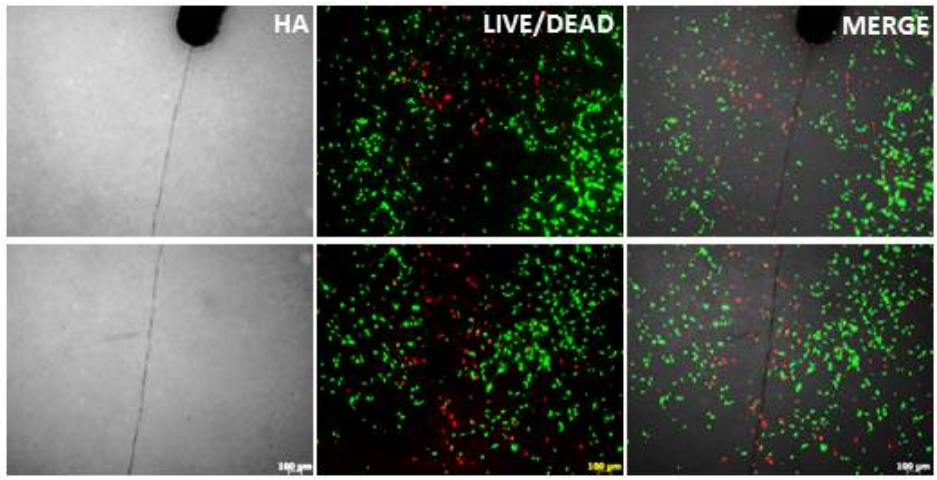

(b)

Figure 5.3: *Effects of crack generation on osteoblast and osteocytes. The sample was inspected (a) before and (b) after the sample was fractured.*

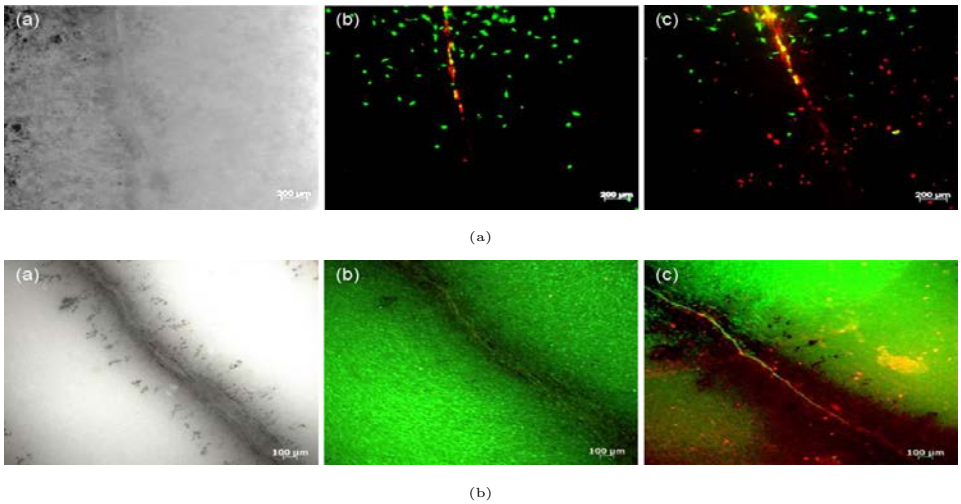

Figure 5.4: *Effects of mechanical stimulus on cracks with (a) osteoblast and (b) osteocytes. Samples were inspected before and after the samples were stimulated.*

decrease in cell viability, to only 50%, after bending in cracked samples. These results were averaged over the whole sample surface so they underestimate the effect of the cracks which only occupy a small portion of the sample. The microscopy results show that, in fact, the cell survival rate near the crack is essentially 0% for osteocytes.

Apoptosis progression in osteocytes after bending was detected by Caspase 3/7 staining (Figure 5.6). This staining uses a fluorogenic peptide that binds to the caspasa-3/7, a protein present in apoptotic cells[119]. The staining visually indicates

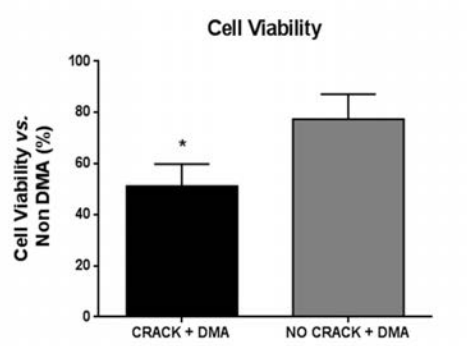

Figure 5.5: *Viabilty of osteocytes on pre-cracked samples and samples without crack.*

the first stages of the apoptosis in cells. In Figure 5.6(c), it can be seen that the maximum levels of apoptosis (green colors) were detected from the middle to the tip of the crack. In contrast, at the crack base and in the clamp area, where there is less flexoelectricity, the cell viability was higher.

Furthermore, we can see in the top part of Figures 5.6, that almost no cells were affected when there was no crack, except a few cells stained green (red arrows).

By checking the bright field image, it seemed that the apoptotic cells coincided with different voids in the sample, but the nature of these voids was not confirmed (Figure 5.6(a)).

However, there remains a puzzling question when comparing the hydroxypatite results with calculations made for bone. In the calculations (Figure 4.4), the expected critical radius to induce apoptosis is smaller than 50 μm; in contrast, in the experiments we observe cells dying at distances as far as 300 μm, even in the pre-cracked samples (so, their death was not caused by mechanical shock). Some of the differences may be due to the simplifying assumptions made in the theoretical model. First, the equations used for the strain around the crack assumed a perfect Mode-I loading system[105], when in reality there are likely to be more components to stress. In addition, the calculation is only for the electric internal field inside the hydroxyapatite, not taking into account the stray field at the surface, the intensity of which depends on the (unknown) dielectric constant of the medium. However, we believe that the most important difference is that the hydroxyapatite samples do not have one single crack: as shown in high resolution scanning electron microscopy images (Figure 5.7), around the main crack there are flaws and small subsidiary cracks that have the effect of enlarging the area of influence of the main crack.

To verify this explanation, experiments were repeated on a TiO_2 single crystal that had similar mechanoelectric properties to hydroxyapatite but, being a single crystal, had almost no defects and thus cracked cleanly. First, the flexoelectric field around a crack was calculated and compared for pure hydroxyapatite and TiO_2. Although the Young's modulus of TiO_2 is higher than hydroxyapatite (and thus it bends less), the higher flexocoupling coefficient compensates for this difference and the final calculations of the flexoelectric field around a crack are very similar, as can be seen in Figures 5.8(a) and 5.8(b). A field of 1 kVm^{-1} was obtained at distances in the micrometer range from the tip of the crack.

For calculations (appendix B), the Young's modulus used for TiO_2 was 230 GPa[120], the critical intensity factor 2.4 $MPam^{-1/2}$ and the flexocoupling value was 4 V. Meanwhile, Young's modulus for hydroxyapatite was 80 GPa, the critical

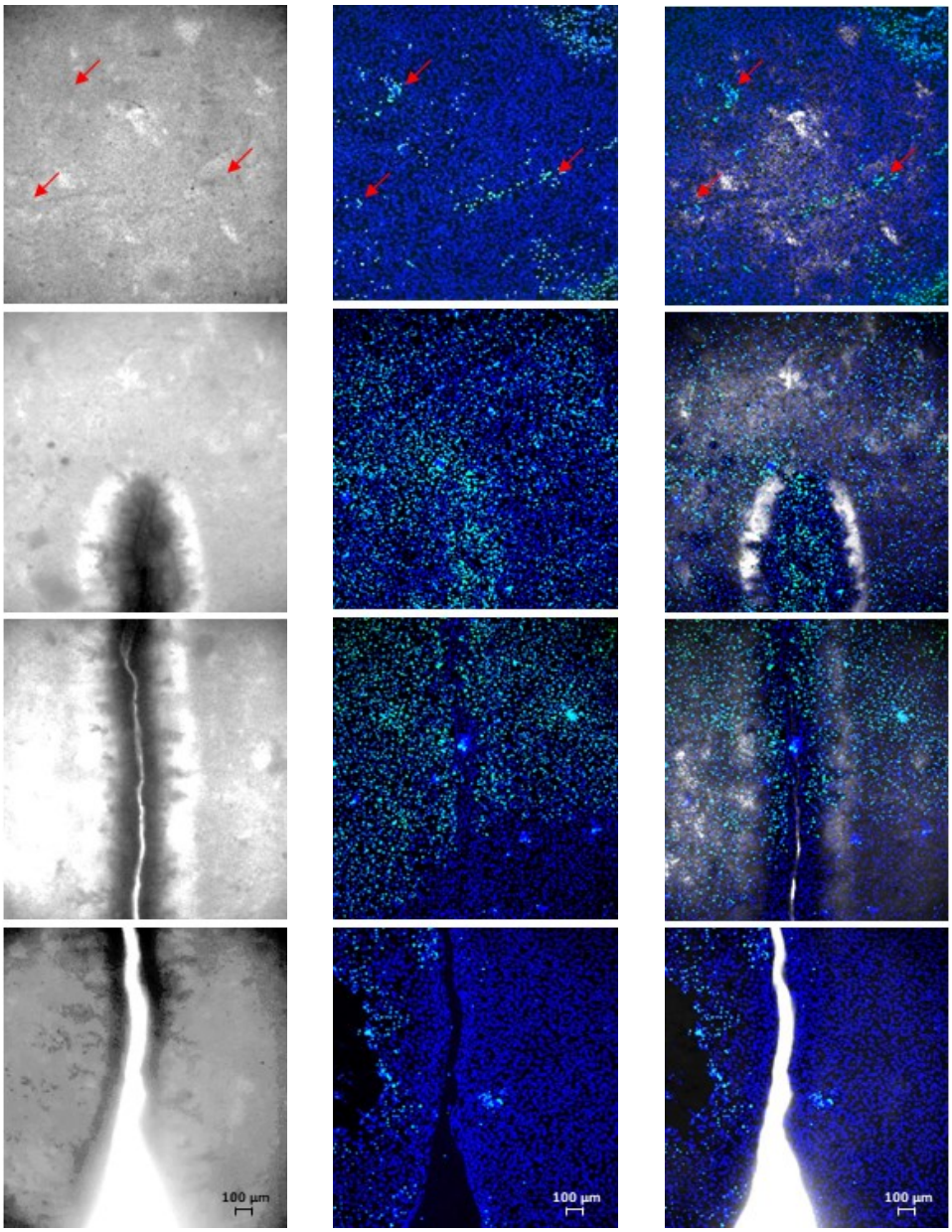

(a) (b) (c)

Figure 5.6: *Apoptosis progression of osteocytes inmediatly after the mechanical stimulus on cracks with caspasa. (a) Brigthfield image of the surface and crack in the sample. (b) Fluorescent image of the cells. (c) Merge of the bright field image and fluorescent image. Blue dots are the nuclei of cells, in green the caspase staining showing the cells that are starting to die. Samples were inspected before and after they were stimulated.*

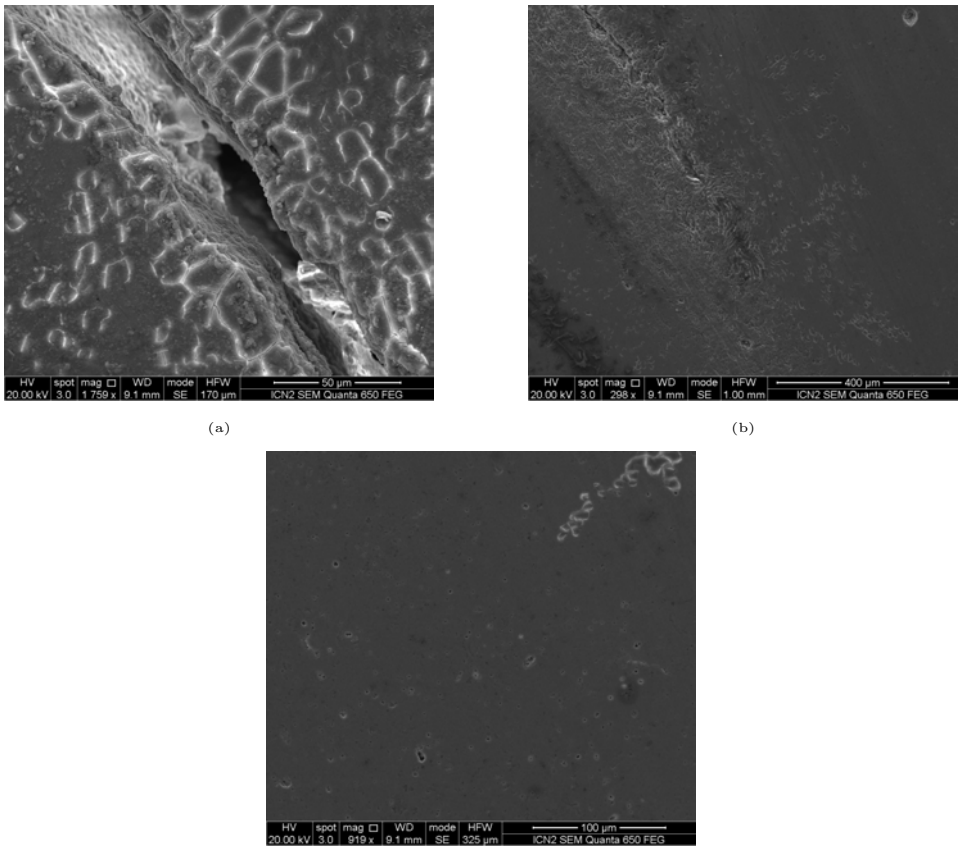

(a) (b)

(c)

Figure 5.7: *Scanning electron microscopy of hydroxyapatite samples (a) around an induced cracks, (b) near the tip of the crack and (c) when there are not cracks. Around the main crack several flaws can be observed, these can be contributing as centers of strain and increasing the influenced area of the flexoelectric field.*

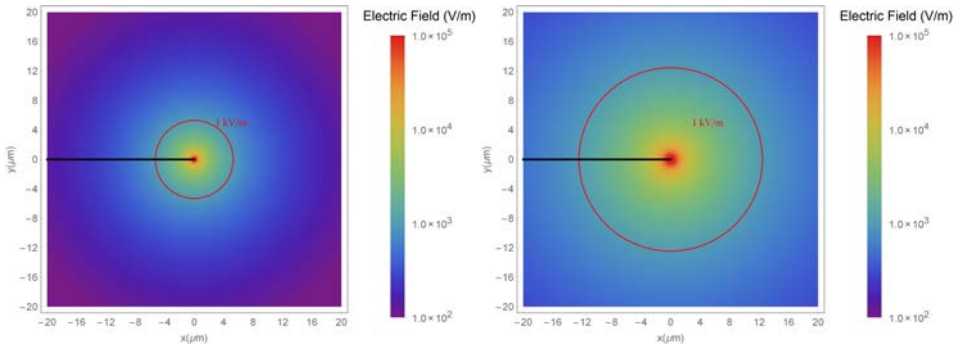

(a) (b)

Figure 5.8: *Calculation of the flexoelectric field around a crack in (a)TiO_2, (b) hydroxyapatite.*

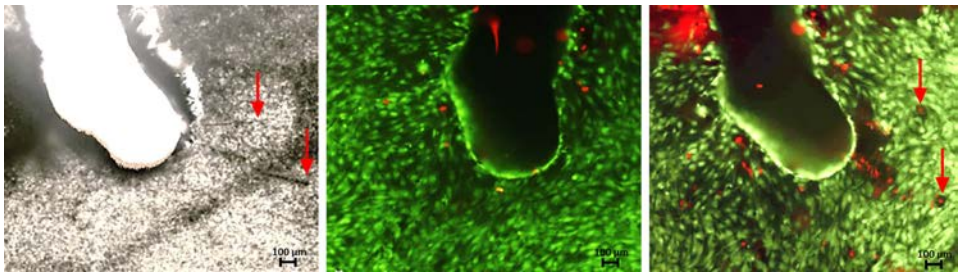

Figure 5.9: *Effects of mechanical stimulus on cracks with osteocytes in TiO_2. From left to right are the bright field, fluorescent image before the stimulation and fluorescence image after stimulation. Red arrows indicate the end of the crack.*

intensity factor was 1 $MPam^{-1/2}$[23] and had a flexocoupling coefficient of $\sim 11\ V$.

Osteocytes were cultured on precracked TiO_2 samples and analyzed before and after 2,5 min of bending as was done preivously with hydroxyapatite. Here, while most of the cells survived, cellular apoptosis was also observed mainly around the crack and only up to very small distances, in accordance with Figure 5.9. The results, show much fewer dead cells in TiO_2 samples, as we hypothesized, because the TiO_2 sample, being monocrystalline has sharper and cleaner cracks, plus its higher dielectric constant means that the flexoelectric field is screened within a shorter distance. In fact, the only region where cells died in TiO_2 were adjacent to the small cracks generated and/or near the notch, where concentrations of strains are larger.

5.2.3 Flexoelectro stimulation of cells

Beside cell death, it is known that weaker electric fields (weaker than those that cause apoptosi) can electrostimulate the repair activity (e.g. mineralization) of bone cells [106, 110]. In order to determine the influence of crack-generated flexoelectricity on bone remodelling, cells were cultured on microcracked hydroxyapatite under osteogenic medium conditions for 15 days. The samples were bent at day 3 of differentiation following the same protocol as before: 2,5 minutes at 5 Hz in the cantilever bending system. The osteoblasts' mineralization on microcracked hydroxyapatite with and without bending was imaged 15 days post-seeding.

Figure 5.10 shows the mineralization in two regions of the same sample, one with crack and another without after 15 days when the sample was not mechanically stimulated. The Figure shows that there is a weak mineralization preferably located following the crack orientation. This is unlikely to be due to flexoelectrcity, because if the crack is not subjected to a mechanical load it cannot generate an electric field. Instead the most likely explanation is that there are higher concentrations of Ca^{+2} ions around cracks due to mineral debris released by the crack itself[97]. Osteoblasts (during the first days of cultivation) will thus seed mainly around the crack and their maturation in those regions will occur first and their mineralization activity will be higher, both things, being a direct consequence of the higher availability of calcium ions.

However, the results of mineralization when the crack was mechanically stimulated (Figure 5.11) show much higher mineralization (red tint) than without the stimulus with similar cell viability. Meanwhile, in the same Figure it is shown that when there are no cracks the mineralization is much weaker. It is thus the combination of structural defects (cracks) plus mechanical loading that favours bone remodelling. Absence of either results in weaker mineralization.

Furthermore, the effect of microcrack bending were examined on a typical osteogenic genetic markers, osteocalcin (OC) at 15 days of osteogenic differentiation by quantitative real time polimerase chain reaction (qRT-PCR) (Figure 5.12). The results demonstrated differences in OC levels between bent and non-bent cracked samples. Specifically, cells on bent cracked surfaces showed greater mRNA levels of OC.

Finally, the protein expression of COL1, the major organic component of bone extracellular matrix, was evaluated by immunofluorescence analysis (Figure 5.13). Results showed that the amount of COL1 was greater around the microcrack in the

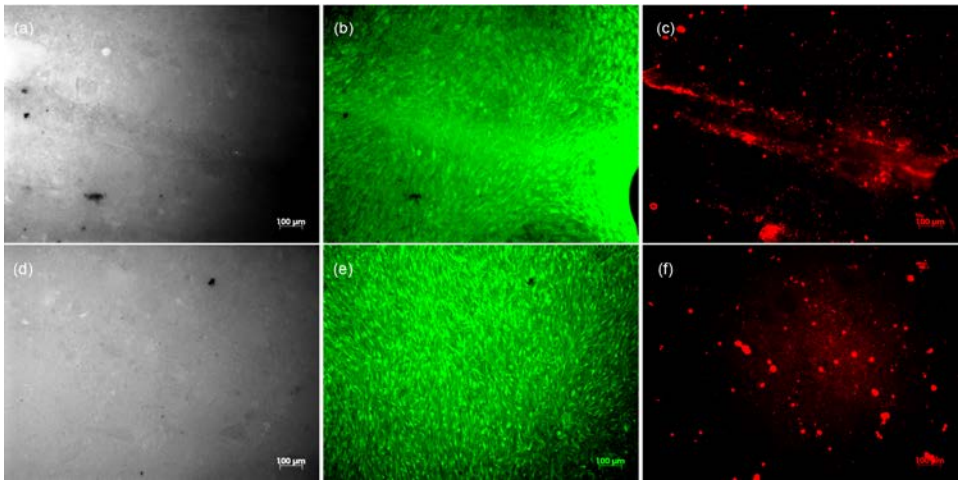

Figure 5.10: *Mineralization in samples with cracks and without cracks when no stimulus was applied to the sample. First two lines show samples with cracks on the surfaces and the las line shows a region without crack. The first column are the images of the surfaces, the second column shows the cell viability and the last column shows in red the mineralization.*

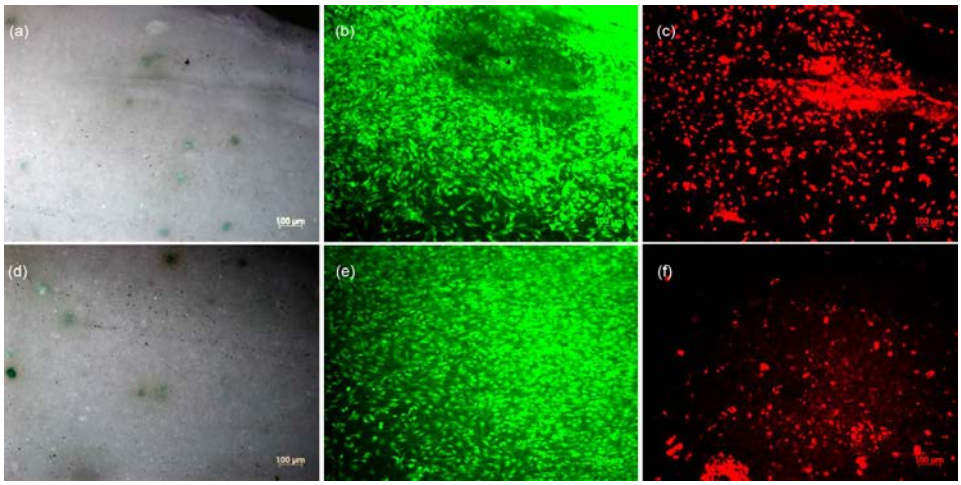

Figure 5.11: *Mineralization in samples with cracks and without cracks when a stimulus was applied to the samples. First two lines show samples with cracks on the surfaces and the last line shows a region without crack. The first column are the images of the surfaces, the second column shows the cell viability and the last column shows in red the mineralization.*

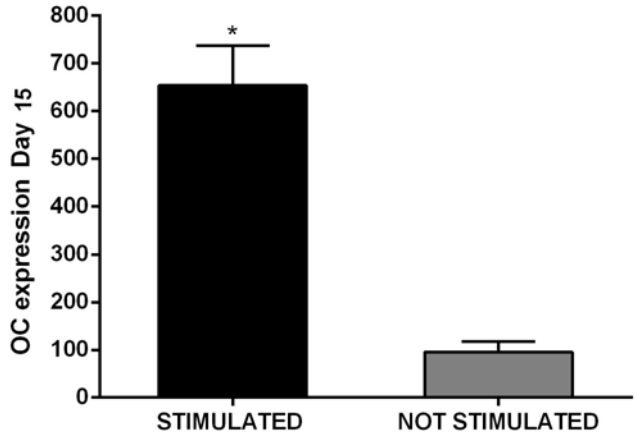

Figure 5.12: *PCR quantification of osteocalcin protein in stimulated samples. The stimulation was done on the third day of cultivation and the levels of OC were measured on day 15. Quantification were normalized with OC gene expression at day 0 and with respect the housekeeping gen: GAPDH.*

bent samples. In addition, while in the base of the tip COL1 was still predominantly located intracellularly around the nucleus of the cells, near the microcrack tip it was secreted into extracellular matrix, showing an advanced stage of differentiation, i.e. osteocytes are already making bone tissue.

Taken together, these results suggest the following effects of flexoelectricity and bone remodellig:

1. Mechanical loading of a crack causes it to generate a flexoelectric field that induces osteocytes apoptosis in the immediate vicinity of the fracture. The chemicals released by dead osteocytes are known to act as the trigger for the initiation of osteoclastic repair activity. The first role of flexoelectricity is thus as a signaling mechanism to trigger the process of remodeling.

2. In microcracks and under long-term culture conditions, flexoelectricity promotes osteoblastic maturation and mineralization around the microcracks, thus acting as an electro-stimulating mechanism to accelerate the reconstruction of the damaged area.

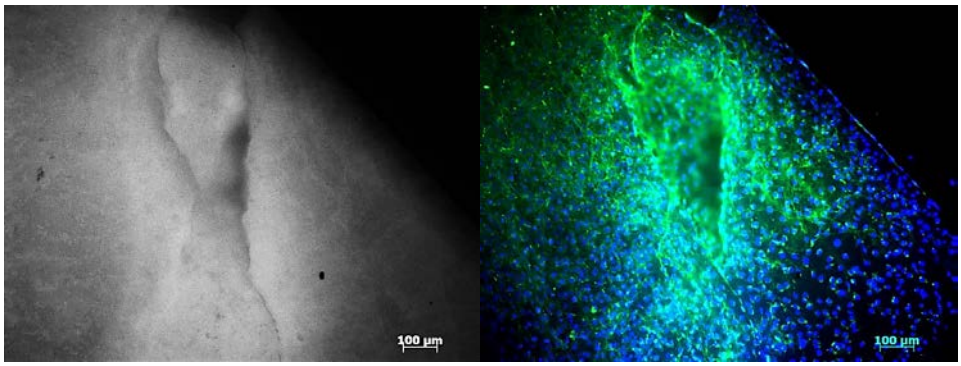

(a) (b)

Figure 5.13: *Fluorescence figure of collagen expression of cells around a crack. (a) Image of the surface with the crack and (b) the fluorescence image where collagen expression can be seen in green, blue spots show the nucleous of cells. Cells far from the crack do not show extracellular collagen expression.*

CHAPTER 6

Flexoelectricity of other biomaterials

An interesting question in the development of natural biomaterials is how different species developed the same solutions to solve similar problems in completely different circumstances, in biology, this is known as "evolutionary convergence".

For example, the structure of bone has many similarities with the structure of bamboo, despite their completely different evolutionary path. Specifically, bone forms tubular structures called osteons and in a very similar way, bamboo also organizes the tissue in layers forming a honeycomb-like cells lattice of circular channels (Figure 6.1) [23]. In both cases, there is also a gradient of porosity, with the outer layers being more compact and the inner layers more porous, with the centre being hollow.

Such hierarchical architectures are in fact common to many species[23, 47, 55–57]. The main reason they developed was because such architectures help to increase flexural rigidity, and also help deflect and stabilize cracks thus increasing the fracture toughness of the whole tissue[23]. A consequence of these architectures is that, being structurally inhomogeneous, they necessarily cause gradients and thus favour flexoelectricity.

In the previous chapters we analyzed bone tissue, an essential hard tissue for vertebrates, performing structural and support functions with outstanding performance and healing capacity which, as shown in this thesis, is assisted by flexoelectricity. In nature, however, there are many other examples of hard tissues with similar characteristics. In this chapter, the flexoelectricity of three natural ceramics is studied as a starting point for further research into the participation of flexoelectricity in physiological processes.

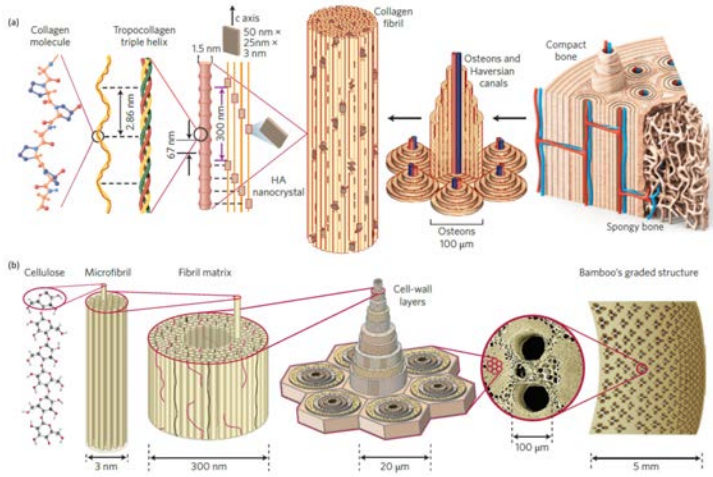

Figure 6.1: *(a) Structure of bone from the nanoscale, where the common building block is collagen and hydroxyapatite to the microscale where osteons formed the compact bone with the Harvesians canals. (b) Analogously bamboo has a hierarchical structure composed by cellulose fribres that form a complex matrix in a honeycomb-like cells. Taken from [23]*

6.1 Teeth

Teeth share with bones the common building elements of hydroxyapatite and collagen[25]. For human beings and other mammals, teeth also contain the hardest material in the body: enamel. Enamel is made of highly crystalline hydroxyapatite which constitutes 97% of its weight. This characteristic motivated the study of flexoelectricity in enamel, because, due to its nearly complete lack of piezoelectric collagen, in principle, enamel should behave very similar to the hydroxyapatite ceramics. In addition, teeth also have a hierarchical structure with gradients of Young's modulus that prevents cracking of the brittle enamel, thanks to the dentin enamel junction (DEJ), where there is an important increase of collagen to absorb mechanical energy[23]. The presence of built-in elasticity gradients in teeth should in principle lead to flexoelectric effects during mastication.

6.1.1 Flexoelectricity of enamel

The enamel samples were examined in order to compare them with the ceramics prepared for the study in Chapter 3 of this thesis. To this end, cow teeth were obtained directly from a slaughter house and were cut and polished in the shape of beams for measurements in the DMA, with the same process used for bones and hydroxyapatite explained in Appendix A. Special care was taken to avoid dentin in the samples so as to minimize the presence of organic material that could induce piezoelectric polarization.

For these measurements, we tried to calculate the flexoelectric coefficient by measuring the polarization as a function of the strain gradient, as we did for hydroxyapatite in Figure 3.4. However, since enamel without dentin is very brittle, high deformations broke the samples, whereas very small deformations did not give a stable signal for reliable measurement using the lock-in amplifier. As a compromise, all the measurements of enamel were done with a vertical displacement of 3 micrometers, which did not break the samples but was still enough to yield a measurable signal. The effective flexoelectric coefficient μ_{eff} was calculated directly from Equations A.1 and A.2.

Figure 6.2, shows the flexoelectric coefficient at different frequencies of stimulus. There was a small decrease in the coefficient as the frequency of the stimulating force was increased; we speculate that at the lowest frequencies there is probably some participation from ionic charge transport that is absent at higher frequencies. The results were, nevertheless, almost the same as those of hydroxyapatite in Chapter 3

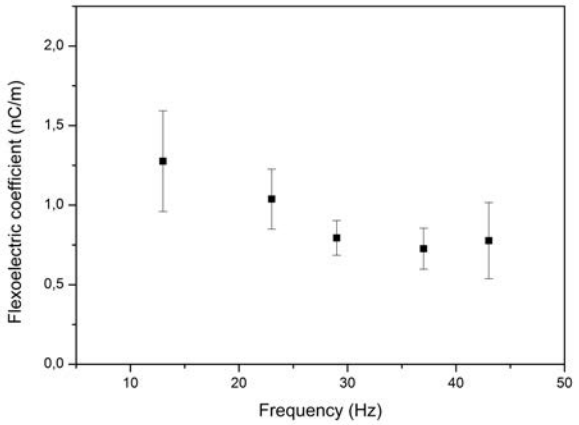

Figure 6.2: *Flexoelectric coeffiecient of teeth for different frequencies. Side one and side two were selected arbitrarily and the sample was rotated to see if there were any important changes.*

which varied from 0.7 to 1.6 nCm^{-1}. For enamel, the flexoelectric coefficient was from 0.6 to 1.5 nCm^{-1} at 13 Hz, the same frequency used to measure hydroxyapatite.

However, for enamel, the flexoelectric fields with flexoelectricity are unlikely to be sensed by any cell as happens in bone, since there are no cells on the surface of the teeth[25]. Teeth do not have the same regenerative properties as bone, although there is evidence of proteins attaching to certain sites of enamel when a crack appears in order to "bridge" the crack and bring together both surfaces[121]. We speculate that perhaps stress concentrations 'indicate' the attaching position for proteins, but direct testing of this hypothesis is outside of the scope of this thesis. On the other hand, it is possible that polarization occurs not just in enamel but also across the whole tooth, including the DEJ, especially because of the mechanical differences between the dentin and enamel[25, 122].

6.1.2 Flexoelectricity of the DEJ

As shown in the theory section 2.2, if there are differences in the elastic constant along a material, stress will induce strain gradient and thus flexoelectric polarization. Teeth are formed by two different tissues with important differences in the crystallinity and elastic constant. As we go from the surface of the tooth, made completely of enamel, to the dentin that has a higher organic content, we see

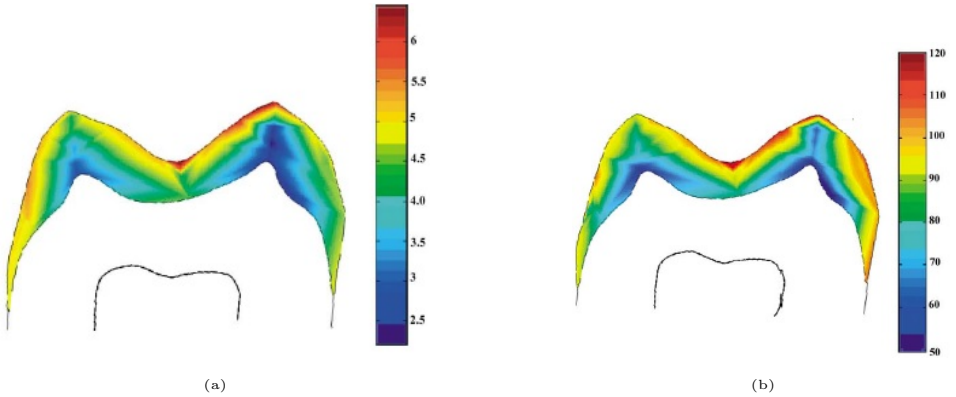

Figure 6.3: *Variation of the (a) hardness and (b) Young's modulus across the thickness of the tooth. Taken from [122].*

that the hardness and Young's modulus of even just the enamel already vary with depth[122, 123], as can be seen in Figure 6.3.

Considering the data of Cuy et al. and Fong et al.[122, 123] the Young's modulus varies from $c_1 = 120\ GPa$ in the enamel to $c_2 = 30\ GPa$. It is therefore possible to calculate μ_{eff} from the polarization generated in a parallel-shaped sample of area A and thickness h stimulated directly with a force F. Samples of the DEJ of cow teeth were prepared for measuring with a compression system described in appendix A. The surfaces of both tissues were polished to ensure flat surfaces without compromising the amount of material of both tissues: enamel and dentin.

The preparation of these samples was not as simple as bone, since the geometry and size of teeth make it difficult to have flat surfaces. In Figure 6.4 is possible to observe the DEJ where differences in density and order are very clear. Moreover, the junction is not flat and usually it goes parallel to the surface of enamel. Nevertheless, the sample was treated as a rectangular cuboid with a linear variation of the elastic constant. In order to calculate the effective flexoelectric coefficient, the slope of the plot of polarization P versus $\frac{F}{Ah}\left(\frac{c_2-c_1}{c_2 c_1}\right)$ was obtained, as in the Equation 2.5. The results are shown in Figure 6.5.

The effective flexoelectric coefficient obtained was $\mu_{eff} = -253\ nCm^{-1}$. This big effective flexoelectric as we move towards the inner (dentin and pulp) region of the teeth suggest that there is probably a contribution from collagen piezoelectricity to the effective flexoelectric coefficient. It is not clear what (if any) is the physiological effect of this relatively large effective flexoelectricity, but we speculate that it might help strengthening the tooth's insertion and/or it could stimulate the creation of

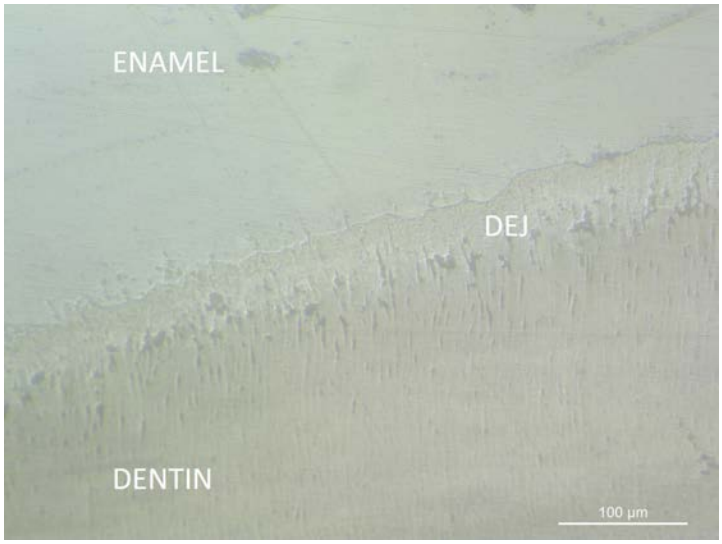

Figure 6.4: *Microscopy image of the dentin-enamel junction.*

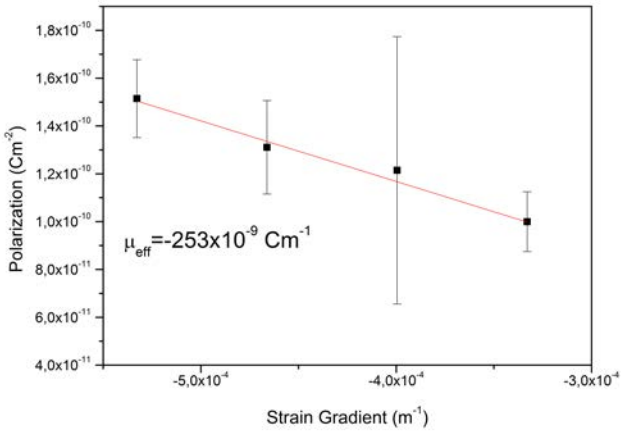

Figure 6.5: *Induced polarization of the DEJ of a tooth by strain gradients to obtain the effective flexoelectric coefficient.*

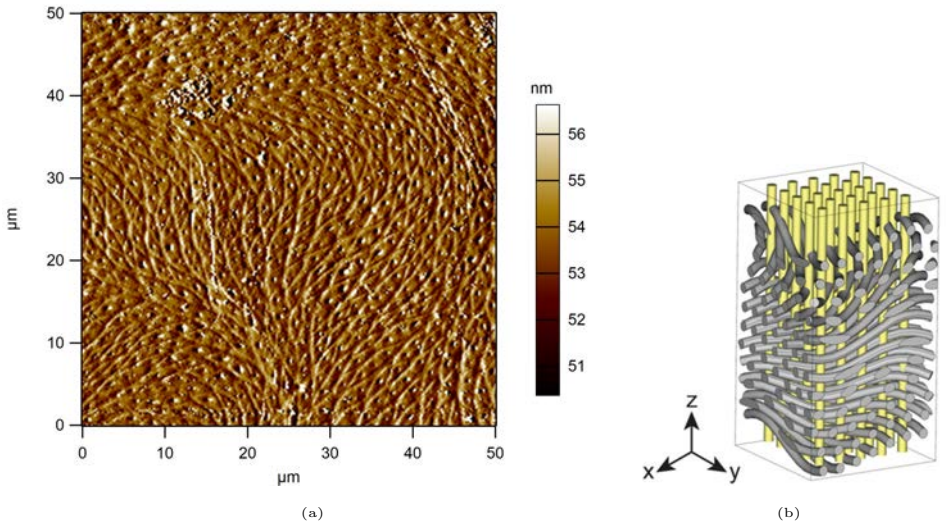

(a) (b)

Figure 6.6: *(a)Topography of the surface of the club.(b) In yellow the mineralized fibers that do up to the surface of the club.*

protein bridges across cracks, as observed by Rivera et. al. [121].

6.2 Stomapod's club

The stomapod is a crustacean notorious for the strength of its club, which it uses to break the shells of its prey. This club divided in three different regions: the impact region, the periodic region and the striated region. We are interested mainly in the impact region, the strongest part of the club and the one responsible for absorbing most of the impact energy.

6.2.1 Impact region

The impact region can also be divided in two different parts: the impact surface and the bulk. Interestingly, the impact region has a very similar structure to teeth, in the sense that it has a very hard surface of a few micrometers that progressively softens with depth[57]. The surface of the club at micrometer scales has mosaic-like pattern (Figure 6.6(a)), probably due to the mineralized fibers in the c-axis described by Yaraghi et.al.[57] (Figure 6.6(b)).

The impact surface has a crystalline hydroxyapatite surface, which has the highest Young's modulus of the club, at values of 60 GPa. Deeper in the club,

hydroxyapatite is ordered in a sophisticated herringbone pattern, which takes the form of a spiral wave thanks to the rotation of chitin fibrils. The amplitude of the waves also decreases with depth. Along this pattern, variations of the Young's modulus are observed. This structure deflects the mechanical energy from the central region towards the perimeter, which is larger and can thus absorb more energy. This allows the club to absorb the impact without provoking major damage to itself or other parts of the body of the shrimp. Figure 6.7 shows images of the structure of the impact region[57].

Two samples of the impact region of the stomapod's club were obtained. The samples were provided by Prof. D. Kisailus's group from the Materials Science and Engineering Program from the University of Riverside in California, USA. Figure 6.8, shows the samples we used for the measurements. The shape of these samples resembles an ovoid, so the most accurate equation to find the effective flexoelectric coefficient is Equation 2.11, where $\mu_{eff} = \left[\left(\frac{hc_1c_2}{2}\frac{A_2+A_1}{A_2c_2-A_1c_1}\right)e_{zz} + \mu_{zz}\right]$

Figure 6.9 shows the polarization of the club as a function of the strain gradient. Two curves are shown: one at 1 Hz and the other at 19 Hz. Higher frequencies would be of interest because the club hits the target at high speed and the contact of the surface with other material during the strike is small. Our DMA system, however, does not allow us to reach frequencies higher than a few tens of Hz. Nevertheless, already going from 1 Hz to 19 Hz we observe a change (a lowering) in the effective flexoelectric coefficient.

Interestingly, just like it happened with teeth, the flexoelectric coefficient is two orders of magnitude higher than pure hydroxyapatite, leading us to believe that chitin could be contributing to the total polarization in the same way as collagen contributes to the effective flexoelectricity of dentin.

We also calculated the effective piezoelectric coefficient of the dactyl club. The measurements are in the fCN^{-1} order. Assuming that the maximum force applied on these clubs during a hit can reach values of 10400g[49], that means inside the impact region of the club a polarization in the order of μCm^{-2} is generated during an impact, this impact will generate a voltage of 1-2 V across the thickness of the impact surface. Besides, if we consider a force of 10400g, the generated current, assuming a linear response in all the range, should be in the order of nanoamperes. The later calculations will result in an electrical power of a few nanoWatts during the the hit.

At this point, we do not yet have a hypothesis for what (if any) is the physiological role that flexoelectricity plays in the stomatopod's club, though we notice that

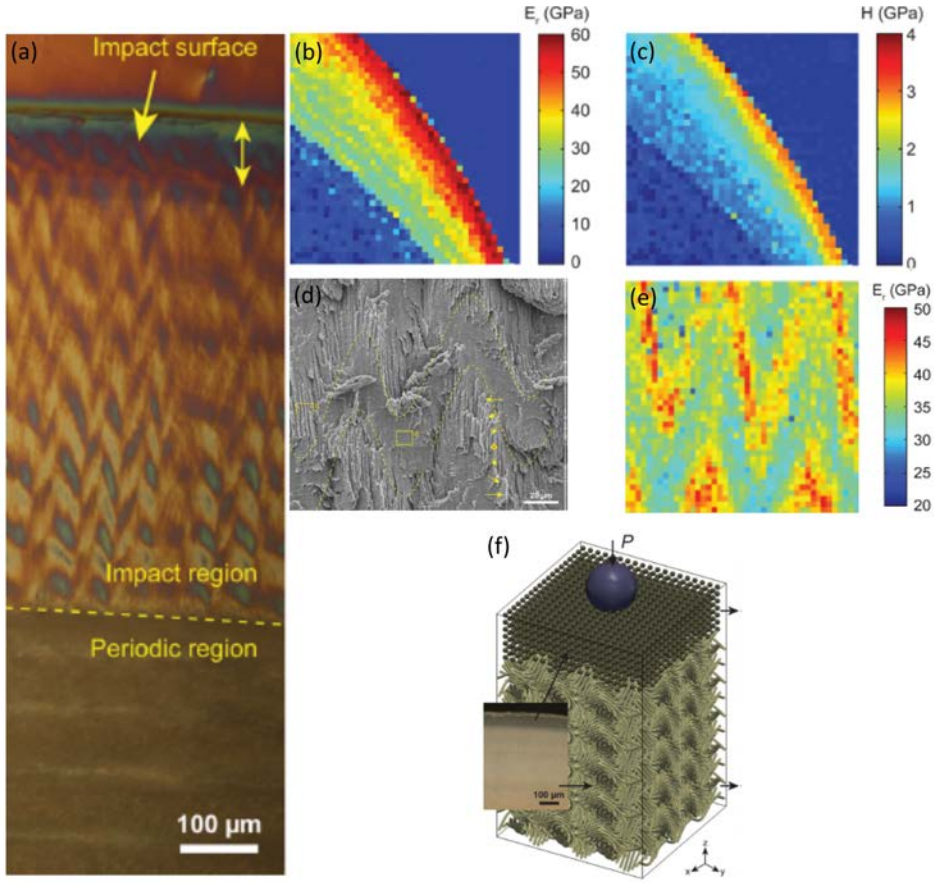

Figure 6.7: *(a)Microscopic image of a transverse cut of the dactyl club where different regions are shown. (b) Variation of the Young's modulus of the club. (c) Variation of the hardness of the club. (d) Scanning electron microscopy image of the tissue of the bulk in the impact region, yellow arrows show the direction of the mineralized fibrils. (e) Associated variation of the Young's modulus to the periodic pattern. (f) Schematic of the impact region showing the crystalline part of the impact surface and the rotating organization of the fibrils in the bulk if the impact region. Images taken from [57]*

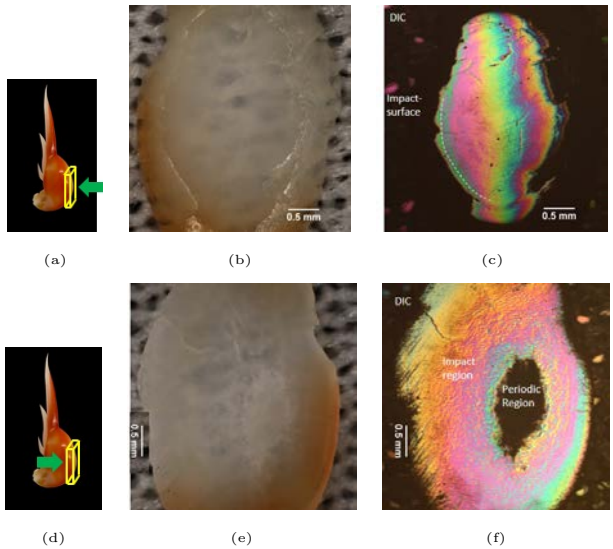

(a) (b) (c)

(d) (e) (f)

Figure 6.8: *Impact region of the samples received for measurements. (a), (b), (c) are the top view of the sample. (c), (d) and (f) are the bottom view, where a small region can be seen in the center that is part of the periodic region of the club. The images were provided by Prof. D. Kisailus's group.*

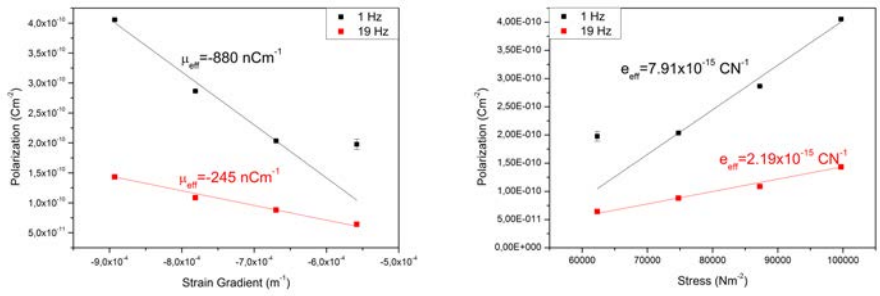

(a) (b)

Figure 6.9: *Polarization of stomapod's club at 1 Hz and 19 Hz produced by (a) strain gradients to calculate the effective flexoelectric coefficient and (b) stress to calculate the effective piezoelectric coefficient.*

flexoelectricity is known to be able to increase a material's toughness [101], which is the defining feature of this crustacean's club.

6.3 Coral Skeleton

As mentioned before, coral skeleton has similar characteristics to bone. In particular, it displays gradients of porosity with similar sizes to the pores in bone. These gradients help the structure of the skeleton to arrest the growth of cracks, as in the case of bone[51]. Furthermore, coral skeleton has high strength during compression (though it is brittle during tension).

These similarities between coral and bone have motivated the utilization of coral and coralline-based materials to produce bone grafts and implant them in animals and humans[53, 54, 124]. Two different kinds of grafts can be found: natural and synthetic. Natural ones have to undergo minimum processes to remove potential contaminants, but the original morphology and chemistry is preserved. Synthetic grafts use natural corals and, via a chemical process, corals mineral (aragonite) is exchanged for apatite, while preserving the morphology[53, 54]. Many clinical studies have evaluated the main results which, Pountus and Giannoudis, have reviewed[54].

Taking into account all the similarities to bone, we wondered whether natural coral can also induce flexoelectric fields in order to facilitate the integration of the graft inside the bone. A small piece of an unidentified species of brached coral was obtained and its structure was examined by scanning electron microscopy (Figure 6.10); branched corals are used in commercial bone grafts[54].

Although the original idea was to observe polarization across the coral's porosity gradient, a closer inspection with SEM did not show a smooth change of porosity (Figures 6.10(d) and 6.10(c)). Therefore, bending induced polarization measurements were made on the dense outer layer of the coral skeleton to measure the flexoelectricity of biologically-produced aragonite.

The measured flexoelectric coefficient of the coral skeleton (Figure 6.11 was exactly the same as that of bones and hydroxyapatite. Table 6.1, shows the results of the flexoelectric coefficient of the measured biomaterials of this thesis. It therefore seems likely -or at least not inconsistent- that this property contributes to the good integration properties of coralline bone grafts, and we propose that flexoelectric compatibility should be explored in other types of materials used for bone implants.

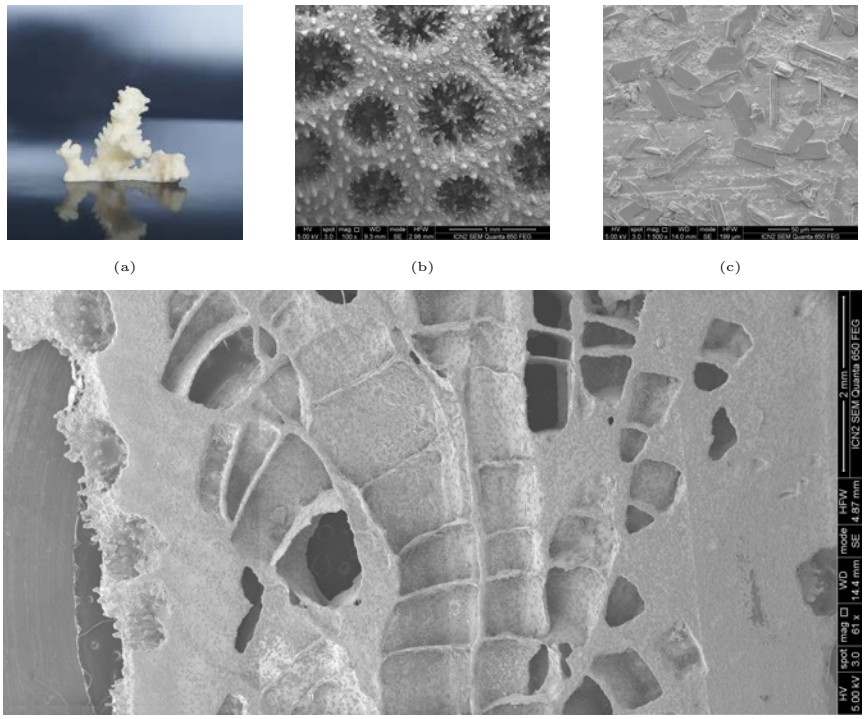

Figure 6.10: *(a) Picture of the coral. (b) SEM image of the surface of the coral, pores of different sizes are formed by aragonite that at the surface form nanoparticles. (c) In the dense layer several crystals are visible but there was no sign of a gradient of porosity. (d) Image of a transverse cut of the coral, at the edge there was a dense compact layer of aragonite, at the center of the coral, pores large sizes were observed.*

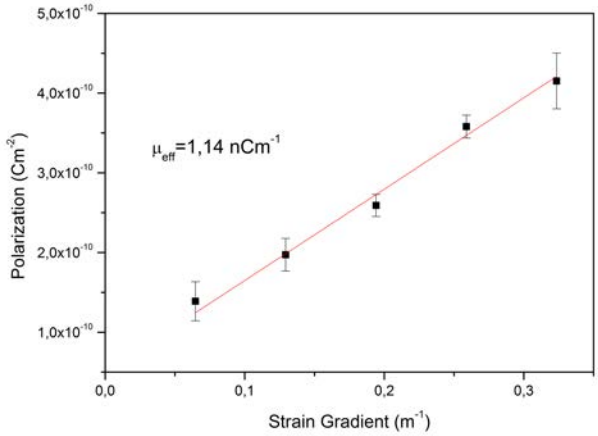

Figure 6.11: *Bending induced polarization of the coral skeleton at 13 Hz.*

Table 6.1: *Meachanoelectric properties of biomaterials measured by the 3-point bending technique.*

	Flexoelectric coefficient (nCm$^-$1)	Dielectric constant (Fm^{-1})	Flexocoupling (V)
Hydroxyapatite	1.1 ± 0.5	9.74×10^{-11}	11 ± 4
Enamel	0.9 ± 0.4	1.36×10^{-10}	6 ± 3
Coral skeleton	1.14 ± 0.08	8.43×10^{-11}	13.0 ± 0.9
Bone (average)	1.5 ± 0.9	1.38×10^{-10}	11 ± 6

CHAPTER 7

Conclusions and Future Work

7.1 Conclusions

The research work presented herein has explored the presence and consequences of strain gradients and therefore flexoelectricity in biomaterials. It has also contributed to the field of mechanoelectric properties of inhomogeneous systems by theoretically relating piezoelectricity and flexoelectricity in experimental conditions typically encountered in biomaterials in which they are indistinguishable. This study has also contributed to determining the physiological importance of flexoelectricity in bones. All these contributions can be summarized as follows:

(i) Different types of gradients (e.g. of porosity, of elasticity, of piezolectrity) can be found in biomaterials, and all of them favour the mechanoelectric polarization of materials. Two models were developed for cases where, respectevely, piezoelectricity is imitated by flexoelectric principles and, conversely, where flexoelectricity is mimicked by piezoelectric materials.

(ii) For a piezoelectric beam to be able to indistinguishably mimic flexoelectricity, that is, to to yield a non-zero solution invariant with respect to space inversion, it is a necessary and a sufficient condition that the piezoelectric coefficient be asymmetrically distributed across the thickness of the beam, i.e. that there is a non-zero net gradient of piezoelectricity.

(iii) Bending-induced polarization in non-piezoelectric hydroxyapatite beams and bones was measured and related to their effective flexoelectric coefficient. For any given curvature, hydroxyapatite flexoelectricity is quantitatively comparable to bone flexoelectricity. Hydroxyapatite flexoelectricity can therefore

account for most of the bending-induced polarization of bones, without needing to invoke collagen piezoelectricity.

(iv) Flexoelectricity pertaining to bone is affected by the direction of the applied curvature, showing the anisotropy of the flexoelectricity. This effect is related to the anisotropic mechanical properties of bone.

(v) At macroscopic scales, the average strain (and thus piezoelectricity, piezoelectricity gradients and streaming potentials) may dictate the global electromechanical response. However, at small scales, the strain gradient, and thus flexoelectricity, is much larger and dominates the local electromechanical response, as in the case of microcracks. This is important because it is at the microscale that cells operate, and thus flexoelectricity can have cytological effects.

(vi) The role of flexoelectricity is to trigger the process of bone remodelling by functioning as a signalling mechanism. Enormous strain gradients around the tip of microcracks generate big enough flexoelectric fields to induce osteocyte's apoptosys, the starting known point of the process of bone remodelling.

(vii) Around microcracks and under long-term culture conditions, flexoelectricity also stimulates osteoblastic maturation and mineralization.

(viii) Coral flexoelectricity was proved to be very similar to flexoelectricity of bone and hydroxyapatite. This property likely contributes to the good integration properties of coralline bone grafts. We therefore propose that flexoelectric compatibility should be explored in other types of materials used for bone implants.

(ix) Gradients of elastic constant are able to polarize samples by strain gradients. These kind of experiments were performed in the enamel-dentin junction and the stomapod's club, for the first time.

7.2 Future work

Each one of the measurements in this thesis has opened a new door for future research.

In the stomapod's club, it would be interesting to determine if it has any physiological role, particularly as regards toughening.

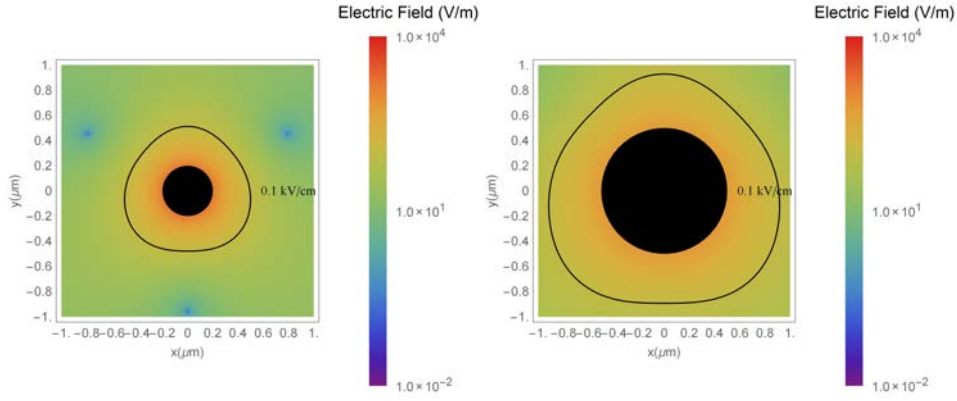

(a) (b)

Figure 7.1: *Calculation of flexoelectric fields around holes of (a) 200 μm and (b) 500 μm in PLLA substrates*

Regarding osteogenesis, it is important to explore further the capacity of flexoelectricity to stimulate cells, particularly osteoblast, and particularly with materials typically used for bone implants and bone grafts.

This would require inducing flexoelectric fields with magnitudes in the safe range for cells and stimulating properties as defined by McCullen et. al. [110]. By inducing flaws, not as sharp as cracks, it is possible to obtain a flexoelectric field with the desired electro-stimulation characteristics. For instance, with a hole in a surface, it would be possible to concentrate stress and form strain gradients that are intense enough to theoretically stimulate calcification but not so intense as to cause apoptosis.

Calculations of such flexoelectric fields are shown in Figure 7.1. In these cases, the felexoelectric fields were calculated for substrates of poliactic acid (PLLA, a common polymer used in bioaplications[125]) with two holes of 200 μm and 500 μm, mechanically stimulated with a portable bending system developed during this thesis. The results are promising for future experiments with cells cultured on PLLA to determine whether or not it is possible to stimulate cells, without killing them. Therefore, we would expect to see a nice radial gradient of mineralization after a few weeks of stimulation. The results for such experiments would be very valuable in determining the effectiveness of PLLA in bone grafts and prosthetic implants using flexoelectricity.

APPENDIX A

Experimental procedures

A.1 Sample preparation and characterization

Most samples used during the thesis were shaped in the same way for bending experiments. Samples, were cut using a diamond wire at low speed in order to avoid damage to the tissue. Both surfaces of the samples were polished up to 0.1 μm grain size disc with an Allied precision polishing system at low velocity to minimize damage to the samples. Finally platinum electrodes were deposited using pulsed laser deposition. We took special care to have low resistance across the electrode ($< 100\Omega$). The quality of the electrodes were checked by measuring the capacitance and dielectric losses, being 0.2 for the latest. Some of the samples had an extra treatment that will be explained bellow.

A.1.1 Bones

The most external parts of bones were cut in such a way that samples were composed only of compact bone. The samples were cut in consideration of the orientation of the collagen inside the bone. Collagen in compact bone is considered the strongest part of the bone due to its large density of hydroxyapatite.

A.1.2 Hydroxyapatite

Hydroxyapatite compact discs were commercially obtained from Clarkson Chromatography Products, INC., with certified purity greater than 95%. We also produced our own hydroxyapatite from bovine bones following the procedure of Ooi, C. et al.[126]. After annealing the bones at 900°C, they had a white aspect. In

order make the compact discs, bones were milled and the powder was sieved to 125 μm particle size. The powder was then uniaxially pressed into pellets of 22.5 mm of diameter under a pressure 25 metric tons. Finally the pellets were air sintered at 1360℃ for 4 hours. Samples were cut and polished using the same procedure as for the bones.

A.2 Flexoelectric measurements

Polarization was induced by a DMA8000 dynamic mechanical analyzer (DMA) of Perkin-Elmer and was measured using the method described by Zubko et al.[65]. The DMA was used to apply a periodic three-point bending stress at room temperature. This periodic signal was used as a reference for a lock-in amplifier, model 830 of Stanford Research Instruments, while the signal obtained from the electrodes fed the measurement channel of the lock-in amplifier, which recorded the bending-induced displacement currents. The current was converted into polarization using $P = I/2\pi\nu A$, where ν is the frequency of the bending force and A is the area of the electrodes. The polarization measured by the lock-in is related to the effective flexoelectric coefficient μ_{eff} by

$$P_3 = \mu_{13}^{eff} \frac{\partial S_{11}}{\partial x_3}, \tag{A.1}$$

and

$$\frac{\partial S_{11}}{\partial x_3} = \frac{12 z_0}{L^3}(L - a) \tag{A.2}$$

where L is the separation between the standing points of the sample, a is the half-length of the electrodes, and z_0 is the maximum vertical deflection in the middle of the sample. Typical values used in our measurements were L=12 mm,a=2 mm and z_0=2 μm. Measurements were taken after all samples had been dried in an oven at a temperature of 90℃ for 7 hours. All the measurements were obtained by measurements at 13 Hz, which in the range of frequencies that covers the characteristic timescales of the periodic loads in vivo[127].

From equationA.1, the effective flexoelectric coefficient is defined as the relation between the polarization and the stress gradient. For more accuracy, several strain gradients were applied to each sample and the flexoelectric coefficient was extracted from the slope of the plots of polarization as a function of strain gradient[19], as can be seen in Figure A.1.

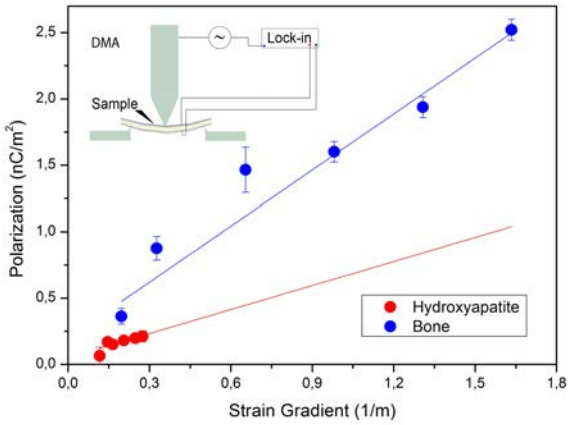

Figure A.1: *Flexoelectric coefficients were calculated as the slopes of the linear fits between the curvature and the bending-induced polarization. Inset: sketch of the measurement apparatus.*

A.3 Compression measurements

By using a DMA8000 dynamic mechanical analyzer (DMA) of Perkin-Elmer, uniform cyclic stress was applied to samples. Meanwhile, induced displacement currents were measured to calculate the polarization. Samples were mounted in between two plates that also worked as electrodes, however, to increase the quality of the electric contact, silver paint was used to cover the surfaces of the samples. A static force was applied to the sample, as a rule of thumb, the static force was at least 3 times bigger than the dynamic force that induced the polarization. Figure A.2 shows a sketch of the system. From the polarization is possible to obtain the effective flexoelectric coefficient μ_{eff} from

$$P_z = \mu_{eff} \frac{\partial S}{\partial x}, \tag{A.3}$$

or the effective piezoelectric coefficient e_{eff}

$$P_z = e_{eff} \sigma_z. \tag{A.4}$$

The value of stress σ_z and strain gradient $\frac{\partial S_{11}}{\partial x_3}$, depend on the geometry of the sample.

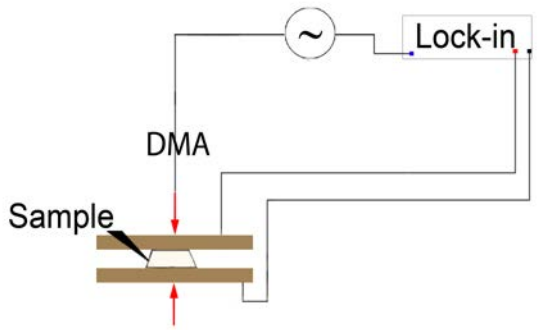

Figure A.2: *Sketch of the compression system used for the measurements of DEJ samples and the club of the stomapod. A dynamic force is applied to sample in between two electrodes. Induced displacement current is measured by a lock in amplifier.*

A.4 Cell experiments

A.4.1 Cell Culture

MC3T3-E1 mouse osteoblastic cells (ECACC General Cell Collection) were seeded at 11.320 $cells/cm^2$ on HA substrates and cultivated in MEMα GlutaMAX™medium (Gibco) supplemented with 10% fetal bovine serum (FBS, Life Technologies) and 1% penicillin/streptomycin (Life Technologies) at 37 ℃ in a 5% CO_2 incubator. For cell maturation studies, the medium was further supplemented with 8 mM β-glycerol phosphate (Sigma-Aldrich), 50 μ g/ml L-ascorbic acid (Sigma-Aldrich) and 10 nM Dexamethasone (Sigma-Aldrich) over 10-15 days, when they were differentiated into osteocytes.

A.4.2 Live/Dead staining

Cell attachment and viability after bending were evaluated qualitatively using Live/Dead staining probes (Live Technologies). The viability was evaluated immediately after bending. Briefly, cells were incubated for 15 minutes at room temperature with a mixture of 2 μM calcein acetoxymethyl ester (Calcein AM) and 4 μM ethidium homodimer-1 (EthD-1). Images of the viable cells (green fluorescence) and

dead cells (red fluorescence) were obtained using a Zeiss Axio Observer Z1m Optical Microscope with fluorescence optics and an Olympus DP30BW camera.

A.4.3 Cell Proliferation Assay

Cell proliferation was quantified measuring the activity of living cells via mitochondrial dehydrogenase activity by EZ4U Cell Proliferation Assay (Biomedica) according to the manufacturer's protocol. In brief, 40 μl of dye solution was added to 400 μl of medium. Then, samples were incubated during 5 hours at 37 ℃ in a 5% CO2 incubator until yield a significant increase in colour intensity. After incubation the absorbance is measured by a microplate-reader at 450 nm and subtracting background absorbance at 620 nm.

A.4.4 Caspase-3/7 staining

CellEvent™Caspase-3/7 green detection reagent was used to detect the progression of apoptosis in 10 days differentiated MC3T3-E1 cells after bending. Briefly, 8 μM of CellEvent™Caspase-3/7 reagent (Invitrogen) and 20 mM Hoechst 33342 nucleic acid stain (Life Technologies) were added directly to the cells in complete osteogenic medium.

A.4.5 Xylenol Orange staining

Xylenol Orange powder (Sigma-Aldrich) was dissolved in distillated water to make a 20mM stock solution, which was added to the ostegenic media overnight at 20 µM for detecting calcium formation. Mineralization was visualized in red using a Zeiss Axio Observer Z1m Optical Microscope with fluorescence optics. At the same time, calcein green staining was used to identify the viability and the amount of cells.

A.4.6 qRT-PCR analyses

The relative expression of the osteogenic marker genes collagen 1a1 (Col1a1) and osteocalcin (OC) at day 10 after stimulation or in control samples was studied by quantitative real-time reverse transcription polymerase chain reaction (qRT-PCR). The total messenger RNA (mRNA) was isolated from the samples using Maxwell RSC simply RNA extraction Kit (Promega). The isolated mRNA was reverse transcribed to cDNA with ISCRIPT Reverse Transcriptase Kit (Bio-Rad). The qRT-PCR mixture contained 50 ng cDNA, 300 nM of forward and reverse primers

and iTaq SYBR Green Supermix (Bio-Rad). The data were normalized to the expression of the housekeeping gene GAPDH. Finally, amplifications were performed in a CFX96 Real-Time PCR Detection System (Bio-Rad).

A.4.7 Scanning electron microscopy

Scanning electron microscopy (SEM) analysis was performed in HA samples. Samples were previously mounted in aluminium stubs and metalized with 5µm of platinum. Images were performed with a Quanta 650 FEG microscope.

A.4.8 Immunofluorescence staining

Col1 production was analyzed by immunofluorescence analaysis. Briefly, cells were fixed with 4% paraformaldehyde (Sigma-Aldrich) supplemented with 0.2% Triton-X-100 (Sigma-Aldrich) for 15 minutes at RT. Then, cells were blocked with 1% BSA (Sigma-Aldrich) for 1h at RT. After 3 PBS washes, cells were incubated with the primary antibody anti-COL1 (Abcam; 1:250) diluted in 1% BSA overnight at 4℃ . After 3 washes, the samples were treated with the secondary antibody Alexa-fluor 488 (Abcam, 1:500) for 1h at RT and washed 3 times again. The nuclei were stained with DAPI (1:1000) during the third wash after the secondary antibody treatment. Finally, the PBS was removed and images were performed with a Zeiss Axio Observer Z1m Optical Microscope with fluorescence optics.

A.4.9 Statistical analysis

Statistical analyses were performed with SPSS Statistics version 21.0 (IBM). The results were analysed by applying the two-way analysis of variance (ANOVA) test for multiple factors. Confidence intervals were fixed at 95% ($P < 0.05$). GraphPad Prism was used to graph all the quantitative data presented as mean and standard deviation (SD). See figure legends for specific information regarding the number of biological replicates (N).

APPENDIX B

Mathematica's codes

B.1 Strain gradient and flexoelectric field around a crack

2D maps of the flexoelectric field, strain and strain gradients were presented for different materials. Following code was developed in Wolfram Mathematica. To present the code as part of this document, the constants were commented in order to see the analytical solution of the equations. By including the constants defined at the beginning of the code, it is able to present the images used for the thesis.

```
(*Constants definition*)
(*Yx=6*10^9*) (*Bone*)(*10000000000*) (*PLLA*)(*80000000000*)
(*HA*)(*230000000000*) (*TiO2*) (*Young's modulus of the material*)
(*Yy=19*10^9*) (*Bone*)(*10000000000*) (*PLLA*)
(*80000000000*) (*HA*)(*230000000000*) (*TiO2*)
(*Yz=18*10^9*) (*Bone*)(*10000000000*) (*PLLA*)
(*80000000000*) (*HA*)(*230000000000 *)(*TiO2*)
(*K=3000000 *)(*Bone*)(*2400000*)(*PLLA and TiO2*)(*1000000*)
(*HA*) (*Critical intensity factor of the material or fractu*)
(*f=10*) (*flexocoupling coefficient. 10 V for bone,
43 for PLLA, 11.29 for HA and 4 for TiO2*)
(*ν=0.2*)(*Bone and HA*)(*0.36*) (*PLLA*) (*0.27*)(*TiO2*)(*Poisson's ratio*)

(*Cartesian equations of strain around a crack
 tip. Transformation of the variables that are cilindrical to cartesians*)
Sx = TransformedField["Polar" → "Cartesian",
    K/(Yx √(2*π*r)) * Cos[θ/2] * (1 - ν - Sin[θ/2] * Sin[3*θ/2] * (1 - ν)), {r, θ} → {x, y}] // Simplify
Sy = TransformedField["Polar" → "Cartesian", K/(Yy * √(2*π*r)) * Cos[θ/2] *
     (1 - ν + Sin[θ/2] * Sin[3*θ/2] * (1 - ν)), {r, θ} → {x, y}] // Simplify
Ss = TransformedField["Polar" → "Cartesian", K*(1 + ν)/(Yz * √(2*π*r)) * Cos[θ/2] * (Sin[θ/2] * Cos[3*θ/2]),
   {r, θ} → {x, y}] // Simplify
(*Definition of the Strain tensor in 2D*)
S = {{Sx, Ss}, {Ss, Sy}}
(*Magnitude of the strain to make a plot*)
SF = Norm[S, "Frobenius"] // Simplify
(*Calculation of the gradients for each cartesian variable*)
∇Sxx = ∂x Sx // Simplify
∇Sxy = ∂y Sx // Simplify
∇Syx = ∂x Sy // Simplify
∇Syy = ∂y Sy // Simplify
∇Ssx = ∂x Ss // Simplify
∇Ssy = ∂y Ss // Simplify
(*Definition of the flexoelectric field. The shear flexocouplin is 0*)
FEx = f * (∇Sxx + ∇Syx) + 0 * (∇Esy)
FEy = f * (∇Syy + ∇Sxy) + 0 * (∇Esx) // Simplify
(*Definition of the vector electric field and its magnitude*)
∇E = {FEx, FEy, 0} // Simplify
V = Norm[∇E] // Simplify
(*Definition of a line to draw in the plot as the crack*)
lineStyle = {Black, Thick};
(*Function that defines a logarithmic bar legend in the plot.  x_ are the variables sizes,
min_ is the lowest value of the Color bar legend
 and max_ is the highest value of the color bar legend*)
LogarithmicScaling[x_, min_, max_] := Log[x/min]/Log[max/min]
(*Function to make the plots. F_ is the function to be plotted;
oder is the scale of the size that will be plotted;
xunits_ and yunits_ are the label written for x and y in the plot;
Fmin_ and Fmax_ are the limit values plotted;
NumberOfTicks_ define the number of thicks in the bar legend;
Label_ is the label for the bar legend; text1_,text2_ and text3_,
are texts used to mark values of the mesh; and mesh_ are the values to define the mesh*)
plotter[F_, lim_, order_, xunits_, yunits_, Fmin_, Fmax_, NumberOfTicks_, Label_,
  text1_, text2_, text3_, mesh_] := DensityPlot[F, {x, -lim, lim}, {y, -lim, lim},
  FrameTicks → {{{{-5/5*lim, -5/5*lim/order}, {-4/5*lim, -4/5*lim/order}, {-3/5*lim,
       -3/5*lim/order}, {-2/5*lim, -2/5*lim/order}, {-1/5*lim, -1/5*lim/order}, {0, 0},
      {1/5*lim, 1/5*lim/order}, {2/5*lim, 2/5*lim/order}, {3/5*lim, 3/5*lim/order},
      {4/5*lim, 4/5*lim/order}, {5/5*lim, 5/5*lim/order}}, None},
    {{{-5/5*lim, -5/5*lim/order}, {-4/5*lim, -4/5*lim/order}, {-3/5*lim,
```

```
        -3 / 5 * lim / order}, {-2 / 5 * lim, -2 / 5 * lim / order}, {-1 / 5 * lim, -1 / 5 * lim / order}, {0, 0},
      {1 / 5 * lim, 1 / 5 * lim / order}, {2 / 5 * lim, 2 / 5 * lim / order}, {3 / 5 * lim, 3 / 5 * lim / order},
      {4 / 5 * lim, 4 / 5 * lim / order}, {5 / 5 * lim, 5 / 5 * lim / order}}, None}}
    (*{x,y}∈Disk[{0,0}, 1/10^5]*), PlotPoints → 100, PlotRange → Full,
  MeshFunctions → {#3 &}, Mesh → mesh,
  MeshStyle → {Directive[Red]},
  ColorFunctionScaling → False,
  ColorFunction → (ColorData["Rainbow"][LogarithmicScaling[#, Fmin, Fmax]] &),
  FrameLabel → {xunits, yunits} , PlotLegends →
   BarLegend[{ColorData["Rainbow"], {0, 1}}, LegendLabel → Label, LegendMarkerSize → 300,
    Ticks → ({LogarithmicScaling[#, Fmin, Fmax], ScientificForm[N[#, 2]]} & /@
        (Fmin (Fmax / Fmin) ^ Range[0, 1, 1 / NumberOfTicks]))],
  Epilog → {Directive[lineStyle], Line[{{-lim, 0}, {0, 0}}],
    Text[Style[text1, 10, FontFamily → Times, Black], {6 / 20 * lim, 0}],
    Text[Style[text2, 10, FontFamily → Times, Red], {5 / 20 * lim, 5 / 20 * lim}],
    Text[Style[text3, 10, FontFamily → Times, Green], {13 / 20 * lim, 13 / 20 * lim}]}]
(*Call of the plots*)
plotter[V, 150/10^6, 1/10^6, "x(μm)", "y(μm)", 10^2, 10^7, 5,
 "Electric Field (V/m)", "10 kV/m", "5 kV/m", "1 kV/m", {{10 * 10^3, 5 * 10^3, 1 * 10^3}}]
plotter[SF, 200/10^6, 1/10^6, "x(μm)", "y(μm)", 10^-3, 10^-1, 2, "Strain", " ", " ", " ", None]
plotter[Abs[∇Sxx], 200/10^6, 1/10^6, "x(μm)", "y(μm)", 10^0,
 10^5, 5, "Strain Gradient ∂Sxx/∂x (m^-1)", " ", " ", " ", None]
plotter[Abs[∇Syx], 200/10^6, 1/10^6, "x(μm)", "y(μm)", 10^0, 10^5,
 5, "Strain Gradient ∂Syy/∂x (m^-1)", " ", " ", " ", None]
```

Out[1]=
$$-\frac{K\,(-1+\nu)\,\text{Cos}\left[\frac{1}{2}\,\text{ArcTan}[x,y]\right]\left(2-\frac{x}{\sqrt{x^2+y^2}}+\text{Cos}[2\,\text{ArcTan}[x,y]]\right)}{2\sqrt{2\pi}\;(x^2+y^2)^{1/4}\,Yx}$$

Out[2]=
$$\frac{K\left(-3+\frac{2x}{\sqrt{x^2+y^2}}\right)(-1+\nu)\,\text{Cos}\left[\frac{1}{2}\,\text{ArcTan}[x,y]\right]^3}{\sqrt{2\pi}\;(x^2+y^2)^{1/4}\,Yy}$$

Out[3]=
$$\frac{K\,y\,(1+\nu)\,\text{Cos}\left[\frac{3}{2}\,\text{ArcTan}[x,y]\right]}{2\sqrt{2\pi}\;(x^2+y^2)^{3/4}\,Yz}$$

Out[4]=
$$\left\{\left\{-\frac{K\,(-1+\nu)\,\text{Cos}\left[\frac{1}{2}\,\text{ArcTan}[x,y]\right]\left(2-\frac{x}{\sqrt{x^2+y^2}}+\text{Cos}[2\,\text{ArcTan}[x,y]]\right)}{2\sqrt{2\pi}\;(x^2+y^2)^{1/4}\,Yx},\ \frac{K\,y\,(1+\nu)\,\text{Cos}\left[\frac{3}{2}\,\text{ArcTan}[x,y]\right]}{2\sqrt{2\pi}\;(x^2+y^2)^{3/4}\,Yz}\right\},\right.$$
$$\left.\left\{\frac{K\,y\,(1+\nu)\,\text{Cos}\left[\frac{3}{2}\,\text{ArcTan}[x,y]\right]}{2\sqrt{2\pi}\;(x^2+y^2)^{3/4}\,Yz},\ \frac{K\left(-3+\frac{2x}{\sqrt{x^2+y^2}}\right)(-1+\nu)\,\text{Cos}\left[\frac{1}{2}\,\text{ArcTan}[x,y]\right]^3}{\sqrt{2\pi}\;(x^2+y^2)^{1/4}\,Yy}\right\}\right\}$$

Out[5]=
$$\frac{1}{2\sqrt{2\pi}}\left(\sqrt{\left(4\,\text{Abs}\left[\frac{K\left(-3+\frac{2x}{\sqrt{x^2+y^2}}\right)(-1+\nu)\,\text{Cos}\left[\frac{1}{2}\text{ArcTan}[x,y]\right]^3}{(x^2+y^2)^{1/4}\,Yy}\right]^2+2\,\text{Abs}\left[\frac{K\,y\,(1+\nu)\,\text{Cos}\left[\frac{3}{2}\text{ArcTan}[x,y]\right]}{(x^2+y^2)^{3/4}\,Yz}\right]^2+\text{Abs}\left[\frac{K\,(-1+\nu)\,\text{Cos}\left[\frac{1}{2}\text{ArcTan}[x,y]\right]\left(2-\frac{x}{\sqrt{x^2+y^2}}+\text{Cos}[2\,\text{ArcTan}[x,y]]\right)}{(x^2+y^2)^{1/4}\,Yx}\right]^2\right)}\right)$$

Out[6]=
$$\frac{K\,y\left(-5\,x^4-4\,x^2\,y^2+y^4+7\,x^3\sqrt{x^2+y^2}-5\,x\,y^2\sqrt{x^2+y^2}\right)(-1+\nu)\,\text{Csc}\left[\frac{1}{2}\text{ArcTan}[x,y]\right]}{8\sqrt{2\pi}\,(x^2+y^2)^{13/4}\,Yx}$$

Out[7]=
$$\frac{1}{4\sqrt{2\pi}\,(x^2+y^2)^{7/4}\,Yx}K\,(-1+\nu)\,\text{Sin}\left[\frac{1}{2}\text{ArcTan}[x,y]\right]\left(-x^2+2\,x\sqrt{x^2+y^2}-3\,x\,y\,\text{Cot}\left[\frac{1}{2}\text{ArcTan}[x,y]\right]+\sqrt{x^2+y^2}\,\text{Cos}[2\,\text{ArcTan}[x,y]]\left(x+y\,\text{Cot}\left[\frac{1}{2}\text{ArcTan}[x,y]\right]\right)+y^2\,\text{Csc}\left[\frac{1}{2}\text{ArcTan}[x,y]\right]^2+2\,x\,y\,\text{Csc}\left[\frac{1}{2}\text{ArcTan}[x,y]\right]^2\text{Sin}[2\,\text{ArcTan}[x,y]]\right)$$

Out[8]=
$$\frac{K\,y^3\left(-17\,x^2-5\,y^2+18\,x\sqrt{x^2+y^2}\right)(-1+\nu)\,\text{Csc}\left[\frac{1}{2}\text{ArcTan}[x,y]\right]^3}{16\sqrt{2\pi}\,(x^2+y^2)^{13/4}\,Yy}$$

Out[9]=
$$\left(3\,K\,(-1+\nu)\,\text{Cos}\left[\frac{1}{2}\text{ArcTan}[x,y]\right]^2\left(-4\,x^2+6\,x\sqrt{x^2+y^2}-4\,x\,y\,\text{Cot}\left[\frac{1}{2}\text{ArcTan}[x,y]\right]+y^2\,\text{Csc}\left[\frac{1}{2}\text{ArcTan}[x,y]\right]^2\right)\text{Sin}\left[\frac{1}{2}\text{ArcTan}[x,y]\right]\right)\Big/\left(4\sqrt{2\pi}\,(x^2+y^2)^{7/4}\,Yy\right)$$

Out[10]=
$$\left(3\,K\,y\,(1+\nu)\left(-x\,\text{Cos}\left[\frac{3}{2}\text{ArcTan}[x,y]\right]+y\,\text{Sin}\left[\frac{3}{2}\text{ArcTan}[x,y]\right]\right)\right)\Big/\left(4\sqrt{2\pi}\,(x^2+y^2)^{7/4}\,Yz\right)$$

Out[11]=
$$\left(K\,(1+\nu)\left((2\,x^2-y^2)\,\text{Cos}\left[\frac{3}{2}\text{ArcTan}[x,y]\right]-3\,x\,y\,\text{Sin}\left[\frac{3}{2}\text{ArcTan}[x,y]\right]\right)\right)\Big/\left(4\sqrt{2\pi}\,(x^2+y^2)^{7/4}\,Yz\right)$$

Out[12]=
$$f\left(\left(K\,y\left(-5\,x^4-4\,x^2\,y^2+y^4+7\,x^3\sqrt{x^2+y^2}-5\,x\,y^2\sqrt{x^2+y^2}\right)(-1+\nu)\,\text{Csc}\left[\frac{1}{2}\text{ArcTan}[x,y]\right]\right)\Big/\left(8\sqrt{2\pi}\,(x^2+y^2)^{13/4}\,Yx\right)+\left(K\,y^3\left(-17\,x^2-5\,y^2+18\,x\sqrt{x^2+y^2}\right)(-1+\nu)\,\text{Csc}\left[\frac{1}{2}\text{ArcTan}[x,y]\right]^3\right)\Big/\left(16\sqrt{2\pi}\,(x^2+y^2)^{13/4}\,Yy\right)\right)$$

Out[13]=
$$\frac{1}{4\sqrt{2\pi}\ (x^2+y^2)^{7/4}\,Yx\,Yy}$$
$$f\,K\,(-1+\nu)\,\text{Sin}\left[\frac{1}{2}\text{ArcTan}[x,y]\right]\left(-x^2\,Yy+2\,x\sqrt{x^2+y^2}\ Yy-3\,x\,y\,Yy\,\text{Cot}\left[\frac{1}{2}\text{ArcTan}[x,y]\right]+\right.$$
$$3\,y^2\,Yx\,\text{Cot}\left[\frac{1}{2}\text{ArcTan}[x,y]\right]^2+\sqrt{x^2+y^2}\ Yy\,\text{Cos}[2\,\text{ArcTan}[x,y]]\left(x+y\,\text{Cot}\left[\frac{1}{2}\text{ArcTan}[x,y]\right]\right)-$$
$$6\,x\,Yx\,\text{Cos}\left[\frac{1}{2}\text{ArcTan}[x,y]\right]^2\left(2\,x-3\sqrt{x^2+y^2}+2\,y\,\text{Cot}\left[\frac{1}{2}\text{ArcTan}[x,y]\right]\right)+$$
$$\left.y^2\,Yy\,\text{Csc}\left[\frac{1}{2}\text{ArcTan}[x,y]\right]^2+2\,x\,y\,Yy\,\text{Csc}\left[\frac{1}{2}\text{ArcTan}[x,y]\right]^2\text{Sin}[2\,\text{ArcTan}[x,y]]\right)$$

Out[14]=
$$\left\{-\left(\left(f\,K\,y\,(-1+\nu)\,\text{Csc}\left[\frac{1}{2}\text{ArcTan}[x,y]\right]\left(-2\left(-5\,x^4-4\,x^2\,y^2+y^4+7\,x^3\sqrt{x^2+y^2}-5\,x\,y^2\sqrt{x^2+y^2}\right)Yy+\right.\right.\right.$$
$$\left.\left.\left.y^2\left(17\,x^2+5\,y^2-18\,x\sqrt{x^2+y^2}\right)Yx\,\text{Csc}\left[\frac{1}{2}\text{ArcTan}[x,y]\right]^2\right)\right)\Big/\left(16\sqrt{2\pi}\ (x^2+y^2)^{13/4}\,Yx\,Yy\right)\right),$$
$$\frac{1}{4\sqrt{2\pi}\ (x^2+y^2)^{7/4}\,Yx\,Yy}f\,K\,(-1+\nu)\,\text{Sin}\left[\frac{1}{2}\text{ArcTan}[x,y]\right]$$
$$\left(-x^2\,Yy+2\,x\sqrt{x^2+y^2}\ Yy-3\,x\,y\,Yy\,\text{Cot}\left[\frac{1}{2}\text{ArcTan}[x,y]\right]+3\,y^2\,Yx\,\text{Cot}\left[\frac{1}{2}\text{ArcTan}[x,y]\right]^2+\right.$$
$$\sqrt{x^2+y^2}\ Yy\,\text{Cos}[2\,\text{ArcTan}[x,y]]\left(x+y\,\text{Cot}\left[\frac{1}{2}\text{ArcTan}[x,y]\right]\right)-$$
$$6\,x\,Yx\,\text{Cos}\left[\frac{1}{2}\text{ArcTan}[x,y]\right]^2\left(2\,x-3\sqrt{x^2+y^2}+2\,y\,\text{Cot}\left[\frac{1}{2}\text{ArcTan}[x,y]\right]\right)+$$
$$\left.y^2\,Yy\,\text{Csc}\left[\frac{1}{2}\text{ArcTan}[x,y]\right]^2+2\,x\,y\,Yy\,\text{Csc}\left[\frac{1}{2}\text{ArcTan}[x,y]\right]^2\text{Sin}[2\,\text{ArcTan}[x,y]]\right),\,0\Big\}$$

Out[15]=
$$\frac{1}{16\sqrt{2\pi}}$$
$$\left(\sqrt{\left(\text{Abs}\left[\left(f\,K\,y\,(-1+\nu)\,\text{Csc}\left[\frac{1}{2}\text{ArcTan}[x,y]\right]\left(-2\left(-5\,x^4-4\,x^2\,y^2+y^4+7\,x^3\sqrt{x^2+y^2}-5\,x\,y^2\sqrt{x^2+y^2}\right)Yy+\right.\right.\right.\right.$$
$$\left.\left.\left.\left.y^2\left(17\,x^2+5\,y^2-18\,x\sqrt{x^2+y^2}\right)Yx\,\text{Csc}\left[\frac{1}{2}\text{ArcTan}[x,y]\right]^2\right)\right)\Big/\left((x^2+y^2)^{13/4}\,Yx\,Yy\right)\right]^2+$$
$$16\,\text{Abs}\left[\frac{1}{(x^2+y^2)^{7/4}\,Yx\,Yy}f\,K\,(-1+\nu)\,\text{Sin}\left[\frac{1}{2}\text{ArcTan}[x,y]\right]\left(-x^2\,Yy+2\,x\sqrt{x^2+y^2}\ Yy-\right.\right.$$
$$3\,x\,y\,Yy\,\text{Cot}\left[\frac{1}{2}\text{ArcTan}[x,y]\right]+3\,y^2\,Yx\,\text{Cot}\left[\frac{1}{2}\text{ArcTan}[x,y]\right]^2+$$
$$\sqrt{x^2+y^2}\ Yy\,\text{Cos}[2\,\text{ArcTan}[x,y]]\left(x+y\,\text{Cot}\left[\frac{1}{2}\text{ArcTan}[x,y]\right]\right)-$$
$$6\,x\,Yx\,\text{Cos}\left[\frac{1}{2}\text{ArcTan}[x,y]\right]^2\left(2\,x-3\sqrt{x^2+y^2}+2\,y\,\text{Cot}\left[\frac{1}{2}\text{ArcTan}[x,y]\right]\right)+$$
$$\left.\left.y^2\,Yy\,\text{Csc}\left[\frac{1}{2}\text{ArcTan}[x,y]\right]^2+2\,x\,y\,Yy\,\text{Csc}\left[\frac{1}{2}\text{ArcTan}[x,y]\right]^2\text{Sin}[2\,\text{ArcTan}[x,y]]\right)\right]^2\right)\right)$$

```
(*Export commands*)
Export["Bone.jpg", plotter[V, 250/10^6, 1/10^6, "x(μm)", "y(μm)", 10^2,
  10^5, 3, "Electric Field (V/m)", " ", " ", " ", None], ImageResolution → 400]
(*Export["Bone_Strain.JPG",plotter[SF,200/10^6,1/10^6, "x(μm)","y(μm)",10^-3,
   10^-1,2,"Strain"," ", " ", " ",None ],ImageResolution→400]
 Export["Bone_Strain Gradient XXX.JPG",plotter[Abs[∇Sxx],200/10^6,1/10^6, "x(μm)","y(μm)",10^0,
   10^5,5,"Strain Gradient ∂Sxx/∂x (m^-1)"," ", "1 kV/m", " ",{{1000}} ],ImageResolution→400]
 Export["Bone_Strain Gradient YYX.JPG",plotter[Abs[∇Syx],200/10^6,1/10^6, "x(μm)","y(μm)",
   10^0,10^5,5,"Strain Gradient ∂Syy/∂x (m^-1)"," ", " ", " ",None ],ImageResolution→400]*)
```

Bibliography

[1] S. M. Kogan, *Piezoelectric effect during inhomogeneous deformation and acoustic scattering of carriers in crystals*, Sov. Phys. Solid State **5** (1964).

[2] R. Maranganti, N. D. Sharma, and P. Sharma, *Electromechanical coupling in nonpiezoelectric materials due to nanoscale nonlocal size effects: Green's function solutions and embedded inclusions*, in *Physical Review B*, Vol. 74 (American Physical Society, 2006) p. 014110.

[3] P. Zubko, G. Catalan, and A. K. Tagantsev, *Flexoelectric Effect in Solids*, Annu. Rev. Mater. Res. **43**, 387 (2013).

[4] P. V. Yudin and a. K. Tagantsev, *Fundamentals of flexoelectricity in solids.*, Nanotechnology **24**, 432001 (2013).

[5] W. L. Indenbom, E. B. Loginov, and M. A. Osipov, *On the microscopic origin of flexoelectricity effect in the smectic C liquid crystals*, Sov. Phys. Crystallogr. **26** (1981).

[6] R. B. Meyer, *PIEZOELECTRIC EFFECTS IN LIQUID CRYSTALS*, Physical Review Letters **22**, 918 (1969).

[7] E. Bursian and N. Trunov, *Nonlocal piezoelectric effect*, Sov. Phys. Solid State **16**, 760 (1974).

[8] A. K. Tagantsev, *Piezoelectricity and flexoelectricity in crystalline dielectrics*, Physical Review B **34**, 5883 (1986).

[9] L. E. Cross, *Flexoelectric effects: Charge separation in insulating solids subjected to elastic strain gradients*, Journal of Materials Science **41**, 53 (2006).

[10] W. Ma and L. E. Cross, *Observation of the flexoelectric effect in relaxor Pb(Mg[sub 1/3]Nb[sub 2/3])O[sub 3] ceramics*, Applied Physics Letters **78**, 2920 (2001).

[11] W. Ma and L. E. Cross, *Flexoelectric effect in ceramic lead zirconate titanate*, Applied Physics Letters **86**, 072905 (2005).

[12] J. Narvaez and G. Catalan, *Origin of the enhanced flexoelectricity of relaxor ferroelectrics*, Applied Physics Letters **104**, 162903 (2014).

[13] A. Biancoli, C. M. Fancher, J. L. Jones, and D. Damjanovic, *Breaking of macroscopic centric symmetry in paraelectric phases of ferroelectric materials and implications for flexoelectricity*, Nature materials **14**, 224 (2015).

[14] L. M. Garten and S. Trolier-McKinstry, *Enhanced flexoelectricity through residual ferroelectricity in barium strontium titanate*, Journal of Applied Physics **117**, 094102 (2015).

[15] J. Narvaez, S. Saremi, J. Hong, M. Stengel, and G. Catalan, *Large Flexoelectric Anisotropy in Paraelectric Barium Titanate*, Physical Review Letters **115**, 037601 (2015).

[16] E. Fukada, G. M. Sessler, J. E. West, A. Berraissoul, and P. Günther, *Bending piezoelectricity in monomorph polymer films*, Journal of Applied Physics **62**, 3643 (1987).

[17] S. Baskaran, X. He, Q. Chen, and J. Y. Fu, *Experimental studies on the direct flexoelectric effect in α -phase polyvinylidene fluoride films*, Applied Physics Letters **98** (2011), 10.1063/1.3599520.

[18] Y. Zhou, J. Liu, X. Hu, B. Chu, S. Chen, and D. Salem, *Flexoelectric effect in PVDF-based polymers*, IEEE Transactions on Dielectrics and Electrical Insulation **24**, 727 (2017).

[19] K. D. Breneman, W. E. Brownell, and R. D. Rabbitt, *Hair cell bundles: flexoelectric motors of the inner ear.*, PloS one **4**, e5201 (2009).

[20] J. Narvaez, F. Vasquez-Sancho, and G. Catalan, *Enhanced flexoelectric-like response in oxide semiconductors.*, Nature **538**, 219 (2016).

[21] T. D. Nguyen, S. Mao, Y.-W. Yeh, P. K. Purohit, and M. C. McAlpine, *Nanoscale flexoelectricity.*, Advanced materials (Deerfield Beach, Fla.) **25**, 946 (2013).

[22] A. Abdollahi, D. Millán, C. Peco, M. Arroyo, and I. Arias, *Revisiting pyramid compression to quantify flexoelectricity: A three-dimensional simulation study*, Physical Review B **91**, 104103 (2015).

[23] U. G. K. Wegst, H. Bai, E. Saiz, A. P. Tomsia, and R. O. Ritchie, *Bioinspired structural materials*, Nature Materials **14**, 23 (2015).

[24] S. Weiner and H. D. Wagner, *THE MATERIAL BONE: Structure-Mechanical Function Relations*, Annual Review of Materials Science **28**, 271 (1998).

[25] J. D. Currey, *Bones: Structure and Mechanics*, 2nd ed. (Princeton University Press, 2002).

[26] N. Reznikov, R. Shahar, and S. Weiner, *Bone hierarchical structure in three dimensions.*, Acta biomaterialia **10**, 3815 (2014).

[27] A. Monro, *The anatomy of the human bones, nerves and lacteal sac and duct*, eight edit ed. (John Donaldson, London, 1775).

[28] G. A. Rodan, *Introduction to bone biology*, Bone **13**, S3 (1992).

[29] J. Behari, *Jawaharlal Nehru University, India*, 1st ed. (John Wiley and Sons (Asia) Pte Ltd, Noida, 2009) p. 501, arXiv:arXiv:1011.1669v3 .

[30] J. C. Anderson and C. Eriksson, *Piezoelectric properties of dry and wet bone.*, Nature **227**, 491 (1970).

[31] A. a. Marino and R. O. Becker, *Piezoelectricity in hydrated frozen bone and tendon*, Nature **253**, 627 (1975).

[32] C. Hatchett and F. R. S. Esq, *Experiments and observations on shell and bone*, Phil. Trans. R. Soc. Lond. **89**, 315 (1799).

[33] W. de Jong, *La substance minerale dans les os*, Recl Trav Chim Pays-Bas Belg **535**, 7 (1925).

[34] P. Fratzl, M. Groschner, G. Vogl, H. Plenk, J. Eschberger, N. Fratzl-Zelman, K. Koller, and K. Klaushofer, *Mineral crystals in calcified tissues: A compar-*

ative study by SAXS, Journal of Bone and Mineral Research **7**, 329 (1992).

[35] A. S. Posner, A. Perloff, and A. F. Diorio, *Refinement of the hydroxyapatite structure*, Acta Crystallographica **11**, 308 (1958).

[36] M. W. Johnson, W. S. Williams, and D. Gross, *Ceramic models for piezoelectricity in dry bone.*, Journal of biomechanics **13**, 565 (1980).

[37] A. H. Rajabi, M. Jaffe, and T. L. Arinzeh, *Piezoelectric materials for tissue regeneration: A review.*, Acta biomaterialia **24**, 12 (2015).

[38] P. Fratzl, H. S. Gupta, E. P. Paschalis, and P. Roschger, *Structure and mechanical quality of the collagen – mineral nano-composite in bone*, Journal of Materials Chemistry **14**, 2115 (2004).

[39] T. C. Lee, A. Staines, and D. Taylor, *Bone adaptation to load: microdamage as a stimulus for bone remodelling.*, Journal of anatomy **201**, 437 (2002).

[40] B. M. Isaacson and R. D. Bloebaum, *Bone bioelectricity: What have we learned in the past 160 years?*, Journal of Biomedical Materials Research - Part A **95**, 1270 (2010).

[41] A. C. Ahn and A. Grodzinsky, *Relevance of Collagen Piezoelectricity to "Wolff's Law": A Critical Review*, Medical Engineering and Physics **31**, 733 (2009).

[42] K. Arvidson, B. M. Abdallah, L. A. Applegate, N. Baldini, E. Cenni, E. Gomez-Barrena, D. Granchi, M. Kassem, Y. T. Konttinen, K. Mustafa, D. P. Pioletti, T. Sillat, and A. Finne-Wistrand, *Bone regeneration and stem cells*, Journal of Cellular and Molecular Medicine **15**, 718 (2011).

[43] M. Capulli, R. Paone, and N. Rucci, *Osteoblast and osteocyte: Games without frontiers*, Archives of Biochemistry and Biophysics **561**, 3 (2014).

[44] R. Florencio-silva, G. Rodrigues, E. Sasso-cerri, M. J. Simões, P. S. Cerri, and B. Cells, *Biology of Bone Tissue : Structure , Function , and Factors That Influence Bone Cells*, **2015** (2015), 10.1155/2015/421746.

[45] O. Verborgt, G. J. Gibson, and M. B. Schaffler, *Loss of Osteocyte Integrity in Association with Microdamage and Bone Remodeling After Fatigue In Vivo **, Journal of Bone and Mineral Research **15**, 60 (2000).

[46] J. E. Bertram and a. a. Biewener, *Bone curvature: sacrificing strength for load predictability?*, Journal of theoretical biology **131**, 75 (1988).

[47] F.-Z. Cui and J. Ge, *New observations of the hierarchical structure of human enamel , from nanoscale to microscale*, Journal of Tissue Engineering and Regerative Medicine **1**, 185 (2007).

[48] M. Garcia, C. Edmiston, R. Marinov, A. Vail, and V. Gruev, *Bio-inspired color-polarization imager for real-time in situ imaging*, Optica **4**, 1263 (2017).

[49] J. C. Weaver, G. W. Milliron, A. Miserez, K. Evans-Lutterodt, S. Herrera, I. Gallana, W. J. Mershon, B. Swanson, P. Zavattieri, E. DiMasi, and D. Kisailus, *The Stomatopod Dactyl Club: A Formidable Damage-Tolerant Biological Hammer*, Science **336**, 1275 (2012).

[50] C. Sheppard, *Coral Reefs: A Very Short Introduction*, 1st ed. (Oxford University Press, New York, 2014).

[51] J. A. Chamberlain, *Mechanical properties of coral skeleton: compressive strength and its adaptive significance*, Paleobiology **4**, 419 (1978).

[52] S. B. Lang, S. a. M. Tofail, a. L. Kholkin, M. Wojtaś, M. Gregor, a. a. Gandhi, Y. Wang, S. Bauer, M. Krause, and a. Plecenik, *Ferroelectric polarization in nanocrystalline hydroxyapatite thin films on silicon.*, Scientific reports **3**, 2215 (2013).

[53] P. V. Giannoudis, H. Dinopoulos, and E. Tsiridis, *Bone substitutes: An update*, Injury **36**, S20 (2005), arXiv:NIHMS150003 .

[54] I. Pountos and P. V. Giannoudis, *Is there a role of coral bone substitutes in bone repair?*, Injury **47**, 2606 (2016).

[55] H. Lowenstam, *Minerals formed by organisms*, Science (New York, N.Y.) **211**, 1126 (1981).

[56] B. J. Rodriguez, S. V. Kalinin, J. Shin, S. Jesse, V. Grichko, T. Thundat, a. P. Baddorf, and a. Gruverman, *Electromechanical imaging of biomaterials by scanning probe microscopy.*, Journal of structural biology **153**, 151 (2006).

[57] N. A. Yaraghi, N. Guarín-Zapata, L. K. Grunenfelder, E. Hintsala, S. Bhowmick, J. M. Hiller, M. Betts, E. L. Principe, J.-Y. Jung, L. Sheppard, R. Wuhrer, J. McKittrick, P. D. Zavattieri, and D. Kisailus, *A Sinusoidally Architected Helicoidal Biocomposite*, Advanced Materials **28**, 6835 (2016).

[58] W. S. Williams and L. Breger, *Piezoelectricity in tendon and bone*, Biomechanics **8**, 407 (1975).

[59] W. S. Williams and L. Breger, *Analysis of Stress Distribution and Piezoelectric Response in Cantilever Bending of Bone and Tendon*, Annals of the New York Academy of Sciences **238**, 121 (1974).

[60] W. S. Williams, *Piezoelectricity and inhomogeneity in ceramics, polymers and bone*, Ferroelectrics **51**, 61 (1983).

[61] D. Gross and W. S. Williamsi, *Streaming Potential and the Electromechanical Response of Physiologically-Moist Bone*, Journal Biomechanics **15**, 277 (1982).

[62] M. Otter, S. Goheen, and W. S. Williams, *Streaming Potentials in Chemically Modified Bone*, Journal of orthopaedic research **6**, 346 (1988).

[63] W. S. Williams, *Piezoelectric effects in biological materials*, Ferroelectrics **41**, 225 (1982).

[64] E. Bursian and O. I. Zaikovskii, *Changes in curvature of ferroelectric film due to polarization* (1968).

[65] P. Zubko, G. Catalan, A. Buckley, P. Welche, and J. Scott, *Strain-Gradient-Induced Polarization in SrTiO3 Single Crystals*, Physical Review Letters **99**, 167601 (2007).

[66] M. S. Majdoub, P. Sharma, and T. Cagin, *Enhanced size-dependent piezoelectricity and elasticity in nanostructures due to the flexoelectric effect*, Physical Review B **77**, 125424 (2008).

[67] S. R. Kwon, W. Huang, L. Shu, F.-G. Yuan, J.-P. Maria, and X. Jiang, *Flexoelectricity in barium strontium titanate thin film*, Applied Physics Letters **105**, 142904 (2014).

[68] A. Abdollahi, C. Peco, D. Millán, M. Arroyo, and I. Arias, *Computational evaluation of the flexoelectric effect in dielectric solids*, Journal of Applied Physics **116**, 093502 (2014).

[69] A. Abdollahi and I. Arias, *Constructive and Destructive Interplay Between Piezoelectricity and Flexoelectricity in Flexural Sensors and Actuators*, Journal of Applied

Mechanics **82**, 121003 (2015).

[70] S. Zhu, B. Jiang, and W. Cao, *Characterization of piezoelectric materials using ultrasonic and resonant techniques*, Proc. SPIE **3341**, 154 (1998).

[71] J. G. Smits, S. I. Dalke, and T. K. Cooney, *The constituent equations of piezoelectric bimorphs*, Sensors and Actuators: A. Physical **28**, 41 (1991).

[72] M. S. Weinberg, *Working Equations for Piezoelectric Actuators and Sensors*, Journal of Microelectromechanical Systems **8**, 529 (1999).

[73] A. K. Tagantsev and A. S. Yurkov, *Flexoelectric effect in finite samples*, Journal of Applied Physics **112**, 044103 (2012).

[74] M. Stengel, *Surface control of flexoelectricity*, Physical Review B **90**, 201112 (2014).

[75] W. Ma and L. E. Cross, *Flexoelectric polarization of barium strontium titanate in the paraelectric state*, Applied Physics Letters **81**, 3440 (2002).

[76] W. Ma and L. E. Cross, *Flexoelectricity of barium titanate*, Applied Physics Letters **88**, 232902 (2006).

[77] Z. Li, S. Chan, M. H. Grimsditch, and E. S. Zouboulis, *The elastic and electromechanical properties of tetragonal BaTiO 3 single crystals*, Journal of Applied Physics **70**, 7327 (1991).

[78] W. Zhu, J. Y. Fu, N. Li, and L. Cross, *Piezoelectric composite based on the enhanced flexoelectric effects*, Applied Physics Letters **89** (2006), 10.1063/1.2382740.

[79] J. Y. Fu, W. Zhu, N. Li, N. B. Smith, and L. Eric Cross, *Gradient scaling phenomenon in microsize flexoelectric piezoelectric composites*, Applied Physics Letters **91** (2007), 10.1063/1.2800794.

[80] B. Chu, W. Zhu, N. Li, and L. E. Cross, *Flexure mode flexoelectric piezoelectric composites*, Journal of Applied Physics **106**, 104109 (2009).

[81] E. Fukada and I. Yasuda, *On the Piezoelectric Effect of Bone*, Journal of the Physical Society of Japan **12**, 1158 (1957).

[82] C. J. Dreyer, *Properties of Stressed Bone*, Nature **4782**, 1217 (1961).

[83] C. A. L. Bassett and R. O. Becker, *Generation of Electric Potentials by Bones in Response to Mechanical Stress*, Science (New York, N.Y.) **137**, 1063 (1962).

[84] A. A. Marino and R. O. Becker, *Piezoelectric Effect and Growth Control in Bone*, Nature **228**, 473 (1970).

[85] A. A. Marino, R. O. Becker, and S. C. Sidney, *Origin of piezoelectric effect in Bone*, Calc. Tiss. Res. **8**, 177 (1971).

[86] J. C. Anderson and C. Eriksson, *Electrical properties of wet collagen.*, Nature **218**, 166 (1968).

[87] R. Hiratai, M. Nakamura, and K. Yamashita, *Role of Collagen and Inorganic Components in Electrical Polarizability of Bone*, J. Vet. Med. Sci **76**, 205 (2014).

[88] S. a. M. Tofail, Y. Zhang, and a. a. Gandhi, *Piezoelectricity of bone from a new perspective*, Proceedings - International Symposium on Electrets , 91 (2011).

[89] S. Singh and H. S. Ranu, *Characterization of bone materials as ultrasonic transducers.*, Biomaterials **7**, 432 (1986).

[90] M. C. Stroe, J. M. Crolet, and M. Racila, *Mechanotransduction in cortical bone and the role of piezoelectricity: a numerical approach.*, Computer methods in biomechanics

and biomedical engineering **16**, 119 (2013).

[91] Y. Zhang, J. M. Tian, and C. Wang, *Piezoelectric Behavior of Biomaterials*, Key Engineering Materials **224-226**, 121 (2002).

[92] W. S. Williams and P. Lawrence, *p-n Junctions and the Piezoelectric Response of Bone*, Nature **232**, 655 (1971).

[93] S. C. Cowin, L. Moss-Salentijn, and M. L. Moss, *Candidates for the Mechanosensory System in Bone*, Journal of Biomechanical Engineering **113**, 191 (1991).

[94] D. Haverty, S. a. M. Tofail, K. T. Stanton, and J. B. McMonagle, *Structure and stability of hydroxyapatite: Density functional calculation and Rietveld analysis*, Physical Review B **71**, 094103 (2005).

[95] S. a. M. Tofail, D. Haverty, F. Cox, J. Erhart, P. Hána, and V. Ryzhenko, *Direct and ultrasonic measurements of macroscopic piezoelectricity in sintered hydroxyapatite*, Journal of Applied Physics **105** (2009), 10.1063/1.3093863.

[96] E. Fukada and I. Yasuda, *Piezoelectric Effects in Collagen*, Japanese Journal of Applied Physics **3**, 502B (1964).

[97] Y. Shu, M. J. Baumann, E. D. Case, R. K. Irwin, S. E. Meyer, C. S. Pearson, and L. R. McCabe, *Surface microcracks signal osteoblasts to regulate alignment and bone formation.*, Materials science & engineering. C, Materials for biological applications **44**, 191 (2014).

[98] R. Lakes, *The Role of Gradients Effects in the Piezoelectricity of Bone*, IEEE Transactions on Biomedical Engineering **BME-27**, 282 (1980).

[99] J. Fu, *Experimental studies of the direct flexoelectric effect in bone materials*, in *APS Meeting Abstracts* (American Physical Society, 2010).

[100] C. Halperin, S. Mutchnik, a. Agronin, M. Molotskii, P. Urenski, M. Salai, and G. Rosenman, *Piezoelectric Effect in Human Bones Studied in Nanometer Scale*, Nano Letters **4**, 1253 (2004).

[101] A. Abdollahi, C. Peco, D. Millán, M. Arroyo, G. Catalan, and I. Arias, *Fracture toughening and toughness asymmetry induced by flexoelectricity*, Physical Review B **92**, 094101 (2015).

[102] T. Norman, D. Vashishtht, and D. Burr, *Fracture Toughness of human bone under tension*, Journal Biomechanics **28** (1994).

[103] D. Taylor, J. A. N. G. Hazenberg, and T. C. Lee, *Living with cracks : Damage and repair in human bone*, Nature materials **6**, 263 (2007).

[104] J. Currey, *Stress concentrations in bone*, Quarterly journal of microscopical science **103**, 111 (1962).

[105] B. Lawn, *Fracture of brittle solids*, second edi ed., edited by E. A. Davis and I. M. Ward FRS (Cambridge University Press, 1993).

[106] L. Khatib, D. E. Golan, and M. Cho, *Physiologic electrical stimulation provokes intracellular calcium increase mediated by phospholipase C activation in human osteoblasts*, The FASEB Journal **18**, 1903 (2004).

[107] H. S. Burr and F. S. C. Northrop, *Evidence for the Existence of an Electro-Dynamic Field in Living Organisms**, Wash. Pub. Genetics Jour. Hered. Jour. Genetics Genetics PROCEEDINGS Shapiro N. J., Biol. Zhur. Genetics Genetics **2**, 284 (1939).

[108] C. T. Brighton, W. Wang, R. Seldes, G. Zhang, and S. R. Pollack, *Signal transduction in electrically stimulated bone cells.*, The Journal of bone and joint surgery. American volume **83-A**, 1514 (2001).

[109] H.-P. Wiesmann, M. Hartig, U. Stratmann, U. Meyer, and U. Joos, *Electrical stimulation influences mineral formation of osteoblast-like cells in vitro*, Biochimica et Biophysica Acta **1538**, 28 (2001).

[110] S. D. McCullen, J. P. McQuilling, R. M. Grossfeld, J. L. Lubischer, L. I. Clarke, and E. G. Loboa, *Application of Low-Frequency Alternating Current Electric Fields Via Interdigitated Electrodes: Effects on Cellular Viability, Cytoplasmic Calcium, and Osteogenic Differentiation of Human Adipose-Derived Stem Cells*, Tissue Engineering Part C: Methods **16**, 1377 (2010).

[111] J. A. Spadaro, *Mechanical and Electrical Interactions in Bone Remodeling **, Bioelectromagnetics **18**, 193 (1997).

[112] J. Deng, K. H. Schoenbach, E. S. Buescher, P. S. Hair, P. M. Fox, and S. J. Beebe, *The effects of intense submicrosecond electrical pulses on cells*, Biophysical Journal **84**, 2709 (2003).

[113] D. E. Clapham, *Calcium Signaling*, Cell **131**, 1047 (2007), arXiv:NIHMS150003 .

[114] M. P. Mattson and S. L. Chan, *Calcium orchestrates apoptosis*, Nature Cell Biology **5**, 1041 (2003).

[115] G. M. Xiong, A. T. Do, J. K. Wang, C. L. Yeoh, K. S. Yeo, and C. Choong, *Development of a miniaturized stimulation device for electrical stimulation of cells*, Journal of Biological Engineering **9**, 1 (2015).

[116] X. Miao, S. Yin, Z. Shao, Y. Zhang, and X. Chen, *Nanosecond pulsed electric field inhibits proliferation and induces apoptosis in human osteosarcoma.*, Journal of orthopaedic surgery and research **10**, 104 (2015).

[117] K. J. McLeod and T. R. Clinton, *The Effect of Low-Frequency Electrical Fields on Osteogenesis*, The Journal of Bone and Joint Surgery **74-A**, 920 (1992).

[118] K. E. Hammerick, A. W. James, Z. Huang, F. B. Prinz, and M. T. Longaker, *Pulsed direct current electric fields enhance osteogenesis in adipose-derived stromal cells.*, Tissue engineering. Part A **16**, 917 (2010).

[119] ThermoFisher Scientific, *CellEvent ™ Caspase-3 / 7 Green Detection Reagent* (2011).

[120] AZoM, *Titanium Dioxide - Titania (TiO2)* (2002).

[121] C. Rivera, D. Arola, and a. Ossa, *Indentation damage and crack repair in human enamel.*, Journal of the mechanical behavior of biomedical materials **21**, 178 (2013).

[122] J. Cuy, A. Mann, K. Livi, M. Teaford, and T. Weihs, *Nanoindentation mapping of the mechanical properties of human molar tooth enamel*, Archives of Oral Biology **47**, 281 (2002).

[123] H. Fong, M. Sarikaya, S. N. White, and M. L. Snead, *Nano-mechanical properties profiles across dentin–enamel junction of human incisor teeth*, Materials Science and Engineering: C **7**, 119 (2000).

[124] M. F. Sciadini, J. M. Dawson, and K. D. Johnson, *Evaluation of bovine-derived bone protein with a natural coral carrier as a bone-graft substitute in a canine segmental defect model*, Journal of Orthopaedic Research **15**, 844 (1997).

[125] N. Barroca, P. M. Vilarinho, M. H. V. Fernandes, P. Sharma, and A. Gruver-

man, *Stability of electrically induced-polarization in poly (L-lactic) acid for bone regeneration*, Applied Physics Letters **101**, 023701 (2012).

[126] C. Ooi, M. Hamdi, and S. Ramesh, *Properties of hydroxyapatite produced by annealing of bovine bone*, Ceramics International **33**, 1171 (2007).

[127] M. B. Schaffler and D. B. Burr, *Stiffness of compact bone: effects of porosity and density*, Journal of Biomechanics **21**, 13 (1988).